Equilibrium and stability of a double inlet system

R.L. Brouwer

M. Sc. thesis
Delft, May 2006

TU Delft
Delft University of Technology

Equilibrium and stability of a double inlet system

Delft, May 2006

R.L. Brouwer

Supervisors:

prof.dr.ir. M.J.F. Stive	TU Delft and WL | Delft Hydraulics
prof.dr.ir. J. van de Kreeke	University of Miami, FI
ir. T.J. Zitman	TU Delft
dr. H.M. Schuttelaars	TU Delft
dr.ir. Z.B. Wang	TU Delft and WL | Delft Hydraulics

TU Delft

Delft University of Technology

Preface

This study forms my Master of Science Thesis. The study is carried out as part of the requirements for the MSc degree of the department of Civil Engineering and Geosciences, Division of Hydraulics and Offshore Engineering at the Delft University of Technology.

This study concerns the cross-sectional equilibrium and stability of a double inlet system. In particular we are interested whether a double inlet system can be in an unconditionally stable equilibrium with its morphological environment.

I would like to thank my supervisors, prof.dr.ir. M.J.F. Stive (Delft University of Technology and WL | Delft Hydraulics), dr.ir. Z.B. Wang (Delft University of Technology and WL | Delft Hydraulics), dr. H.M. Schuttelaars (Delft University of Technology) and especially prof.dr.ir. J. van de Kreeke (University of Miami, Fl) and ir. T.J. Zitman (Delft University of Technology) for sharing their knowledge and support during this study. Furthermore, I would like to thank my fellow graduate students at Delft University of Technology for the pleasant stay. Finally, I would like to thank my soon to be wife, family and friends for their support during the years I spent in Delft.

Delft, May 2006

Ronald Brouwer

Summary

Barrier island coasts are a common feature in many parts of the world. An example is the Wadden coast of The Netherlands, Germany and Denmark. These coasts consist of barrier islands separated by tidal inlets with at the landward side tidal basins. Characteristic for the Wadden Sea is that the tidal basins are not completely separated, but are connected via topographic highs allowing exchange of water between the basins. As a result the tidal inlets that connect the basins to the North Sea will interact. The focus in this thesis is on the effect of this interaction on the cross-sectional equilibrium and stability of tidal inlets that are part of a double inlet system. The knowledge gained in this study will help to develop rational management plans for this kind of system.

In determining the equilibrium values and stability of cross-sectional areas of the inlets use is made of flow diagrams. A flow diagram consists of the equilibrium flow curves of each inlet and a flow field showing the adaptation of the inlet cross-sections after the system has been removed from equilibrium. Each intersection of the equilibrium flow curves represents a stable or unstable equilibrium. The equilibrium flow curve for each inlet is the locus of the values of the cross-sectional areas for which the velocity amplitude in the inlet equals the equilibrium velocity i.e. approximately 1 m/s according to ESCOFFIER [1940].

As a start the double inlet system is schematized as a basin connected to the ocean by two channels. The water surface area of the basin is assumed constant and water levels are assumed to fluctuate uniformly. On the seaward side a simple harmonic, semi-diurnal tide is used to force the system. Analyzing the double inlet system under these conditions by means of the flow diagrams leads to the conclusion that a stable equilibrium of the two inlets does not exist. Ultimately only one inlet remains open and the other will close. This confirms the earlier conclusions of VAN DE KREEKE [1990] and BORSJE [2003] concerning the cross-sectional stability of multiple inlet systems.

Double inlet systems such as those in the Wadden Sea where the basins are interconnected show that some kind of equilibrium is possible. Apparently the assumption of a uniformly fluctuating water level in the basin in previous modeling efforts is too restrictive and invalid as the basin is not deep enough and the overall length scale is not small compared to the length of the tidal wave. A better schematization is a set of two interconnected single inlet systems where in each basin the surface level fluctuates uniformly but with different amplitude and phase. In the model schematization this is implemented by adding a partition with opening between the two basins representing the topographic high. The opening has a length, measured in the current direction, and cross-sectional area. Analysis of the double inlet system with partition and opening leads to the conclusion that such systems can be unconditionally stable, sometimes even have multiple stable equilibriums. Investigations with a variable cross-sectional area of the opening between the basins showed that three configurations can be distinguished. For a relatively small cross-sectional area of this opening the basins hardly interact and the double inlet system almost behaves like two single inlet systems, yielding an unconditionally stable equilibrium for each inlet. For a relatively large cross-sectional area the influence of the opening is negligible and the system behaves like a double inlet system with a uniformly fluctuating water level, yielding a situation where ultimately one

of the two inlets will close while the other remains open. In between these two configurations a transition area exists where the opening has a noticeable influence on the interaction between the two basins. This leads to situations where two unconditionally stable equilibriums exist.

This insight in the behaviour of coupled basins can be used to predict the effect of for instance dredging in the vicinity of the topographic high, thus enlarging the interaction between the basins. Consider a double inlet system in equilibrium for which the stability conditions of the transition area are applicable. When enlarging the cross-sectional area of the opening until the stability conditions are valid belonging to a double inlet system with a uniformly fluctuating water level, one inlet closes while the other remains open. This kind of observations could be useful for future management plans for double inlet systems.

To determine the deeper cause of the existence of multiple stable equilibriums in the transition area a series of numerical experiments was carried out. After several model runs it appeared that the formulation of the friction term in the inlets connected to the ocean and the opening between the basins is paramount. A linear friction for the opening results in one stable equilibrium regardless of the formulation of the friction in the inlets. A non-linear formulation of the friction in the opening results in multiple stable equilibriums regardless of the formulation of the friction in the inlets. For a further understanding of the existence and behaviour of multiple stable equilibriums a mathematical stability analysis needs to be carried out.

To verify whether the model presented in this study generates plausible results it was applied to the Texel and Vlie basins in the western Wadden Sea. Results showed that the model is not able to accurately reproduce the water motion in the Texel and Vlie basins. The assumption of a uniformly fluctuating water level within each basin is too restrictive. Measurements showed that in the Texel and Vlie basin considerable differences in water level amplitude and phase exist depending on location. In addition in the present model the hypsometry is not taken into account. To further improve the calculation of the equilibrium and stability conditions of a double inlet system it is proposed to add the hypsometry to the present model and to investigate the use of a 2D model for the hydrodynamics.

In spite of certain shortcomings the present model still provides useful information. The model does prove that incorporating a partition with opening between the two basins leads to a situation where stable equilibriums are possible. This finding is an important step in a further understanding of double inlet systems.

Table of Contents

List of figures

List of tables

List of symbols

Symbol	Units	Meaning
A	$[m^2]$	Cross-sectional area of inlet below MSL
A_b	$[m^2]$	Surface area of basin
A_E	$[m^2]$	Equilibrium cross-sectional area of inlet below MSL
B	[m]	Width of inlet channel
C	[-]	Empirical constant
c	$[m^3/m^3]$	Actual sediment concentration
c_e	$[m^3/m^3]$	Local equilibrium sediment concentration
c_E	$[m^3/m^3]$	Overall equilibrium sediment concentration
c_f	[-]	Bed friction factor
g	$[m/s^2]$	Gravitational acceleration
h_0	[m]	Water level outside an inlet
h_{01}	[m]	Water level outside inlet 1
h_{02}	[m]	Water level outside inlet 2
h_1	[m]	Water level in basin 1
h_2	[m]	Water level in basin 2
h_b	[m]	Water level in a basin
L	[m]	Length of an inlet channel
m	[-]	Summation of entrance and exist loss coefficient
n	[-]	Power in the equation for the local equilibrium sediment concentration
P	$[m^3]$	Tidal prism
P_E	$[m^3]$	Tidal prism when an inlet is at equilibrium
Q	$[m^3/s]$	Channel discharge
q	[-]	Empirical constant
R	[m]	Hydraulic radius of the cross-sectional area of a channel
t	[s]	Morphological time
T	[s]	Tidal period
u	[m/s]	Velocity in an inlet
w	[m/s]	Vertical exchange coefficient
α	[rad]	Phase of the water level in a basin
β	[rad]	Angle of the slope of a channel with the horizontal
γ	[-]	Coefficient for the hydraulic radius
δ	$[m^3/s]$	Horizontal exchange rate
ζ	[rad]	Phase of the discharge in channel 1
θ	[rad]	Phase of the discharge in channel 2
λ	[-]	Factor for transition between linear and non-linear friction
τ	[s]	Damping factor
φ	[rad]	Phase of the water level in the ocean off inlet 1
χ	[-]	Friction coefficient
ψ	[rad]	Phase of the water level in the ocean off inlet 2
ω	[rad/s]	Angular frequency
ω_0	[rad/s]	Natural or Helmholz frequency
Δt	[s]	Time step

Subscript	Meaning
1,2,3	Inlet 1, inlet 2, inlet 3
b	Tidal basin
e	Local equilibrium
E	Overall equilibrium

Superscript	Meaning
^	Amplitude

1. Introduction

1.1 Background

Barrier island coasts can be found in many parts of the world. A well-known example is the Wadden coast of The Netherlands, Germany and Denmark. These coasts are characterized by barrier islands that are separated by tidal inlets with at the landward side a tidal basin. Barrier island, tidal inlet and tidal basin constitute a sand sharing system meaning that a change in the sand volume in one will affect the sand volume and morphology of the other elements. Changes can be the result of natural phenomena such as accelerated sea level rise and storm surges or can be attributed to human activity. Examples of human activity are land reclamation and gas extraction. It is important that the physical dynamics of these sand sharing systems is understood. When translated in a quantitative predictive manner, this knowledge will allow predicting the consequences of both natural and man-induced changes. In turn this can be used to develop a rational management plan for the sand sharing system.

One of the characteristics of the Wadden Sea tidal basins is that they are not completely separated. Rather, the boundaries between the basins are formed by a tidal divide or in terms of morphology a topographic high extending between the middle of the barrier island and the main land. The topographic high limits, but still allows some exchange of water between the basins. As a result the tidal basins and the inlets that connect the basins to the North Sea will interact. The interest in this thesis is on the effect of this interaction on the cross-sectional equilibrium and stability of the inlets.

1.2 Area of interest

The Dutch Wadden Sea has been the subject of many studies and as a result a wealth of information exists on bathymetry, tides, morphological changes etc. In this study the western part of the Dutch Wadden Sea (Figure 1) is used to provide the necessary guidance for the analysis of the cross-sectional equilibrium and stability of multiple interacting inlets. To a leading order the western Dutch Wadden Sea consists of two basins, The Texel Basin and The Vlie Basin. These basins are connected to the North Sea by respectively the inlets Marsdiep and Vlie. The basins are separated by a topographic high, represented by the white lines. In the figure four locations are added where water levels are measured. These locations are Texel North Sea, Terschelling North Sea, Harlingen and Kornwerderzand.

Figure 1: Area of interest.

1.3 Previous studies

VAN DE KREEKE [1990] investigated the equilibrium and stability of a double inlet system. The inlet cross-sectional areas are assumed to be in equilibrium when the velocity amplitude is approximately 1 m/s [ESCOFFIER, 1940]. Determining the stability of the equilibrium cross-sectional areas requires calculating the relationship between the velocity amplitude in one inlet as a function of the cross-sectional areas of both inlets. This relationship is referred to as the closure surface. In determining the closure surface the water surface area of the basin was assumed constant and water levels were assumed to fluctuate uniformly. In the dynamics of the inlet flow, inertia was neglected and friction was linearized. The governing equations were solved analytically. His conclusion was that under these conditions a stable equilibrium of the two inlets is not possible. Ultimately only one inlet will remain open and the other will close.

BORSJE [2003] studied the same problem as VAN DE KREEKE [1990]. He used the same continuity conditions but in describing the dynamics of the inlet flow included inertia and non-linear friction. The governing equations were solved using the harmonic method i.e. the basin water level and inlet discharges are assumed to fluctuate as a simple sine function. For a given combination of cross-sectional areas of the two inlets the amplitudes of the first harmonic of the inlet velocities were determined using an iterative method. Computations were carried out for different values of basin area, inlet lengths and friction factors. The results of the computations confirmed the earlier conclusion by VAN DE KREEKE [1990] that under the assumption of a constant basin surface area and uniformly fluctuating basin water level a stable equilibrium for the two inlets is not possible.

To introduce a semi-open boundary between the basins, BORSJE [2003] divided the basin in two parts separated by a partition. An opening in the partition allowed flow between the two basins. The water level in the individual basins is assumed to fluctuate uniformly. In general the amplitudes and phase of these fluctuations will be different for each of the basins. The dynamics of the flow in the opening is described by the same equation as for the inlets connecting the basins and ocean. The harmonic method was used to solve the system of equations. Results showed that depending on the size of the opening one or more combinations of inlet cross-sectional areas could be found that represented stable equilibriums.

1.4 Objectives

The harmonic method as used in BORSJE [2003] requires iterating about the amplitudes of the inlet discharges. Values of the amplitudes are selected and with these values new amplitudes are calculated until the solution converges. In case of a double inlet system with partition and opening, three discharge amplitudes are involved in the iteration process. Already in the study by BORSJE there were indications that this iteration process not always converged. This was confirmed by initial computations carried out as part of the present study. For this reason it was decided to abandon the harmonic solution and *to develop a finite difference technique to solve the equations governing the water motion.*

In the studies VAN DE KREEKE [1990] and BORSJE [2003], the equilibrium values and stability of cross-sectional areas were determined using equilibrium flow curves. For the definition of equilibrium flow curve see Section 2.3.1. A more sophisticated way of judging the stability of a set of inlet cross-sectional areas is by means of a flow diagram[1]. The idea of using a flow diagram was derived from a paper on stability of river bifurcations by WANG ET AL (1995).
Constructing a flow diagram requires a model describing the adaptation of an inlet cross-section after it has been removed from equilibrium. In this study *flow diagrams will be used to determine the cross-sectional stability of inlets that are part of a) a double inlet system and b) a double inlet system with partition and opening.*

[1] In literature flow diagrams are also referred to as phase diagrams and phase planes.

The results of BORSJE [2003] when including a partition with opening suggest that depending on the size of the opening one or more stable equilibriums exist. *The existence of multiple stable equilibriums will be further investigated* by carrying out a series of numerical experiments with different formulations of the dynamics of the inlet flow including linear and non-linear friction.

Finally, *the model that includes the partition and opening will be used to explain the stability of the inlets connecting the Texel and Vlie basin to the ocean.*

In summary, the objectives of the present study are:

- To develop a finite difference method to solve the equations governing the water motion.
- To determine the cross-sectional stability of tidal inlets that are part of a double inlet system or double inlet system with partition and opening using flow diagrams
- To investigate the effect of the formulation of the inlet dynamics on the number of stable inlets.
- To apply the model that includes partition and opening to the Texel and Vlie basins.

1.5 Reader

In the following chapter the basic principles of determining the equilibrium and stability of tidal inlets are discussed using a single inlet and double inlet system (without partition) as examples. The construction of a flow diagram and its use in determining the stability of an inlet is illustrated. The hydrodynamic equations for the single, double and double inlet with partition and opening are presented in Chapter 3 together with a finite difference solution. Making use of the finite difference solution and the flow diagram the equilibrium and stability of a double inlet system and a double inlet system with partition and opening are presented in respectively Chapters 4 and 5. In Chapter 6 results of numerical experiments, carried out to investigate the occurrence of multiple stable equilibriums, are summarized. Results of the application of the stability models (Chapter 3) for the Marsdiep - Vlie system can be found in Chapter 7. In the final Chapter 8, a summary of results and conclusions together with recommendations for future research are presented.

2. Morphodynamics; equilibrium and stability

2.1 General approach

For purposes of this study the inlets are schematized to a channel(s) and basin(s). The channel(s) connect the basin(s) to the ocean. They are assumed to have a uniform cross-section. To determine the equilibrium value of the cross-sectional area of a channel use is made of the concept first presented by ESCOFFIER [1940] i.e. when at equilibrium channels take on a cross-sectional area for which the amplitude of the tidal velocity is approximately 1 m/s. The stability of the equilibrium cross-sectional area is investigated using a flow diagram to be discussed in more detail in sections 2.2.2 and 2.3.2. To calculate the flow diagram use is made of the morphodynamic, semi-empirical model ASMITA [STIVE *et al.*, 1996]. This model describes the adaptation of a cross-sectional area when out of equilibrium. The main features of ASMITA are summarized in Appendix A. In the following the general approach for determining the equilibrium and stability is illustrated for a single inlet system and a double inlet system.

2.2 Single inlet system

2.2.1 Equilibrium

The equilibrium cross-sectional area of the channel is determined from the well-known cross-sectional area tidal prism relationship of inlets at equilibrium [O'BRIEN, 1931]:

$$A_E = C \cdot P_E^q \tag{2.1}$$

In this expressions: A_E = equilibrium cross-sectional area of the inlet below MSL [m^2]
P_E = tidal prism when inlet is at equilibrium [m^3]
C and q are empirical constants; C has a dimension [1/m]

In general, the relationship between tidal prism and cross-sectional area from hydrodynamics can be formally written as:

$$P = f(A) \tag{2.2}$$

Instead of the tidal prism, in the following, the amplitude of the tidal velocity in the inlet is introduced as the characteristic hydrodynamic parameter. Assuming a simple harmonic velocity variation, the relation between tidal prism and velocity amplitude is:

$$P = \frac{TA\hat{u}}{\pi} \tag{2.3}$$

in this expression:			
	P	= tidal prism	[m^3]
	T	= tidal period	[s]
	A	= cross-sectional area of the inlet below MSL	[m^2]
	û	= amplitude of the velocity in the inlet	[m/s]

Substituting in Equation (2.1), the expression for the equilibrium velocity is:

$$\hat{u}_E = \frac{\pi}{C^{1/q} \cdot T} A_E^{\frac{1-q}{q}} \tag{2.4}$$

In terms of the velocity amplitude and making use of Equation (2.3), Equation (2.2) can be formally written as:

$$\hat{u} = f(A) \tag{2.5}$$

This relationship is referred to as the closure curve.

Equations (2.4) and (2.5) determine the values of the equilibrium cross-sectional area(s). Values of C and q are to be determined from a set of inlets that are in equilibrium and are located in the same wave, tide and sedimentary environment as the subject inlet. For most inlets and taking P as the tidal prism for average tide condition the value of q is close to 1. In particular to a good approximation for the Wadden Sea inlets q = 1 and C = $6.8 \cdot 10^{-5}$ m^{-1}, VAN DE KREEKE [1998]. With these values and taking T = 44,712 s it follows from Equation (2.4) that for the Wadden Sea inlets $\hat{u}_E = \frac{\pi}{CT} \approx 1\, m/s$. The closure curve, The functional form of Equation (2.5), follows from the hydrodynamic model to be discussed in Chapter 3. A typical shape of the closure curve is presented in Figure 2a. The intersection with $\hat{u} = \hat{u}_E$ yields the two equilibrium cross-sectional areas A_{E1} and A_{E2}.

2.2.2 Stability

To determine whether the two equilibrium cross-sectional areas A_{E1} and A_{E2} are stable or unstable use is made of Equation (2.6) describing the adaptation of a cross-sectional area when out of equilibrium (Appendix A):

$$\frac{dA}{dt} = \frac{wBc_E\delta}{\delta + wBL}\left(\left(\frac{\hat{u}}{\hat{u}_E}\right)^n - 1\right) \tag{2.6}$$

In this expression:			
	A	= cross-sectional area of the inlet below MSL	[m^2]
	B	= width of the inlet channel	[m]
	L	= length of the inlet channel	[m]
	c_E	= overall equilibrium sediment concentration	[m^3/m^3]
	δ	= horizontal exchange rate	[m^3/s]
	w	= vertical exchange coefficient	[m/s]
	û	= velocity amplitude	[m/s]
	$\hat{u}_E$	= equilibrium velocity amplitude	[m/s]
	t	= morphological time	[s]

With û being a function of A, the general shape of $\frac{dA}{dt}$ as a function of A is presented in Figure 2b. For $\hat{u} = \hat{u}_E$ the inlet is in equilibrium and $\frac{dA}{dt} = 0$. Parameter values used to construct Figure 2b are presented in Table 1. In general there will be two equilibrium cross-sectional areas. An equilibrium cross-section A_E represents a stable equilibrium when in the neighbourhood of A_E, $\frac{dA}{dt}$ and $A - A_E$ have opposite signs. Conversely, when $\frac{dA}{dt}$ and $A - A_E$ have the same signs the equilibrium is unstable.
It follows that A_{E1} represents an unstable and A_{E2} represents a stable equilibrium.

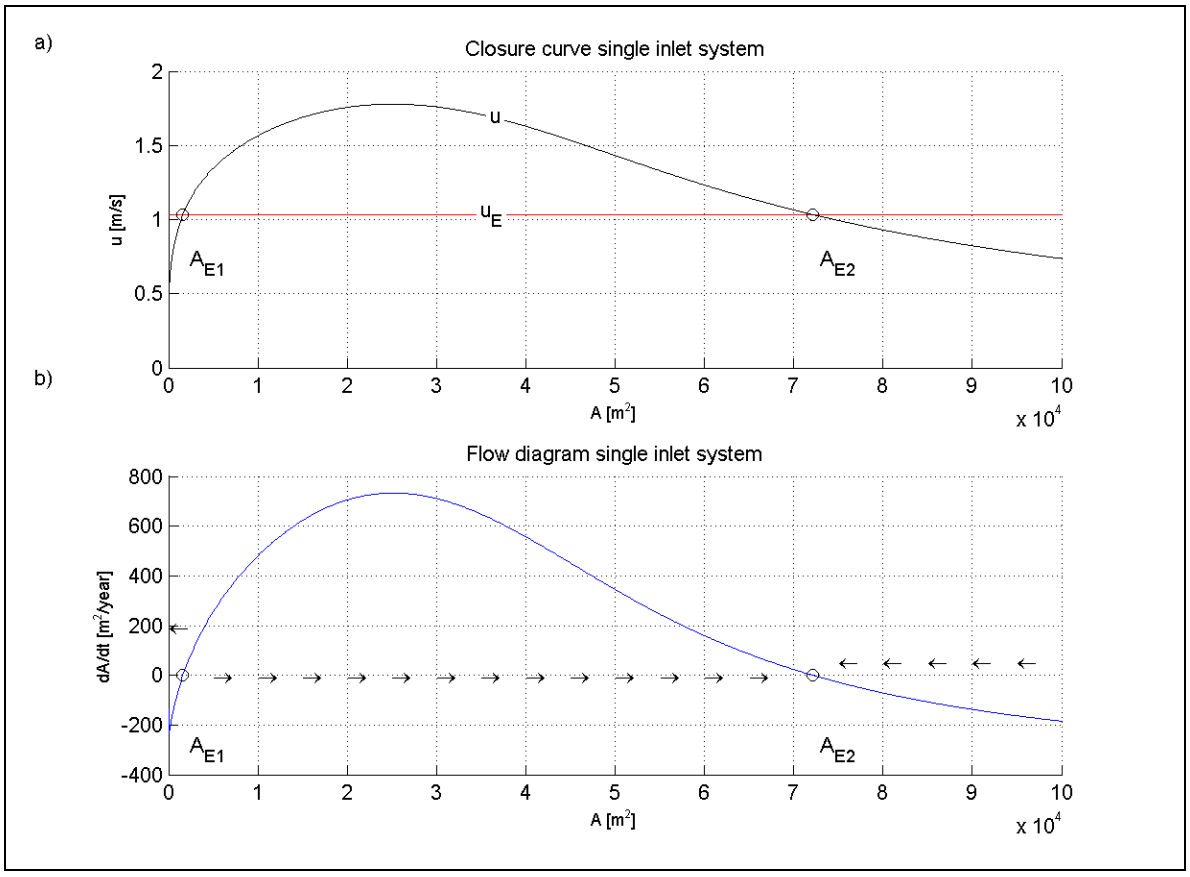

Figure 2: a) Closure curve and b) The rate of change of the cross-sectional areas as a function of cross-sectional area and the corresponding flow diagram. The values of the parameters used in the calculations are presented in Table 1

Table 1: Parameter values used for Figure 2

Parameter	Value	Parameter	Value
L	5,000 [m]	n	3
A_b	$6.56 \cdot 10^8$ [m^2]	m	1
β	π/180 [rad]	δ	3,000 [m^3/s]
c_f	0.004 [-]	w	0.02 [m/s]
$\hat{h}_0$	0.75 [m]	c_E	$2 \cdot 10^{-5}$ [-]

An alternative way of illustrating the (in)stability of an equilibrium is by use of a flow diagram. For this a vector $\frac{\overline{dA}}{dt}$ is defined with magnitude $\frac{dA}{dt}$ and a direction along the A-axis. This results in a vector plot as shown in Figure 2b. Because in this application only the direction of the vector is of interest, vectors are given a unit length. It follows from the vector plot that when slightly enlarging A_{E1} the cross-section will increase until it reaches the value A_{E2}. When slightly decreasing the value of A_{E1} the inlet will close. When changing the values of A_{E2} in the range of $A_{E1} < A < \infty$ the inlet cross-sectional area will always return to the value A_{E2}. Therefore A_{E1} represents an unstable and A_{E2} represents a stable equilibrium.

2.3 Double inlet system

2.3.1 Equilibrium

Evaluating the cross-sectional equilibrium and stability for a double inlet system follows along the same lines as for the single inlet. The equilibrium relationships, Equations (2.1) and (2.4) hold for both inlets. Values of the equilibrium velocity and the amplitude of the actual velocity in the inlets, respectively Equations (2.4) and (2.5) are now functions of A_1 and A_2. A_1 and A_2 are the cross-sectional areas of inlets 1 and 2. Therefore, as before taking q = 1,

$$\hat{u}_{E_1} = \hat{u}_{E_2} = \frac{\pi}{CT} \tag{2.7}$$

and

$$\hat{u}_1 = f(A_1, A_2) \tag{2.8}$$

$$\hat{u}_2 = f(A_1, A_2) \tag{2.9}$$

$\hat{u}_1(A_1, A_2)$ and $\hat{u}_2(A_1, A_2)$ are the two-dimensional counterpart of the closure curve and are henceforth referred to as the closure surfaces. The general shape of these closure surfaces is presented in Figure 3 and Figure 4.

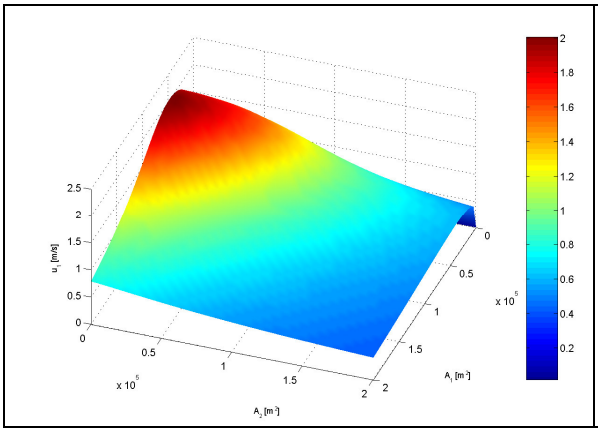

Figure 3: Closure surface for inlet 1. For paramater values used in calculation see Table 2.

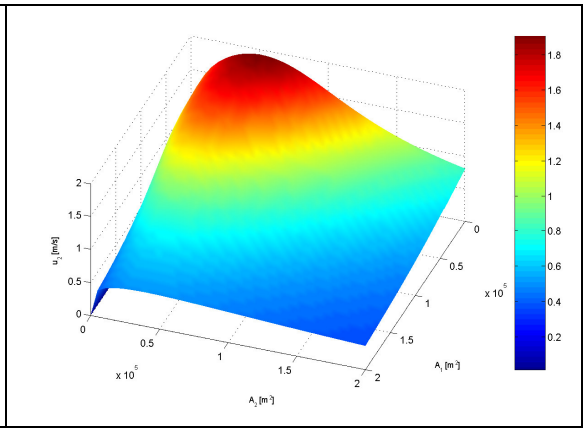

Figure 4: Closure surface for inlet 2. For parameter values used in calculations see Table 2.

Table 2: Parameter values used for Figure 3 and Figure 4

Parameter	Value	Parameter	Value
L_1	5,000 [m]	n	3
L_2	6,000 [m]	m	1
A_b	$14 \cdot 10^8$ [m^2]	δ	3,000 [m^3/s]
$\beta_1 = \beta_2$	π/180 [rad]	w	0.02 [m/s]
$c_{f,2} = c_{f,2}$	0.004 [-]	c_E	$2 \cdot 10^{-5}$ [-]
$\hat{h}_{0,1} = \hat{h}_{0,2}$	0.75 [m]		

The locus of the values (A_1, A_2) for which $\hat{u}_1 = \hat{u}_{E1}$ (= the equilibrium flow curve for inlet 1) is the intersection of the closure surface and the horizontal plane $\hat{u}_1 = \hat{u}_{E1}$. The general shape of the equilibrium flow curve for inlet 1 is presented in Figure 5. Similarly the general shape of equilibrium flow curve for inlet 2 is presented in Figure 6.

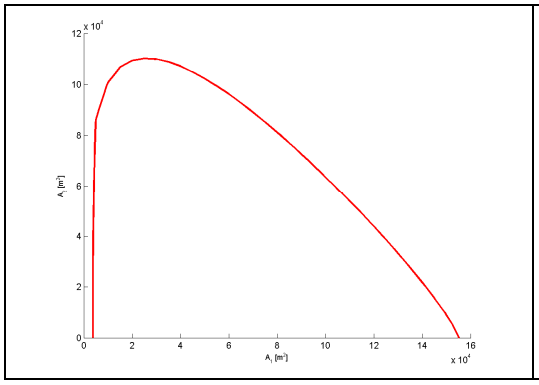

Figure 5: Equilibrium flow curve for inlet 1

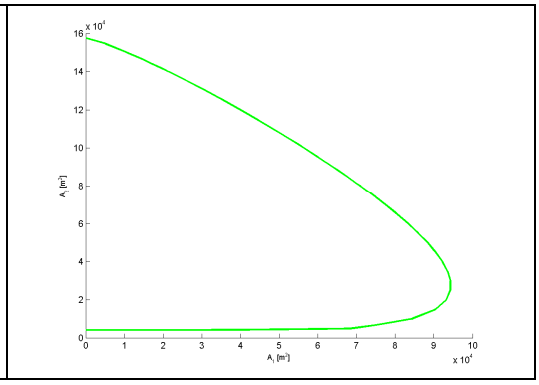

Figure 6: Equilibrium flow curve for inlet 2

The intersection(s) of the two equilibrium flow curves represents combinations of (A_1, A_2) values for which both inlets are in equilibrium.

2.3.2 Stability

To determine whether these equilibriums are stable use is made of the flow diagram. The governing equations describing the rate of change of the cross-sectional area are when using the ASMITA model (Appendix A):

$$\frac{dA_1}{dt} = \frac{wB_1 c_E \delta}{\delta + wB_1 L_1}\left(\left(\frac{\hat{u}_1}{\hat{u}_E}\right)^n - 1\right) \tag{2.10}$$

$$\frac{dA_2}{dt} = \frac{wB_2 c_E \delta}{\delta + wB_2 L_2}\left(\left(\frac{\hat{u}_2}{\hat{u}_E}\right)^n - 1\right) \tag{2.11}$$

Here δ, w, c_E are assumed to be the same for both inlets. Because $\hat{u}_1$ and $\hat{u}_2$ are functions of A_1 and A_2, $\frac{dA_1}{dt}$ and $\frac{dA_2}{dt}$ are functions of A_1 and A_2.
To construct the flow diagram a vector

$$\frac{\overline{dA}}{dt} = \frac{dA_1}{dt}\bar{e}_1 + \frac{dA_2}{dt}\bar{e}_2 \tag{2.12}$$

is introduced, where $\bar{e}$ is the unit vector. $\frac{dA_1}{dt}\bar{e}_1$ is a vector with magnitude $\frac{dA_1}{dt}$ and a direction of the A_1-axis. $\frac{dA_2}{dt}\bar{e}_2$ is a vector with magnitude $\frac{dA_2}{dt}$ and a direction of the A_2-axis. Giving $\frac{\overline{dA}}{dt}$ a unit length the flow diagram together with the two equilibrium flow curves are presented in Figure 7.

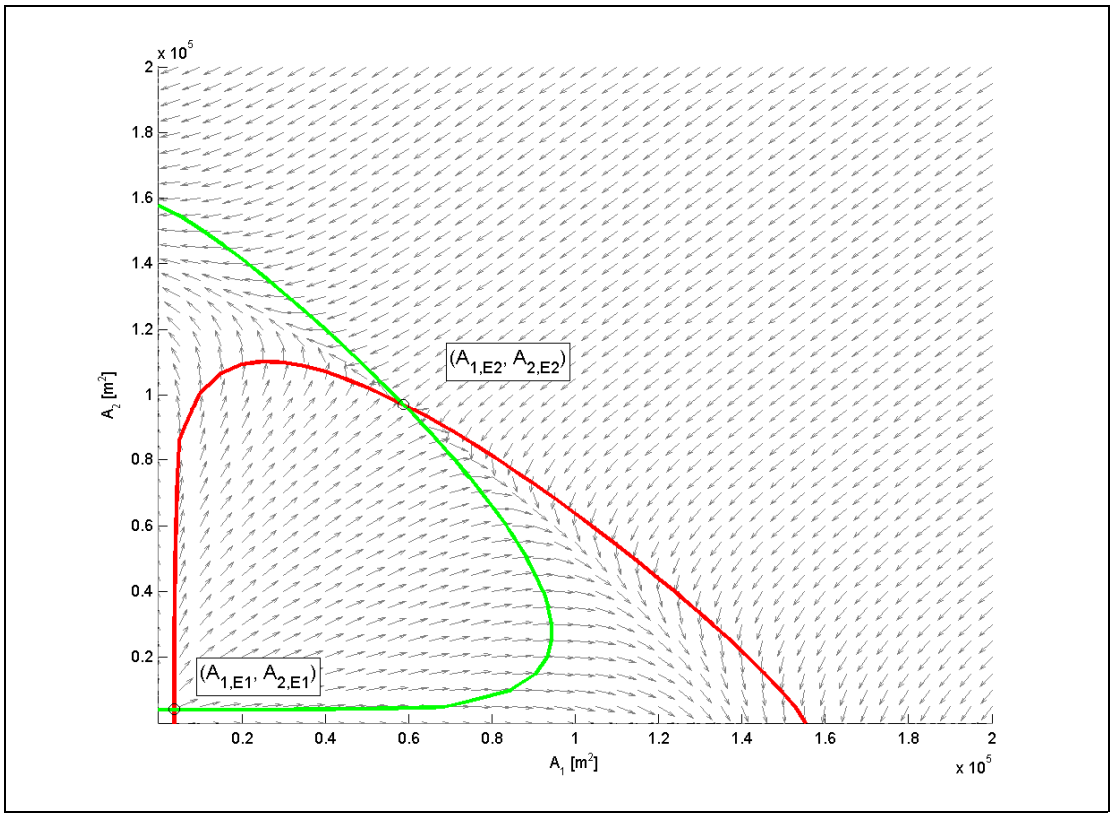

Figure 7: Flow diagram and equilibrium flow curves for a double inlet system

The flow diagram yields two combinations of equilibrium cross-sectional areas ($A_{1,E1}$, $A_{2,E1}$) and ($A_{1,E2}$, $A_{2,E2}$). An expanded version of the flow diagram in the vicinity of those equilibriums are presented in Figure 8a and Figure 8b. In Figure 8b “streamlines” have been added. Streamlines and vectors show that neither of these equilibriums is stable. When given a slight deviation from equilibrium, cross-sectional areas do not return to the equilibrium values. Both inlets close or at best one inlet will remain open; see Figure 7.

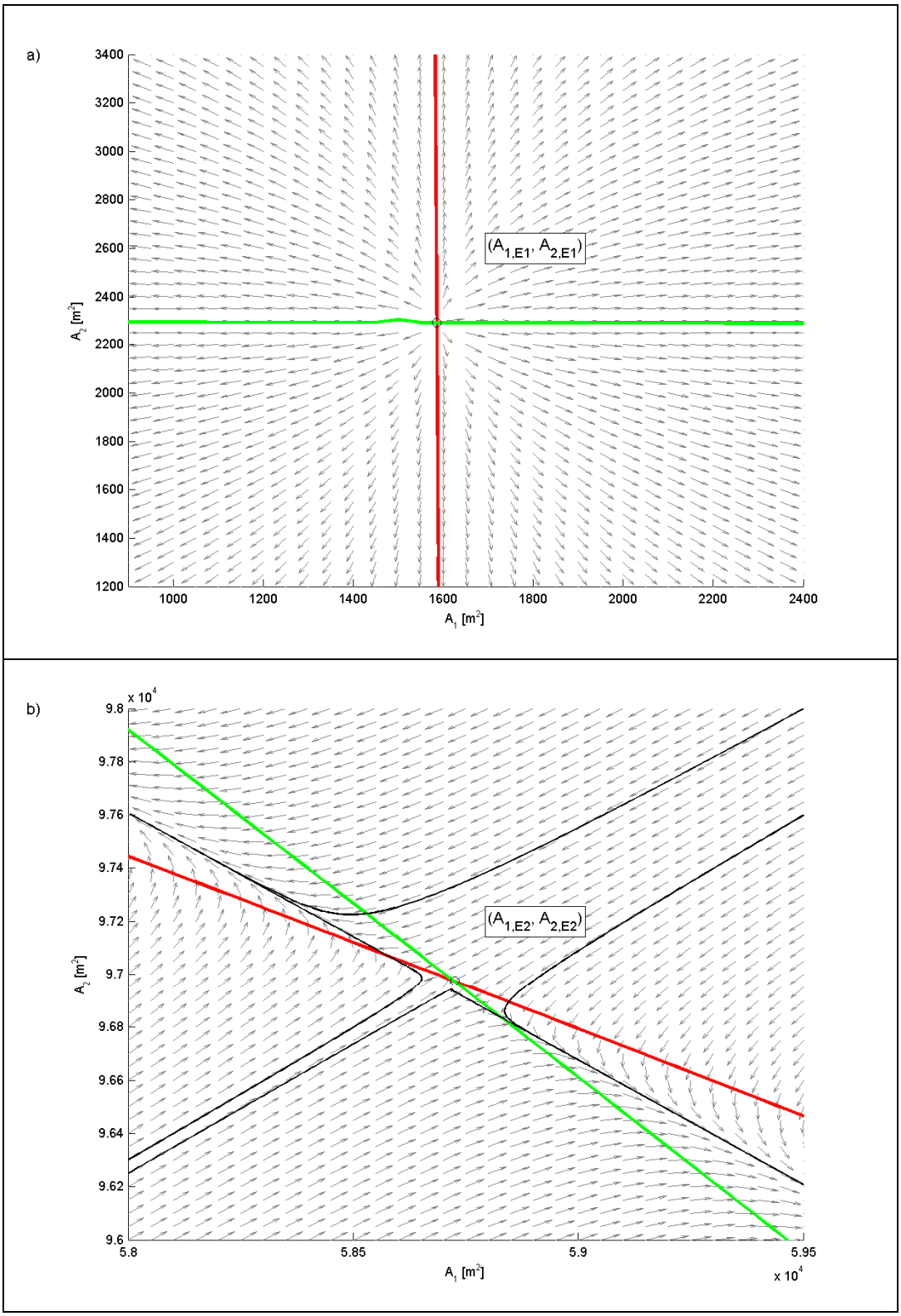

Figure 8: a) Flow diagram in vicinity of equilibrium state ($A_{1,E1}$, $A_{2,E1}$) and b) Flow diagram in vicinity of equilibrium state ($A_{1,E2}$, $A_{2,E2}$)

3. Hydrodynamics

Calculating the equilibrium cross-sectional areas and determining the stability of these equilibriums requires that the amplitudes of the inlet velocities are known as functions of the cross-sectional areas. For this the hydrodynamic equations for a single inlet, a double inlet and a double inlet with opening between two basins are presented (see also BORSJE [2003]). To solve the governing equations the harmonic method is used for the single inlet and double inlet. In addition, for the double inlet and double inlet with opening the governing equations are solved using a finite difference method.

3.1 Single inlet system

3.1.1 Hydrodynamic equations

The single inlet system can be schematized as a channel connecting a basin with the ocean (Figure 9).

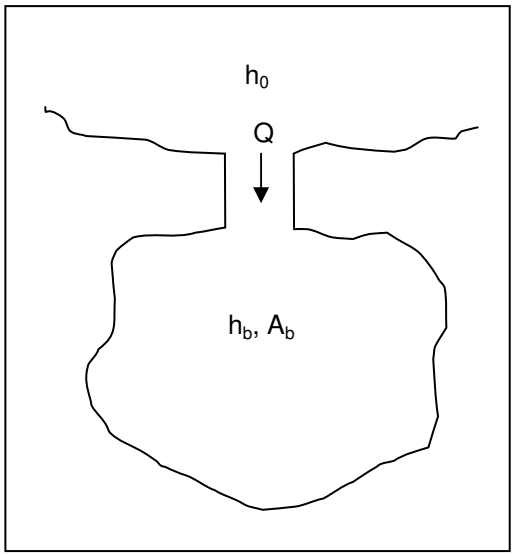

Figure 9: Schematization of a single inlet system

The water motion is forced by a semi-diurnal ocean tide

$$h_0(t) = \hat{h}_0 \cos \omega t \qquad (3.1)$$

Assuming a uniformly fluctuating water level in the basin and a basin size that is small compared to the length of the tidal wave, so that $h_b = h_b(t)$, continuity can be expressed as:

$$Q = A_b \frac{dh_b}{dt} \tag{3.2}$$

in which:	Q	= the channel discharge (flood is positive)	[m^3/s]
	A_b	= the surface area of the basin	[m^2]
	h_b	= the water level in the basin	[m]

A second equation that describes the dynamics of a single inlet system is the equation of motion:

$$M \frac{dQ}{dt} = h_0 - h_b - \chi \frac{|Q|Q}{gA^2} \tag{3.3}$$

with

$$\chi = \frac{mR + 2c_f L}{2R} \tag{3.4}$$

and

$$M = \frac{L}{gA} \tag{3.5}$$

in which:	L	= the length of the channel	[m]
	g	= the gravitational acceleration	[m/s^2]
	A	= the cross-sectional area of the channel with respect to MSL	[m^2]
	h_0	= the water level outside the inlet	[m]
	m	= summation of entrance and exit loss coefficient	[-]
	R	= the hydraulic radius of the cross-sectional area of the channel	[m]
	c_f	= bed friction factor	[-]
	χ	= coefficient which is the summation of entrance, exit and friction losses	[-]

The left-hand side of Equation (3.3) represents the local acceleration, the first two terms on the right-hand side the pressure gradient and the third term on the right-hand side bottom friction.
Assuming the channel cross-section remains geometrically similar and has a triangular shape with β as the angle of the slope of the channel banks, the hydraulic radius can be written as:

$$R = \gamma \sqrt{A} \tag{3.6}$$

With

$$\gamma = \tfrac{1}{2}\sqrt{\sin\beta\cos\beta} \tag{3.7}$$

3.1.2 Harmonic method

In the harmonic method for the equation of motion the friction term in Equation (3.3) is linearized. In applying the basic concept of the harmonic method, where Q is a simple harmonic function of t, one finds:

$$|Q|Q \cong \frac{8}{3\pi}\hat{Q}Q \tag{3.8}$$

In this simplification we assume that there is no generation of higher harmonics due to non-linear interactions. Making use of Equation (3.8), Equation (3.3) can be written as:

$$M\frac{dQ}{dt} + WQ = h_0 - h_b \tag{3.9}$$

with

$$W = \frac{8}{3\pi}\chi\frac{\hat{Q}}{gA^2} \tag{3.10}$$

Substituting Equation (3.2) in Equation (3.9) a non-linear second order non-homogeneous differential equation similar to the equation governing the damped spring-mass system arises:

$$MA_b\frac{d^2h_b}{dt^2} + \tau\frac{dh_b}{dt} + h_b = h_0 \tag{3.11}$$

with the damping factor

$$\tau = WA_b = \frac{8}{3\pi}\chi\left(\frac{A_b}{A}\right)^2\frac{\omega\hat{h}_b}{g} \tag{3.12}$$

Introducing the natural or Helmholz frequency

$$\omega_0 = \frac{1}{\sqrt{MA_b}} = \sqrt{\frac{g}{L}\frac{A}{A_b}} \tag{3.13}$$

The solution to Equation (3.11) is of the form

$$h_b(t) = \hat{h}_b\cos(\omega t - \alpha) \tag{3.14}$$

with

$$\hat{h}_b = \frac{\hat{h}_0}{\sqrt{\left(1-\frac{\omega^2}{\omega_0^2}\right)^2 + (\omega\tau)^2}} \tag{3.15}$$

and

$$\tan\alpha = \frac{\omega\tau}{\left(1-\frac{\omega^2}{\omega_0^2}\right)} \tag{3.16}$$

Substituting the expression for τ from Eq. (3.12) in Eq. (3.15) it follows that:

$$\hat{h}_b = \sqrt{\frac{-\left(1-\frac{\omega^2}{\omega_0^2}\right)^2 + \sqrt{\left(1-\frac{\omega^2}{\omega_0^2}\right)^4 + 4F^2\hat{h}_0^2}}{2F^2}} \tag{3.17}$$

with

$$F = \frac{8}{3\pi}\chi\left(\frac{A_b}{A}\right)^2\frac{\omega^2}{g} \tag{3.18}$$

The amplitude of the discharge in the inlet is related to the amplitude of the basin tide by:

$$\hat{Q} = A_b\omega\hat{h}_b \tag{3.19}$$

The value of the velocity amplitude follows from:

$$\hat{u} = \frac{\hat{Q}}{A} \tag{3.20}$$

3.1.3 Results

Water levels and velocities calculated with the harmonic method are presented in Figure 10. The parameter values used in the calculations are presented in Table 3.

Table 3: Parameter values single inlet system

Parameter	Value	Parameter	Value
c_f	0.004 [-]	T	44,712 [s]
m	1 [-]	β	π/180 [rad]
L	5,000 [m]	g	9.81 [m/s^2]
$\hat{h}_0$	0.75 [m]	ω	1.41·10^{-4} [s^{-1}]
A	25,000 [m^2]	Δt	36 [s]
A_b	6.56·10^8 [m^2]		

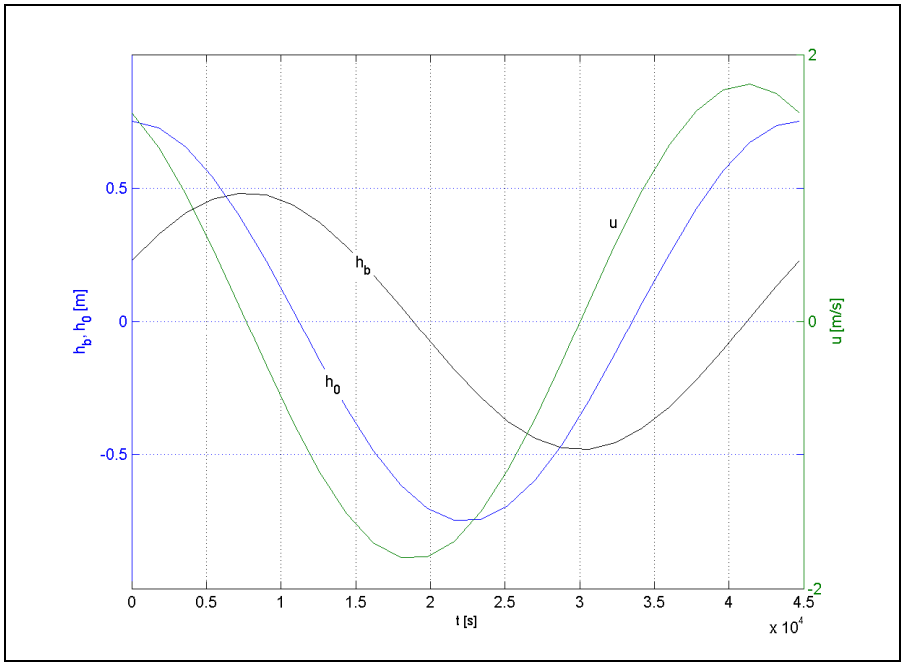

Figure 10: Water motion for a single inlet system

In agreement with the continuity equation (Equation (3.2)), when the velocity is zero the water level in the basin reaches a maximum or a minimum. As a first approximation, neglecting $\frac{du}{dt}$ in the equation of motion (Equation (3.3)):

$$h_0 - h_b = \chi \frac{|u|u}{g} \tag{3.21}$$

When the velocity is zero, the water levels inside and outside are equal. It follows that with the assumption that $\frac{du}{dt} = 0$ water levels intersect at the maximum and minimum of the basin tide. This is in reasonable agreement with the calculation. To verify whether the assumption $\frac{du}{dt} = 0$ can be justified the different terms in the equation of motion, Equation (3.9), are evaluated. Each term in the equation of motion is a harmonic function

of t with amplitude of respectively $M\omega\hat{Q}$, $\sqrt{\hat{h}_0^2 + \hat{h}_b^2 - 2\hat{h}_0\hat{h}_b\cos\alpha}$ and $\chi\frac{\hat{Q}^2}{gA^2}$. Using the amplitude values of $\hat{h}_0$, $\hat{h}_b$ and û in Figure 10 and the parameter values in Table 3:

Acceleration term: $M\omega\hat{Q} = 0.095$ (3.22)

Pressure gradient: $\sqrt{\hat{h}_0^2 + \hat{h}_b^2 - 2\hat{h}_0\hat{h}_b\cos\alpha} = 0.285$ (3.23)

Friction term: $\chi\frac{\hat{Q}^2}{gA^2} = 0.286$ (3.24)

It follows that the acceleration term is indeed small compared to the other terms but is not negligible.

3.2 Double inlet system

The double inlet system is schematized as a basin connected to the ocean by two channels (Figure 11). The entire basin is assumed to react uniformly to external forcing.

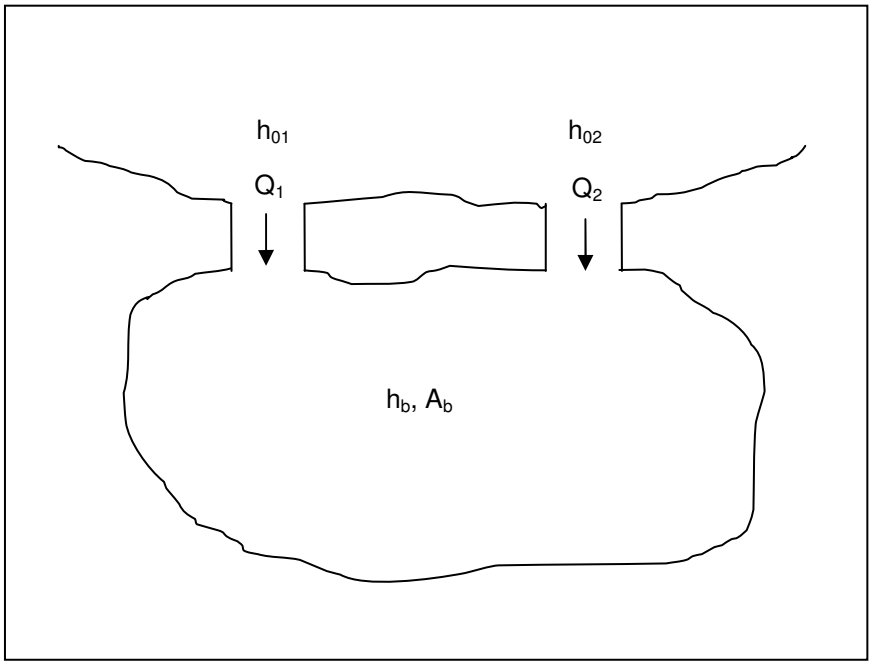

Figure 11: Schematization of a double inlet system

Similar to the single inlet system, a semi-diurnal ocean tide is used to force the system. Amplitudes and phases of the ocean tide can be different for the two inlets. Following BORSJE [2003], if the tide is represented by a simple sinusoidal function, this will result in the following expressions:

$$h_{01}(t) = \hat{h}_{01}\cos(\omega t + \psi) \tag{3.25}$$

$$h_{02}(t) = \hat{h}_{02}\cos(\omega t + \varphi) \tag{3.26}$$

3.2.1 Hydrodynamic equations

Similar to the single inlet system the continuity equation and the equation of motion are used to describe the hydrodynamics of the double inlet system. The continuity equation contains an extra discharge term for the second inlet, resulting in:

$$Q_1 + Q_2 = A_b \frac{dh_b}{dt} \tag{3.27}$$

For each inlet the equation of motion can be written as:

$$M_1 \frac{\partial Q_1}{\partial t} + \chi_1 \frac{|Q_1| Q_1}{g A_1^2} = h_{01} - h_b \tag{3.28}$$

$$M_2 \frac{\partial Q_2}{\partial t} + \chi_2 \frac{|Q_2| Q_2}{g A_2^2} = h_{02} - h_b \tag{3.29}$$

with

$$\chi_i = \frac{m_i R_i + 2 c_{f,i} L_i}{2 R_i} \tag{3.30}$$

and

$$M_i = \frac{L_i}{g A_i} \tag{3.31}$$

This set of equations can be solved with the harmonic method and the finite difference method.

3.2.2 Harmonic method

For the harmonic method Equations (3.28) and (3.29) need to be linearized in the same way as done for the single inlet system. Using Equation (3.8) it follows:

$$M_1 \frac{\partial Q_1}{\partial t} + W_1 Q_1 = h_{01} - h_b \tag{3.32}$$

$$M_2 \frac{\partial Q_2}{\partial t} + W_2 Q_2 = h_{02} - h_b \tag{3.33}$$

with

$$W_i = \frac{8}{3\pi} \chi_i \frac{\hat{Q}_i}{g A_i^2} \tag{3.34}$$

For the solution to the set of Equations (3.27), (3.32) and (3.33) reference is made to BORSJE [2003] appendix A. The solutions are of the form:

$$Q_1(t) = \hat{Q}_1 \cos(\omega t + \zeta) \tag{3.35}$$

$$Q_2(t) = \hat{Q}_2 \cos(\omega t + \theta) \tag{3.36}$$

$$h_b(t) = \hat{h}_b \cos(\omega t + \alpha) \tag{3.37}$$

In the following the expressions for the amplitudes and phases of Q_1, Q_2 and h_b are presented.

$$\hat{Q}_1 = \sqrt{\frac{C^2 + D^2}{A^2 + B^2}} \tag{3.38}$$

$$\tan\zeta = \frac{AD - BC}{AC + BD} \tag{3.39}$$

$$\hat{Q}_2 = \sqrt{\frac{E^2 + F^2}{A^2 + B^2}} \tag{3.40}$$

$$\tan\theta = \frac{AF - BE}{AE + BF} \tag{3.41}$$

$$\hat{h}_b = \sqrt{\frac{G^2 + H^2}{A^2 + B^2}} \tag{3.42}$$

$$\tan\alpha = \frac{AH - BG}{AG + BH} \tag{3.43}$$

with

$$
\begin{aligned}
A &= W_1\left(1-A_bM_2\omega^2\right)+W_2\left(1-A_bM_1\omega^2\right)\\
B &= \omega\left(M_1+M_2+A_b\left(W_1W_2-M_1M_2\omega^2\right)\right)\\
C &= \hat{h}_{01}\cos\psi\left(1-A_bM_2\omega^2\right)-\hat{h}_{01}\sin\psi\left(A_bW_2\omega\right)-\hat{h}_{02}\cos\varphi\\
D &= \hat{h}_{01}\cos\psi\left(A_bW_2\omega\right)+\hat{h}_{01}\sin\psi\left(1-A_bM_2\omega^2\right)-\hat{h}_{02}\sin\varphi\\
E &= \hat{h}_{02}\cos\varphi\left(1-A_bM_1\omega^2\right)-\hat{h}_{02}\sin\varphi\left(A_bW_1\omega\right)-\hat{h}_{01}\cos\psi\\
F &= \hat{h}_{02}\cos\varphi\left(A_bW_1\omega\right)+\hat{h}_{02}\sin\varphi\left(1-A_bM_1\omega^2\right)-\hat{h}_{01}\sin\psi\\
G &= \hat{h}_{01}\left(W_2\cos\psi-M_2\omega\sin\psi\right)+\hat{h}_{02}\left(W_1\cos\varphi-M_1\omega\sin\varphi\right)\\
H &= \hat{h}_{01}\left(W_2\sin\psi+M_2\omega\cos\psi\right)+\hat{h}_{02}\left(W_1\sin\varphi+M_1\omega\cos\varphi\right)
\end{aligned}
\tag{3.44}
$$

The parameters W_1 and W_2 contain the as yet unknown value of Q_1 and Q_2. The computations start by assuming values of Q_1 and Q_2 and substituting those in W_1 and W_2. New values of Q_1 and Q_2 are then calculated until the solution converges.

3.2.3 Finite difference method

The finite difference method solves the set of equations introduced in section 3.2.1 numerically. To that end the continuity equation (Eq. (3.27) and the equations of motion (Eqs. (3.28) and (3.29)) need to be discretized:

$$M_1\frac{Q_1^{(i+1)}-Q_1^{(i)}}{\Delta t}+K_1^{(i)}Q_1^{(i+1)}=h_{01}^{(i+1)}-h_b^{(i+1)} \tag{3.45}$$

$$M_2\frac{Q_2^{(i+1)}-Q_2^{(i)}}{\Delta t}+K_2^{(i)}Q_2^{(i+1)}=h_{02}^{(i+1)}-h_b^{(i+1)} \tag{3.46}$$

$$Q_1^{(i+1)}+Q_2^{(i+1)}=A_b\frac{h_b^{(i+1)}-h_b^{(i)}}{\Delta t} \tag{3.47}$$

with

$$K^{(i)}=\chi_i\frac{|Q_i|}{gA_i^2} \tag{3.48}$$

Here, the superscript refers to the time step. Rewriting Equations (3.45), (3.46) and (3.47), by placing the unknown variables $Q^{(i+1)}$ and $h_b^{(i+1)}$ at the left-hand side and the known variables $Q^{(i)}$, $h_b^{(i)}$ and $h_0^{(i+1)}$ on the right-hand side and writing this in matrix notation, results in the following expression:

$$\begin{pmatrix} \frac{M_1}{\Delta t} + K_1^{(i)} & 0 & 1 \\ 0 & \frac{M_2}{\Delta t} + K_2^{(i)} & 1 \\ 1 & 1 & -\frac{A_b}{\Delta t} \end{pmatrix} \begin{pmatrix} Q_1^{(i+1)} \\ Q_2^{(i+1)} \\ h_b^{(i+1)} \end{pmatrix} = \begin{pmatrix} h_{01}^{(i+1)} + Q_1^{(i)} \frac{M_1}{\Delta t} \\ h_{02}^{(i+1)} + Q_2^{(i)} \frac{M_2}{\Delta t} \\ -h_b^{(i)} \frac{A_b}{\Delta t} \end{pmatrix} \tag{3.49}$$

This equation is solved using MATLAB. The solution is a time series for Q and h_b. For the stability analysis we are interested in the amplitude of the first harmonic $\hat{Q}\cos(\omega t + \alpha)$ of the discharge. $\hat{Q}$ and α are obtained by a least square method (see appendix B).

3.2.4 Results

For the specific case where the tides of both inlets are the same, water levels and velocities calculated with the harmonic and finite difference method are presented in Figure 12. Both models yield practically the same results. The parameter values used in the calculations are presented in Table 4.

Table 4: Parameter values double inlet system

Parameter	Value	Parameter	Value
$c_{f,1} = c_{f,2}$	0.004 [-]	$\hat{h}_{01} = \hat{h}_{02}$	0.75 [m]
$\beta_1 = \beta_2$	π/180 [rad]	$\varphi = \psi$	0 [rad]
m	1 [-]	g	9.81 [m/s^2]
$L_1 = L_2$	5,000 [m]	ω	$1.41 \cdot 10^{-4}$ [s^{-1}]
$A_1 = A_2$	25,000 [m^2]	T	44,712 [s]
A_b	$14 \cdot 10^8$ [m^2]	Δt	36 [s]

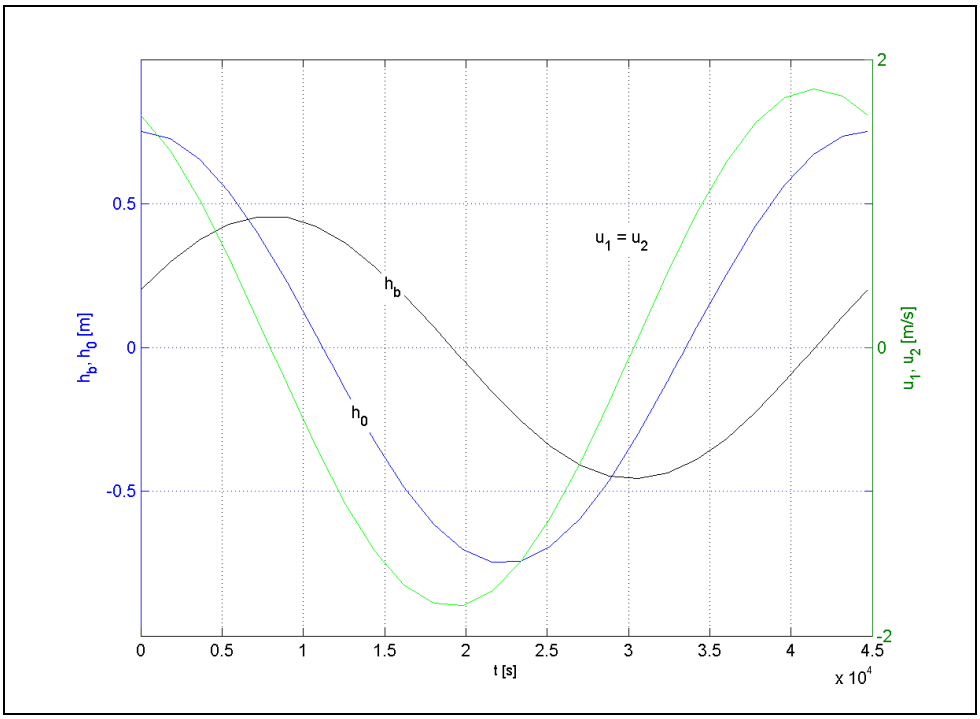

Figure 12: Water motion for a double inlet system

With $M_1 = M_2$, $\chi_1 = \chi_2$ and $h_{01} = h_{02}$, $Q_1 = Q_2$. Therefore using Equation (3.27), the basin level reaches a maximum or a minimum when $Q_1 = Q_2 = 0$ and thus $u_1 = u_2 = 0$. Furthermore, when the velocities are zero and neglecting $\frac{du}{dt}$ in the Equations of motion (3.28) and (3.29), it follows that the water level in the basin intersects the water level outside at its maximum or its minimum (see also Section 3.1.3).

Note that because the basin surface area of the double inlet system is twice the size of the basin surface area of the single inlet system and the ocean tides for both systems are the same, Figure 10 and Figure 12 are the same.

3.3 Double inlet system with partition

To calculate the velocities in the inlets in the presence of a topographic high a partition with opening is introduced. This will result in the two basins having different fluctuating water levels. Figure 13 shows the schematization of the double inlet system with partition and opening.

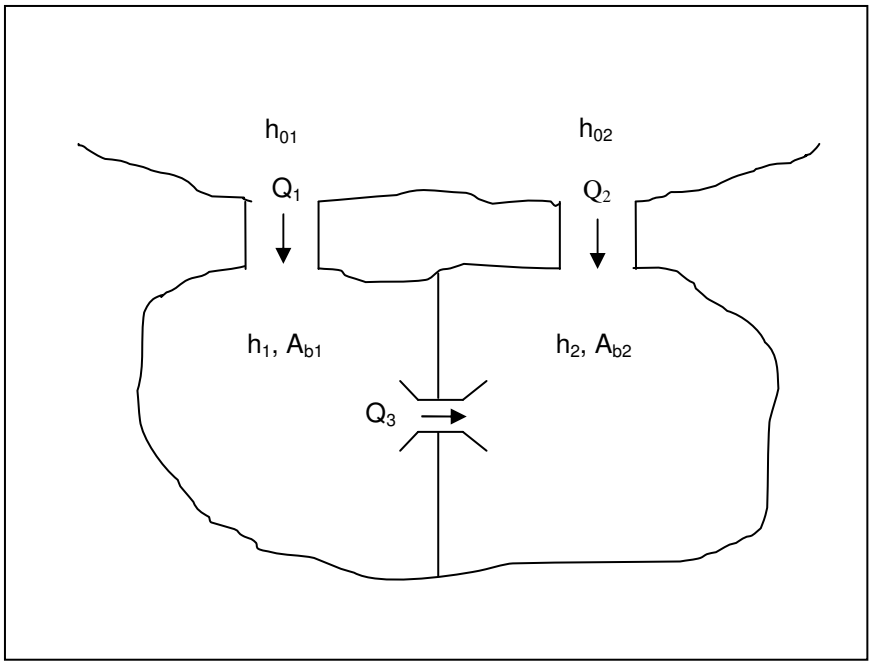

Figure 13: Schematization of a double inlet system with partition

The expressions for the tidal forcing of the system are given by Equations (3.25) and (3.26).

3.3.1 Hydrodynamic equations

The continuity equations for respectively basin 1 and basin 2 are:

$$Q_1 - Q_3 = A_{b1}\frac{\partial h_1}{\partial t} \tag{3.50}$$

$$Q_2 + Q_3 = A_{b2}\frac{\partial h_2}{\partial t} \tag{3.51}$$

The equation of motion for each inlet are:

$$M_1\frac{\partial Q_1}{\partial t} + \chi_1\frac{|Q_1|Q_1}{gA_1^2} = h_{01} - h_1 \tag{3.52}$$

$$M_2\frac{\partial Q_2}{\partial t} + \chi_2\frac{|Q_2|Q_2}{gA_2^2} = h_{02} - h_2 \tag{3.53}$$

$$M_3\frac{\partial Q_3}{\partial t} + \chi_3\frac{|Q_3|Q_3}{gA_3^2} = h_1 - h_2 \tag{3.54}$$

with

$$\chi_i = \frac{m_i R_i + 2c_{f,i} L_i}{2R_i} \tag{3.55}$$

and

$$M_i = \frac{L_i}{gA_i} \tag{3.56}$$

Initial calculations using the harmonic method showed that this method for the double inlet with partition not always converged. Therefore, only the finite difference method will be applied to this problem.

3.3.2 Finite difference method

For the double inlet system with partition a finite difference method avoids the iteration that caused problems with the harmonic method. The selected finite difference form of the equations is:

$$Q_1^{(i+1)} \left(\frac{M_1}{\Delta t} + K_1^{(i)} \right) + h_1^{(i+1)} = h_{01}^{(i+1)} + Q_1^{(i)} \frac{M_1}{\Delta t} \tag{3.57}$$

$$Q_2^{(i+1)} \left(\frac{M_2}{\Delta t} + K_2^{(i)} \right) + h_2^{(i+1)} = h_{02}^{(i+1)} + Q_2^{(i)} \frac{M_2}{\Delta t} \tag{3.58}$$

$$Q_3^{(i+1)} \left(\frac{M_3}{\Delta t} + K_3^{(i)} \right) - h_1^{(i+1)} + h_2^{(i+1)} = Q_3^{(i)} \frac{M_3}{\Delta t} \tag{3.59}$$

$$-Q_1^{(i+1)} + Q_3^{(i+1)} + h_1^{(i+1)} \frac{A_{b1}}{\Delta t} = h_1^{(i)} \frac{A_{b1}}{\Delta t} \tag{3.60}$$

$$-Q_2^{(i+1)} - Q_3^{(i+1)} + h_2^{(i+1)} \frac{A_{b2}}{\Delta t} = h_2^{(i)} \frac{A_{b2}}{\Delta t} \tag{3.61}$$

In matrix form this set of equations transforms into:

$$\begin{pmatrix} \frac{M_1}{\Delta t}+K_1^{(i)} & 0 & 0 & 1 & 0 \\ 0 & \frac{M_2}{\Delta t}+K_2^{(i)} & 0 & 0 & 1 \\ 0 & 0 & \frac{M_3}{\Delta t}+K_3^{(i)} & -1 & 1 \\ -1 & 0 & 1 & \frac{A_{b1}}{\Delta t} & 0 \\ 0 & -1 & -1 & 0 & \frac{A_{b2}}{\Delta t} \end{pmatrix} \begin{pmatrix} Q_1^{(i+1)} \\ Q_2^{(i+1)} \\ Q_3^{(i+1)} \\ h_1^{(i+1)} \\ h_2^{(i+1)} \end{pmatrix} = \begin{pmatrix} h_{01}^{(i+1)}+Q_1^{(i)}\frac{M_1}{\Delta t} \\ h_{02}^{(i+1)}+Q_2^{(i)}\frac{M_2}{\Delta t} \\ Q_3^{(i)}\frac{M_3}{\Delta t} \\ h_1^{(i)}\frac{A_{b1}}{\Delta t} \\ h_2^{(i)}\frac{A_{b2}}{\Delta t} \end{pmatrix} \qquad (3.62)$$

To obtain the amplitudes and phases of the five unknown the least square method is used (see appendix B).

3.3.3 Results

Water levels and velocities calculated with the finite difference method are presented in Figure 14. The parameter values used in the calculation are presented in Table 5.

Table 5: Parameter values double inlet system with partition

Parameter	Value	Parameter	Value
$c_{f,1} = c_{f,2} = c_{f,3}$	0.004 [-]	$\hat{h}_{01} = \hat{h}_{02}$	0.75 [m]
m	1 [-]	$\beta_1 = \beta_2 = \beta_3$	π/180 [rad]
$L_1 = L_2$	5,000 [m]	φ = ψ	0 [rad]
L_3	1,000 [m]	g	9.81 [m/s^2]
$A_{b,1} = A_{b,2}$	7·10^8 [m^2]	ω	1.41·10^{-4} [s^{-1}]
$A_1 = A_2$	25,000 [m^2]	T	44,712 [s]
A_3	10,000 [m^2]	Δt	36 [s]

The water motion of the double inlet system with partition is shown in Figure 14. Because of symmetry $u_3 = 0$, $u_1 = u_2$ and $h_{b1} = h_{b2}$. Ocean and basin water levels approximately intersect at the maximum of the basin water level; they would intersect at the maximum if $\frac{du}{dt}$ were zero. In agreement with continuity, velocities are zero when the basin tide is maximum. Because the two basin surface areas are the same and together equal to the basin surface area of the double inlet system Figure 12 and Figure 14 are the same.

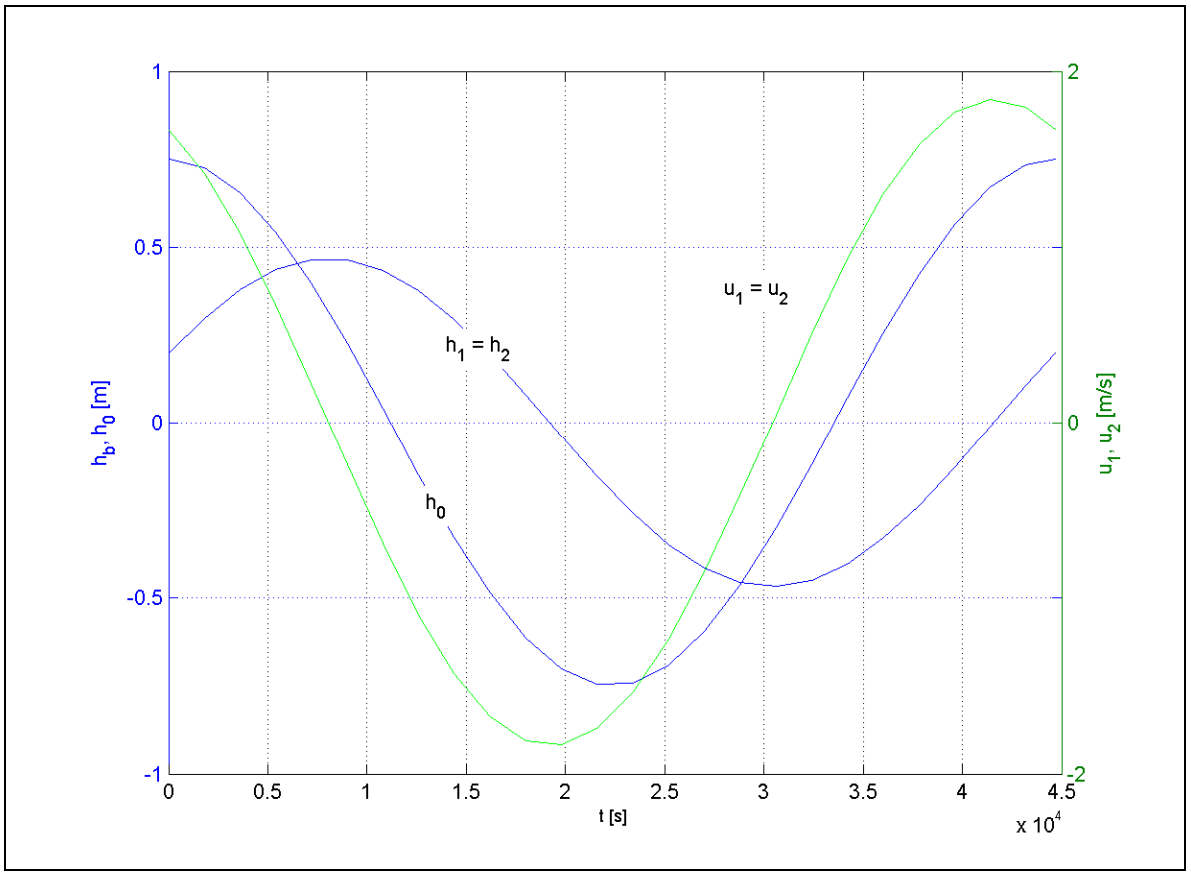

Figure 14: Water motion for a double inlet system with partition; $u_3 = 0$

4. Stability of a double inlet system

4.1 Introduction

In Chapter 3 two different kinds of double inlet systems were introduced, a double inlet system without partition and a double inlet system with partition and opening. In this chapter the stability of a double inlet system without partition will be discussed in more detail.

An inlet is called stable when after a small change, due to a perturbation, the cross-sectional area unconditionally returns to its equilibrium value. In previous studies the stability of double inlet systems has been evaluated using equilibrium flow curves. In Section 2.3.1 the equilibrium flow curve for inlet 1 was introduced as the locus of the values (A_1, A_2) for which $\hat{u}_1 = \hat{u}_{E1}$. Similarly, the equilibrium flow curve for inlet 2 is the locus of the values (A_1, A_2) for which $\hat{u}_2 = \hat{u}_{E2}$. Examples of the general shape of the equilibrium flow curves and their relative position in the [A_1, A_2] plane are presented in Figure 15 [VAN DE KREEKE, 1990]. Figure 15a shows an example where there are four sets of [A_1, A_2] for which both inlets have cross-sectional areas that are in equilibrium with the tidal conditions. Figure 15b, c and d show examples with only two sets of equilibrium cross-sectional areas. The bold parts of the equilibrium flow curves in Figure 15 represent stable equilibrium cross-sectional areas; i.e., referring to the equilibrium flow curve for inlet 1, for a given value of A_2 the corresponding value of A_1 on the bold part of the curve represents a stable equilibrium value of A_1. It follows that a condition for the simultaneous existence of stable equilibrium cross-sectional areas for two inlets is that the bold parts of the equilibrium flow curves intersect. This only occurs for figures Figure 15a and b. VAN DE KREEKE [1990] investigated the stability of multiple inlets and stated that for a double inlet system with a uniformly fluctuating water level in the basin only the configuration of the equilibrium flow curves with four sets of equilibrium cross-sectional areas allows an unconditionally stable set of cross-sections. To justify his statement he used a lumped-parameter model with linearized friction and neglected inertia. In Section 3.1.3 it is shown that in the equation of motion (3.3) this acceleration term is indeed small compared to the other two terms, but cannot be neglected. In the following the double inlet system is further analysed for stability using the dynamic equations including inertia and non-linear friction.

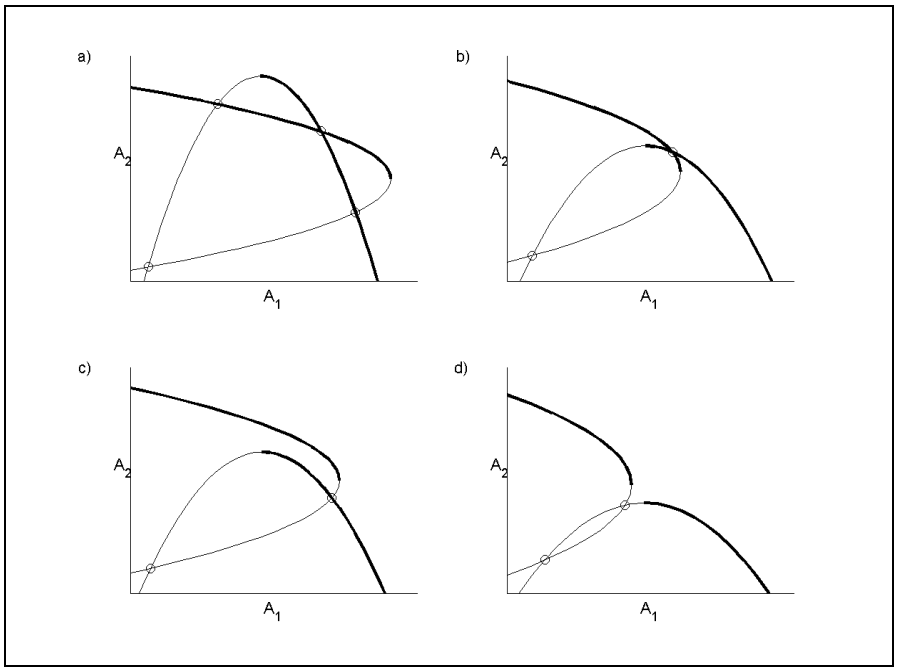

Figure 15: Examples of the general shape of the equilibrium flow curves (VAN DE KREEKE, 1990)

4.2 Stability analysis

In analyzing the stability of a double inlet system without partition use is made of the flow diagrams including the equilibrium flow curves introduced in Chapter 2. These diagrams show the number of intersections between the equilibrium flow curves and whether they are stable or unstable. We are interested in whether a double inlet system can be unconditionally stable. To answer this question, five cases are discussed. First the flow diagrams for each case are analyzed in a qualitative manner. After analyzing the flow diagrams a discussion on the stability of the double inlet system is presented. Particular attention is given to the influence of the inlet lengths on the stability of a double inlet system. With this in mind the values for the channel lengths L_1 and L_2 are taken as variables in the five cases. The channel length L_1 is 5,000 m and the channel length L_2 is varied between 1,000 m and 5,000 m. Other relevant inlet dimensions and flow related properties are the same for the five cases. Values are typical for the western Wadden Sea (see Table 6).

Table 6: Parameter values double inlet system

Parameter	Value	Parameter	Value
$c_{f,1} = c_{f,2}$	0.004 [-]	$\beta_1 = \beta_2$	$\pi/180$ [rad]
m	1 [-]	$\varphi = \psi$	0 [rad]
$\hat{h}_{01} = \hat{h}_{02}$	0.75 [m]	g	9.81 [m/s^2]
A_b	$14 \cdot 10^8$ [m^2]	ω	$1.41 \cdot 10^{-4}$ [s^{-1}]
Δt	36 [s]	T	44,712 [s]

Case I: $L_1 = L_2 = 5{,}000$ m

The first case is a symmetric situation, where $L_1 = L_2 = 5{,}000$ m. The flow diagram (Figure 16a) yields two combinations of equilibrium cross-sectional areas ($A_{1,E1}$, $A_{2,E1}$) and ($A_{1,E2}$, $A_{2,E2}$). From this figure it can be seen that the first combination of equilibrium cross-sectional areas ($A_{1,E1}$, $A_{2,E1}$) is unstable. The second combination ($A_{1,E2}$, $A_{2,E2}$) is more critical. The flow diagram in the vicinity of this point is presented in Figure 16b. In this figure the streamlines (black) and vectors (grey) show that this point is not unconditionally stable i.e. only in case of a deviation from equilibrium for which $A_1 = A_2$ could the cross-sectional areas return to the position ($A_{1,E2}$, $A_{2,E2}$).

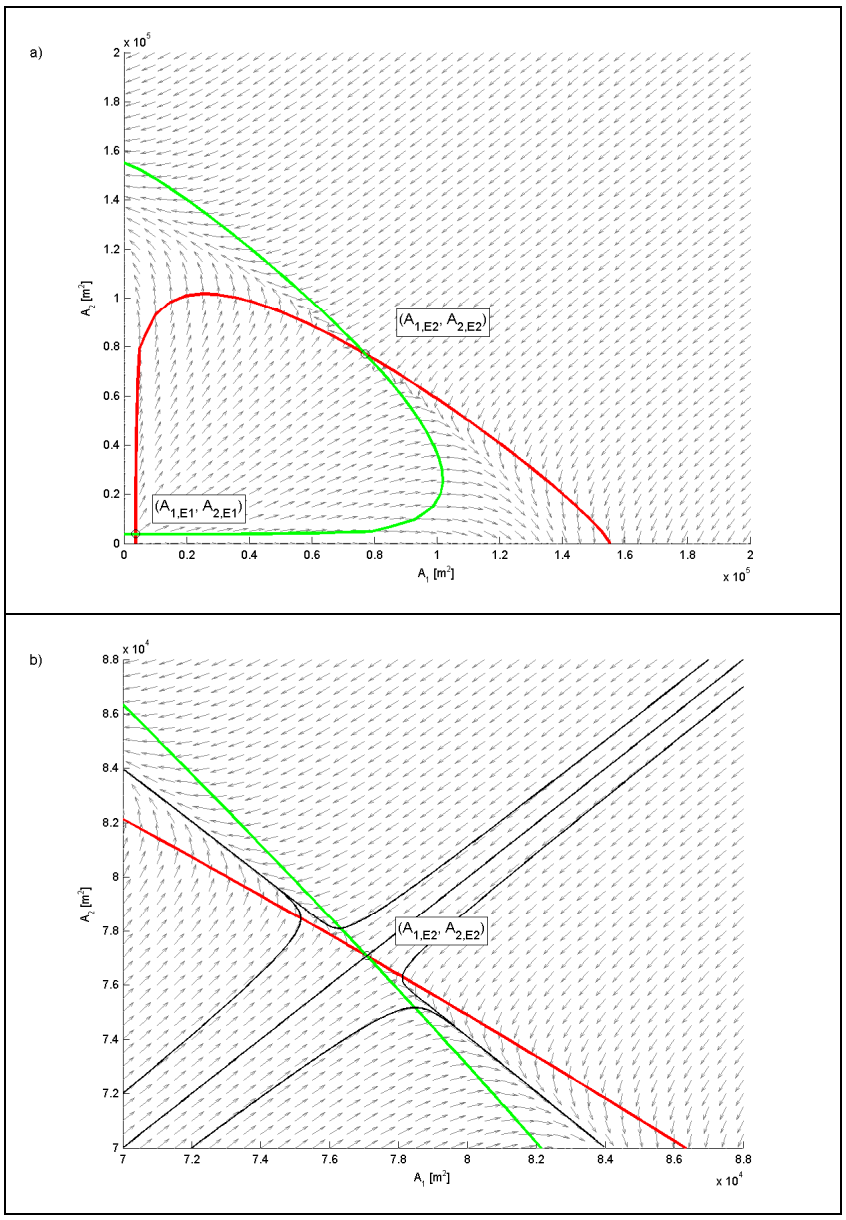

Figure 16: a) Flow diagram and equilibrium flow curves (red for inlet 1 and green for inlet 2) for a double inlet system with $L_1 = L_2 = 5{,}000$ m and b) Close-up equilibrium ($A_{1,E2}$, $A_{2,E2}$)

Case II: L_1 = 5,000 m and L_2 = 4,000 m

In the second case the length of the second channel is smaller than the length of the first channel. Again, the flow diagram (Figure 17a) yields two combinations of equilibrium cross-sectional areas ($A_{1,E1}$, $A_{2,E1}$) and ($A_{1,E2}$, $A_{2,E2}$). The figure shows that by reducing the length of the second channel the second equilibrium ($A_{1,E2}$, $A_{2,E2}$) shifts down and to the right. Figure 17b shows the flow diagram in the vicinity of the second equilibrium. The streamlines (black) and vectors (grey) show that this equilibrium is not unconditionally stable.

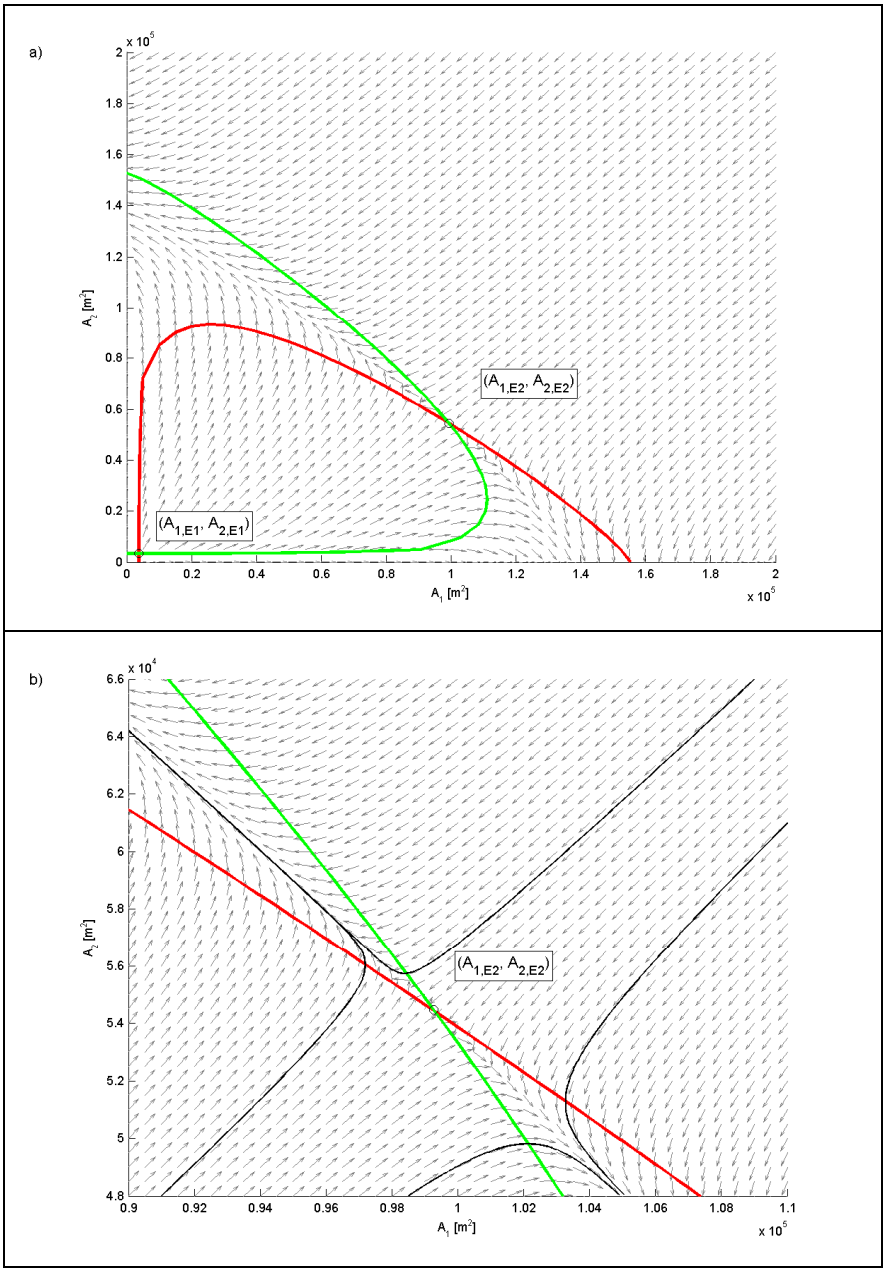

Figure 17: a) Flow diagram and equilibrium flow curves (red for inlet 1 and green for inlet 2) for a double inlet system with L_1 = 5,000 m and L_2 = 4,000 m and b) Close-up equilibrium ($A_{1,E2}$, $A_{2,E2}$)

Case III: L_1 = 5,000 m and L_2 = 3,000 m

In case III the length of the second channel is reduced to 3,000 m. The second equilibrium ($A_{1,E2}$, $A_{2,E2}$) shifts even more down and to the right (Figure 18a). The equilibrium flow curves (red for inlet 1 and green for inlet 2) still intersect each other at the stable branch of the curves. The close-up of the second equilibrium ($A_{1,E2}$, $A_{2,E2}$), Figure 18b, shows that this equilibrium is not unconditionally stable.

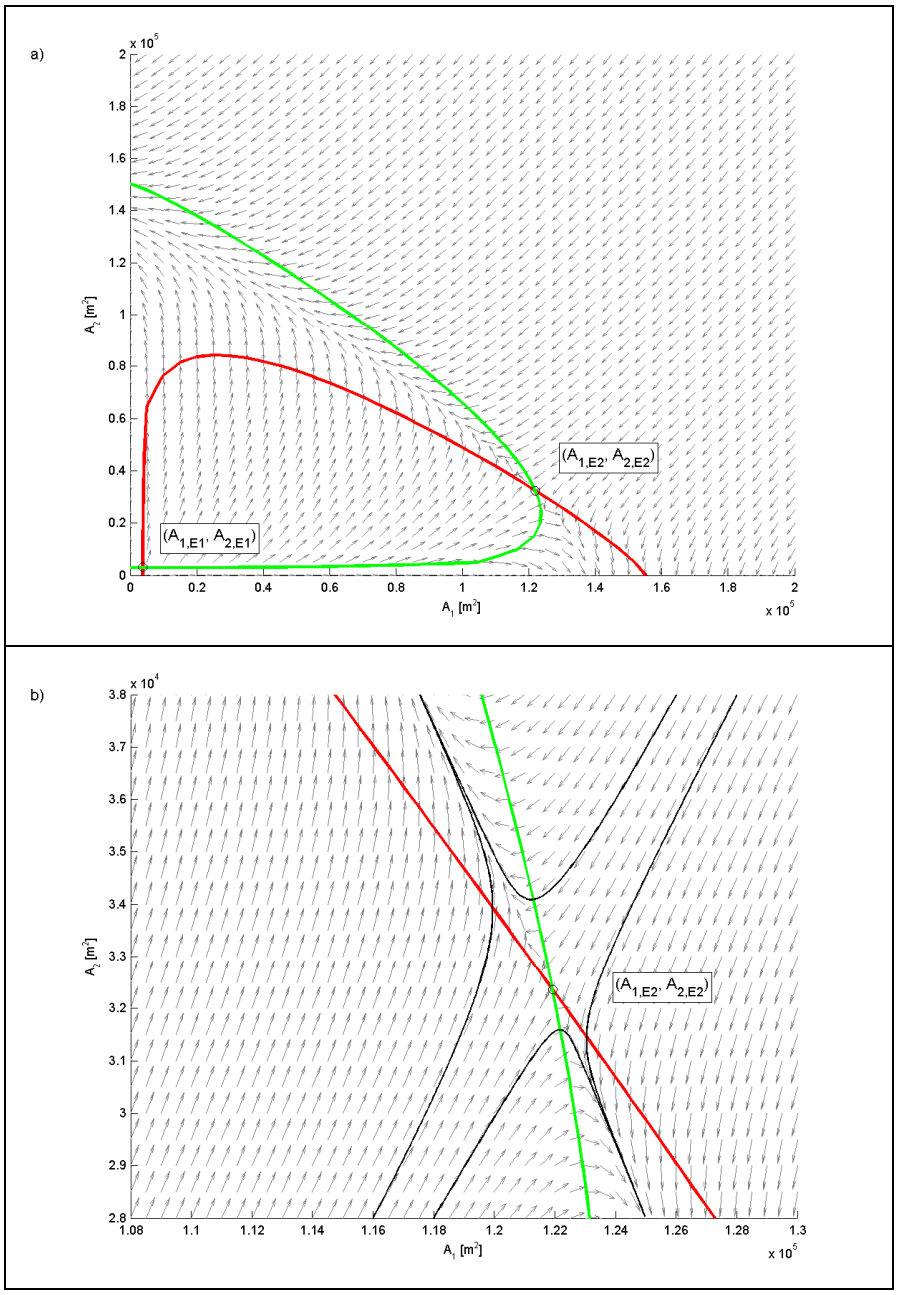

Figure 18: a) Flow diagram and equilibrium flow curves (red for inlet 1 and green for inlet 2) for a double inlet system with L_1 = 5,000 m and L_2 = 3,000 m and b) Close-up equilibrium ($A_{1,E2}$, $A_{2,E2}$)

Case IV: L_1 = 5,000 m and L_2 = 2,000 m

With the second channel length reduced to 2,000 m the equilibrium flow curves intersect each other for the first time at the unstable branch of the curves (Figure 19a). This suggests that the second equilibrium ($A_{1,E2}$, $A_{2,E2}$) is not unconditionally stable. The flow diagram in the vicinity of this point together with the streamlines (black) and vectors (grey), illustrated in Figure 19b, show that this is indeed the case.

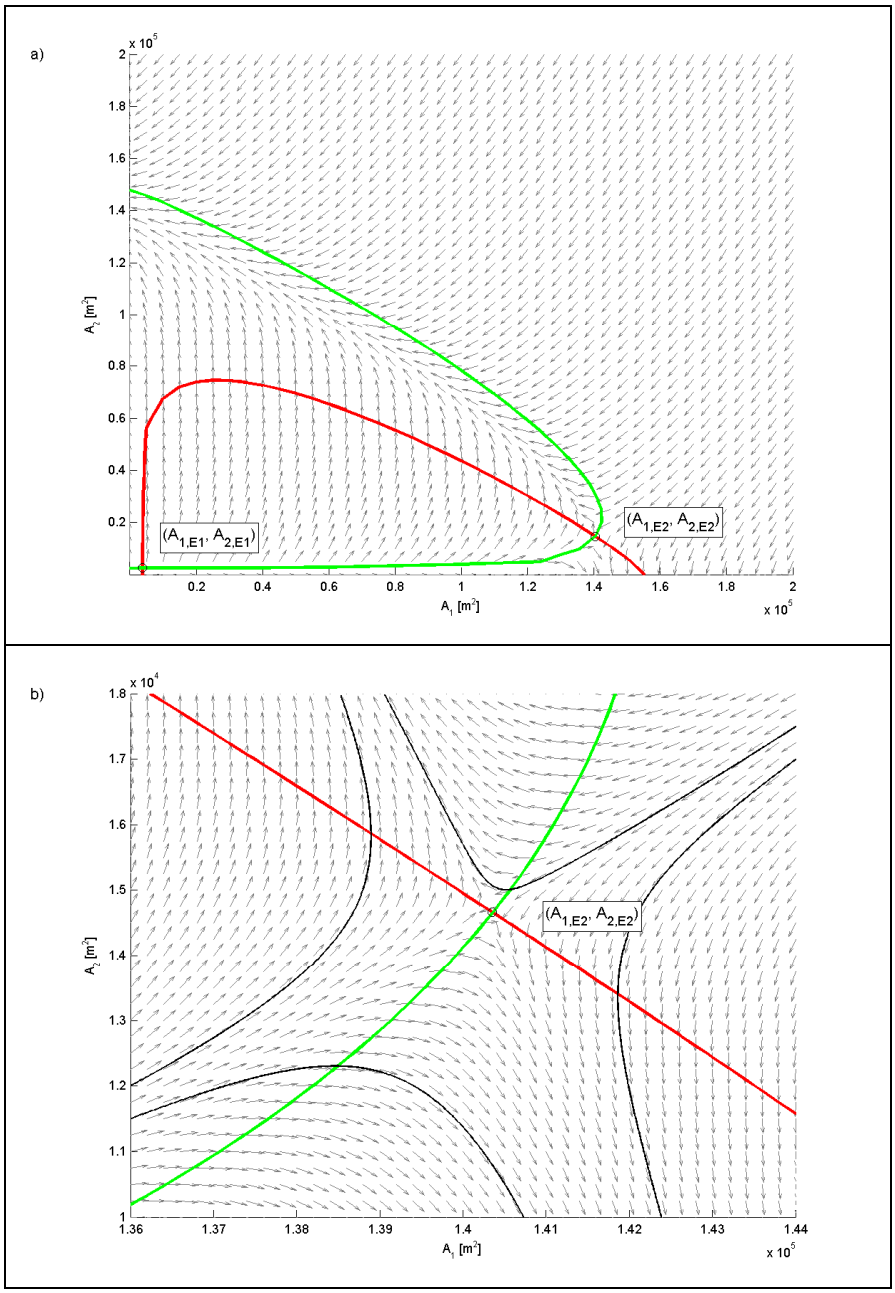

Figure 19: a) Flow diagram and equilibrium flow curves (red for inlet 1 and green for inlet 2) for a double inlet system with L_1 = 5,000 m and L_2 = 2,000 m and b) Close-up equilibrium ($A_{1,E2}$, $A_{2,E2}$)

Case V: L_1 = 5,000 m and L_2 = 1,000 m

In the last case the second channel length is 1,000 m. From the flow diagram in Figure 20a it follows that the second equilibrium has shifted along the unstable branch of the equilibrium flow curves. In the close-up of this equilibrium, Figure 20b, the streamlines are left out, because the vectors already show that this equilibrium is unstable.

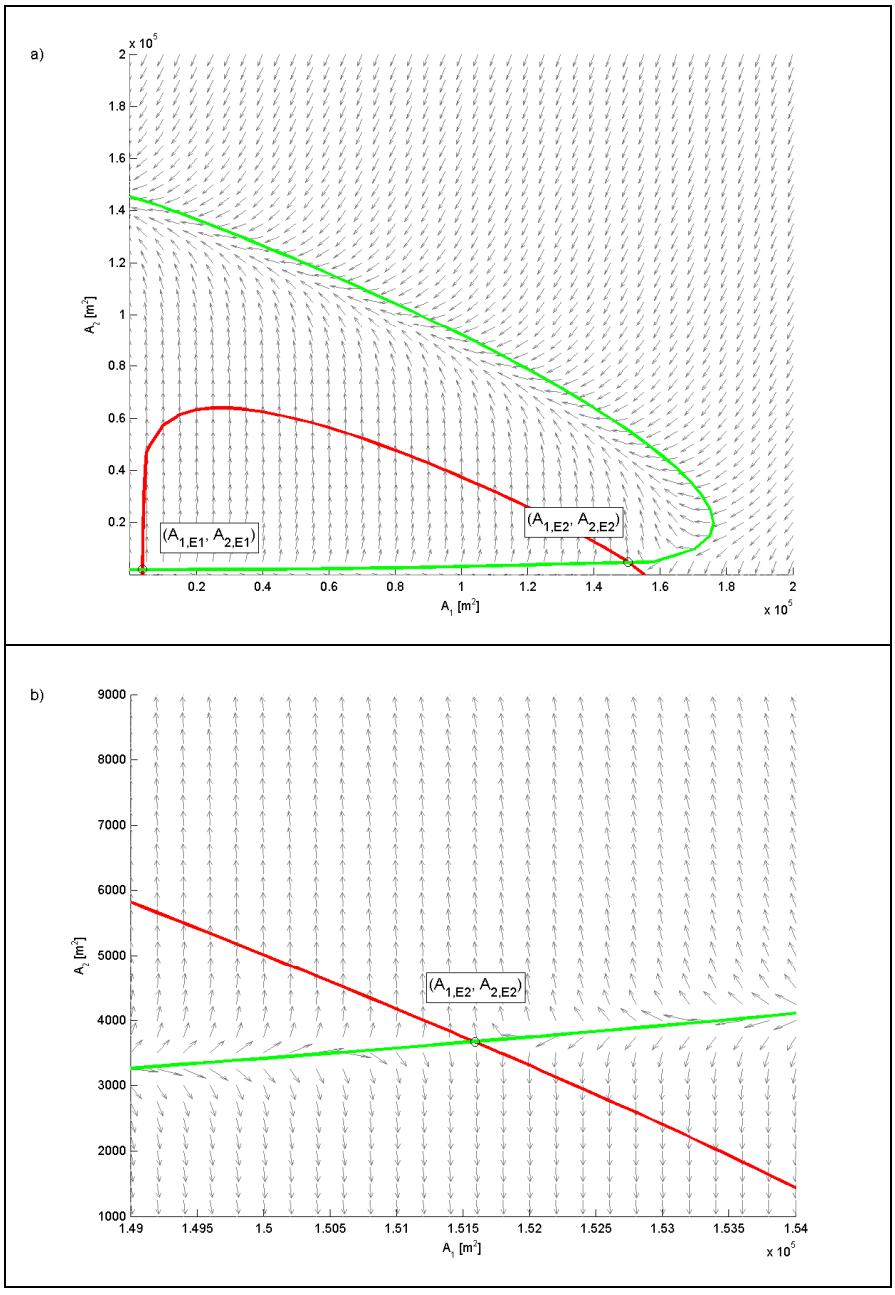

Figure 20: a) Flow diagram and equilibrium flow curves (red for inlet 1 and green for inlet 2) for a double inlet system with L_1 = 5,000 m and L_2 = 1,000 m and b) Close-up equilibrium ($A_{1,E2}$, $A_{2,E2}$)

4.3 Discussion

The five cases analyzed above show that any combination of the inlet lengths L_1 and L_2 leads to unstable equilibrium situations. Apparently, a double inlet system with a uniformly fluctuating basin water level can never be unconditionally stable. To be precise, a double inlet system with a uniformly fluctuating water level always leads to a situation where one of the two inlets closes while the other remains open, thus changing into a single inlet system. In the introduction of this chapter it was stated that in order for a double inlet system with a uniformly fluctuating water level to reach an unconditionally stable equilibrium four intersections between the equilibrium flow curves of the two inlets are needed (see Figure 15a). The cases discussed before generate only configurations with two intersections between the equilibrium flow curves and thus the system cannot be unconditionally stable. The conclusion drawn from the flow diagrams thus confirms the earlier conclusion by VAN DE KREEKE [1990] and BORSJE [2003].

The foregoing implies that when a single inlet system turns into a basin with two inlets, for instance due to breaching of a surrounding barrier during a storm, the newly developed double inlet system will return to a single inlet system. The present analysis is not conclusive with regards to whether ultimately the original inlet or the new inlet will remain open. However, a flow diagram, as presented in this study could provide some insight in this problem.

The apparent instability of a double inlet system seems to disagree with the existence of such inlet systems present in the Dutch Wadden Sea. However, a feature that sofar has not been accounted for in the stability analysis is that water levels in the Wadden Sea as a whole do not fluctuate uniformly. Rather inlets are connected to basins that are partly separated by topographic highs resulting in different water level variations on either side of the topographic high. To account for this effect a partition with opening is added to the model (see also Section 3.3). In the following chapter such a double inlet system with partition and opening between the two basins will be analyzed.

5. Stability of a double inlet system with partition

5.1 Introduction

In Chapter 4 the stability of a double inlet system with a uniformly fluctuating basin water level is discussed. Based on five cases and previous studies by VAN DE KREEKE [1990] and BORSJE [2003], the conclusion is that a double inlet system with a uniformly fluctuating water level always leads to a situation where one of the two inlets closes while the other remains open, thus changing into a single inlet system. However, observations in double inlet systems such as the Texel and Vlie basin in the western Wadden Sea show that some kind of equilibrium is present. These basins are separated from each other by a topographic high adapting its position according to the tidal wave entering the Texel and Vlie basins. A stronger propagating tidal wave in the Texel basin than in the Vlie basin will cause the topographic high to shift towards the Vlie basin and vice versa. The topographic high can be implemented in the model by means of an opening between the two basins (Figure 13). The opening having a finite length and cross-sectional area allows the model to simulate the propagating tidal wave. This configuration causes the basins to have separately fluctuating water levels. In the following sections the stability of a double inlet system with opening is investigated using the flow diagram introduced in Chapter 2. The objective is to see whether incorporating a topographic high between the two basins leads to an unconditionally stable equilibrium of the two inlets.

5.2 Stability analysis

For the stability analysis of a double inlet system with opening use is made of the flow diagrams previously discussed. In determining the stability of a double inlet system with partition and opening different approaches can be taken. In the present study emphasis is on the influence of the topographic high as simulated by the addition of a partition and opening. This is an important added feature in comparison with the double inlet system discussed in Chapter 4.

In the analysis the effect of the cross-sectional area of the opening and the location of the partition on the stability will be investigated. To investigate the effect of the cross-sectional area of the opening (A_3) seven cases are considered with gradually increasing value of A_3. To promote the pellucidness of the seven cases a symmetrical situation is used in which the two inlet lengths and two horizontal basin areas are the same. The effect of the location of the partition is investigated by means of four cases. Four different positions of the partition are considered resulting in four combinations of the areas of the sub-basins. In all four cases the total horizontal basin area is the same and taken equal to the basin area used in Chapter 4. Other relevant inlet parameters are taken in the range of the western Wadden Sea. Because the main interest in this chapter

is on the effect of the cross-sectional area of the opening and the position of the partition on the stability of the inlets, these parameters are taken the same for each case.

5.2.1 Effect of the cross-sectional area of the opening on the stability

In this section seven cases with different cross-sectional area of the opening are presented. Cross-sectional areas for which computations were carried out are 5,000, 10,000, 20,000, 30,000, 40,000, 50,000 and 100,000 m^2. Other relevant parameters are presented in Table 7.

Table 7: Parameter values double inlet system with partition

Parameter	Value	Parameter	Value
$c_{f,1} = c_{f,2} = c_{f,3}$	0.004 [-]	$\beta_1 = \beta_2 = \beta_3$	π/180 [rad]
m	1 [-]	$\varphi = \psi$	0 [rad]
$L_1 = L_2$	5,000 [m]	g	9.81 [m/s^2]
L_3	1,000 [m]	ω	$1.41 \cdot 10^{-4}$ [s^{-1}]
$A_{b,1} = A_{b,2}$	$7 \cdot 10^8$ [m^2]	Δt	36 [s]
$\hat{h}_{01} = \hat{h}_{02}$	0.75 [m]	T	44,712 [s]

Case I: A_3 = 5,000 m^2

The flow diagram (Figure 21a) yields four combinations of equilibrium cross-sectional areas ($A_{1,E1}$, $A_{2,E1}$), ($A_{1,E2}$, $A_{2,E2}$), ($A_{1,E3}$, $A_{2,E3}$) and ($A_{1,E4}$, $A_{2,E4}$). From this figure it can be seen that the first three combination of equilibrium cross-sectional areas ($A_{1,E1}$, $A_{2,E1}$), ($A_{1,E2}$, $A_{2,E2}$) and ($A_{1,E3}$, $A_{2,E3}$) are unstable, because the vectors (grey) are pointed away from these points. The fourth combination ($A_{1,E4}$, $A_{2,E4}$) represents an unconditionally stable equilibrium with $A_{1,E4} = A_{2,E4}$. The latter is to be expected, because of the symmetry of the problem. Figure 21b shows the close-up of this equilibrium. In this figure all vectors are directed towards this equilibrium and the streamlines (black) end in this equilibrium. In section 4.1 it was already outlined that only a configuration of the equilibrium flow curves with four sets of equilibrium cross-sectional areas allows an unconditionally stable set of cross-sections. This is true for Figure 21a. Water levels and velocities when the inlets are in stable equilibrium are those presented in Figure 14.

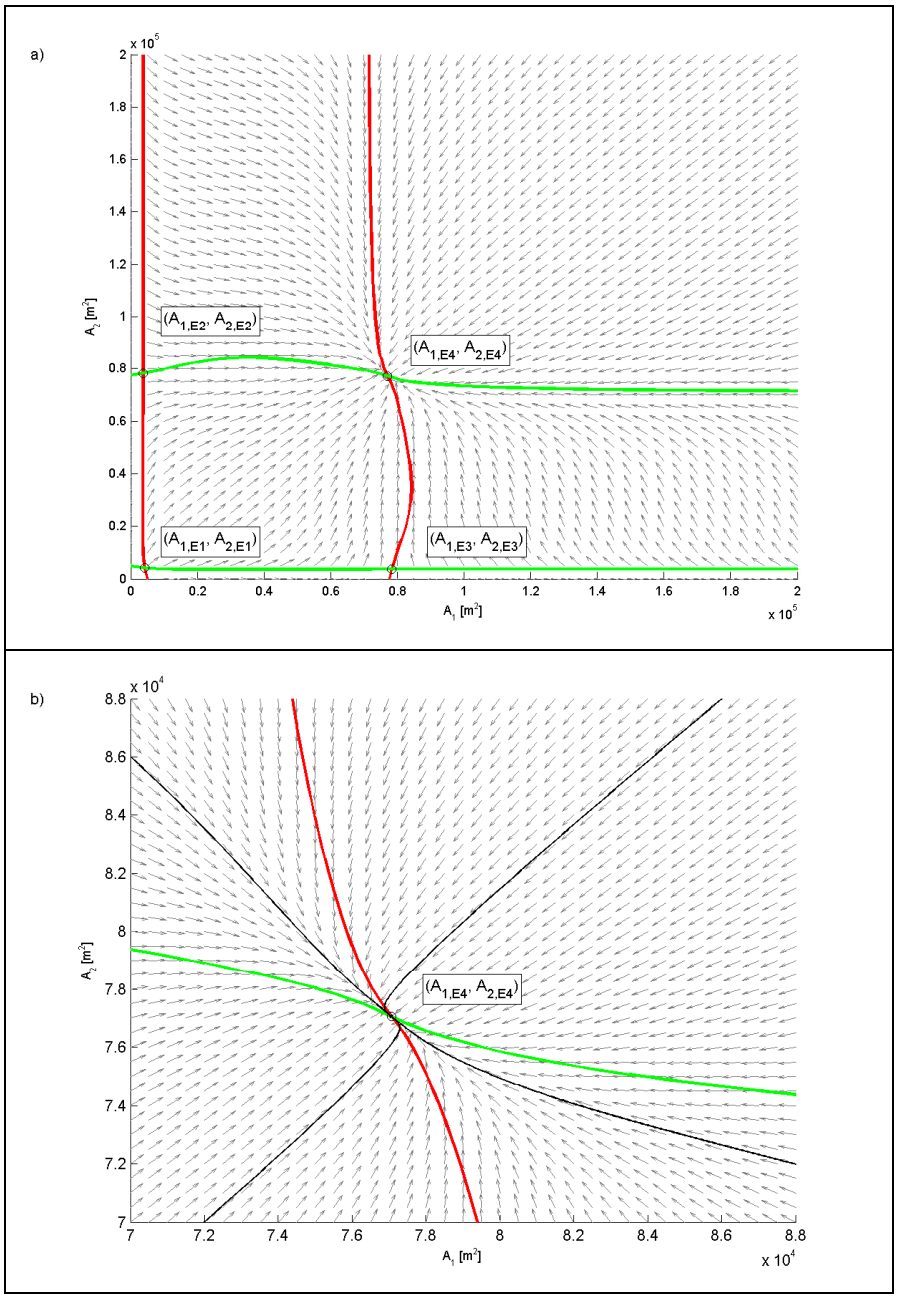

Figure 21: a) Flow diagram and equilibrium flow curves (red for inlet 1 and green for inlet 2) for a double inlet system with partition with A_3 = 5,000 m^2 and b) Close-up equilibrium ($A_{1,E4}$, $A_{2,E4}$)

Case II: A_3 = 10,000 m^2

The flow diagram (Figure 22a) shows four combinations of equilibrium cross-sectional areas, just like in Figure 21a. The fourth combination of equilibrium cross-sectional areas ($A_{1,E4}$, $A_{2,E4}$) represents an unconditionally stable equilibrium. A detailed flow diagram around this equilibrium is presented in Figure 22b. Water levels and velocities when the inlets are in stable equilibrium are those presented in Figure 14.

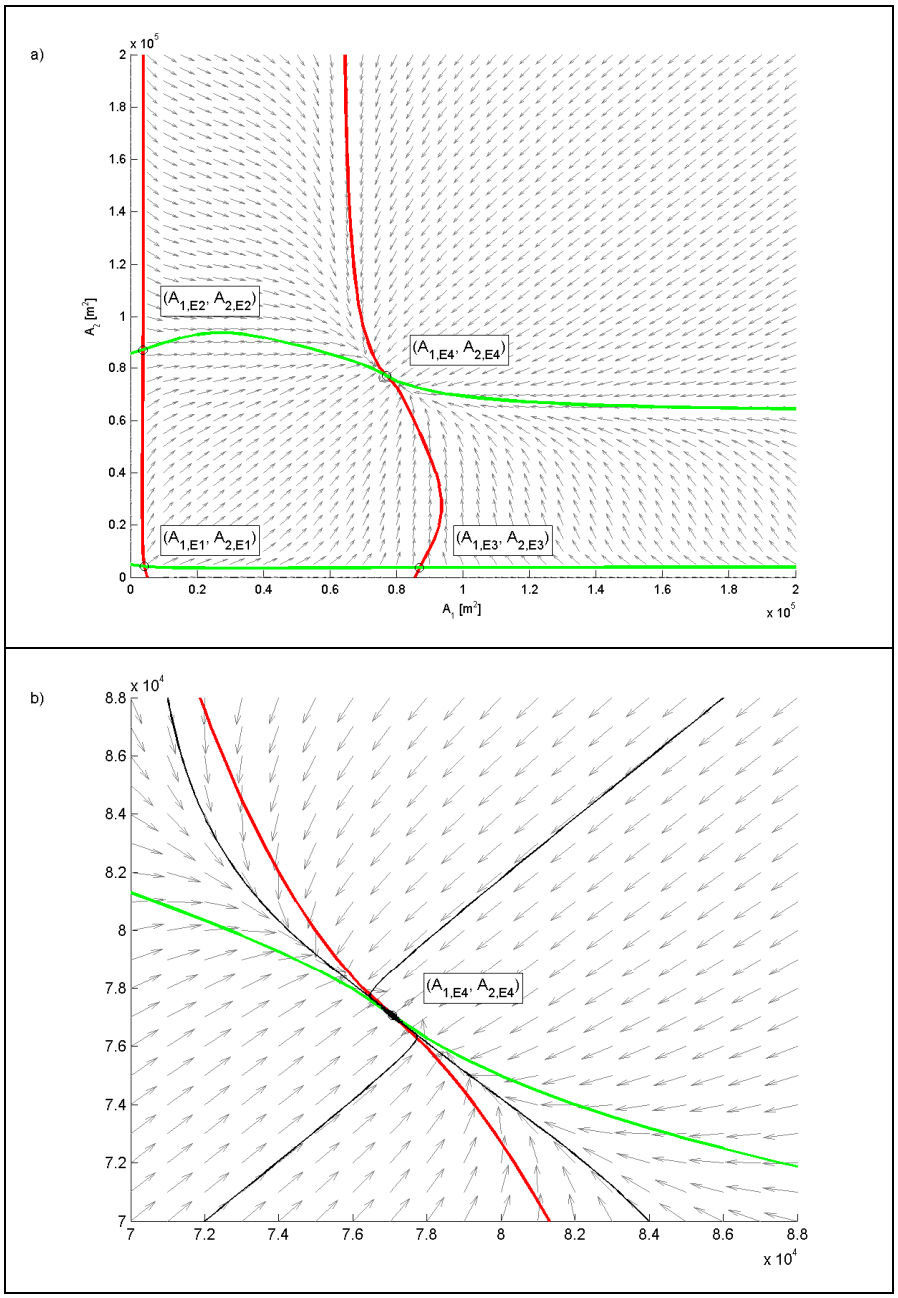

Figure 22: a) Flow diagram and equilibrium flow curves (red for inlet 1 and green for inlet 2) for a double inlet system with partition with A_3 = 10,000 m^2 and b) Close-up equilibrium ($A_{1,E4}$, $A_{2,E4}$)

Case III: $A_3 = 20{,}000\ m^2$

From the previous two flow diagrams it can be seen that enlarging of A_3 from 5,000 m^2 to 10,000 m^2 results in an increased interaction between the two basins. The equilibrium flow curves in Figure 22a and Figure 21a show a curvature between the second and fourth equilibrium and between the third and fourth equilibrium. Note that the fourth equilibrium is the same for A_3 = 5,000 m^2 and A_3 = 10,000 m^2. This curvature is more pronounced in Figure 22a than in Figure 21a meaning that the basins have more interaction.

The flow diagram for case III (Figure 23a) again shows an increased interaction between the basins. Instead of four, six combinations of equilibrium cross-sectional areas are found. The two extra combinations lie in the neighbourhood of the fourth equilibrium ($A_{1,E4}$, $A_{2,E4}$) and are each others mirror image. Figure 23b shows a close-up of this situation. Remarkable is that the fourth equilibrium is no longer stable. The fifth and sixth equilibriums are unconditionally stable; hence, a situation of multiple stable equilibriums. Contrary to the (fourth) stable equilibriums for A_3 = 5,000 m^2 and A_3 = 10,000 m^2, for the (fifth and sixth) stable equilibriums for A_3 = 20,000 m^2 the velocity in the opening is no longer zero.

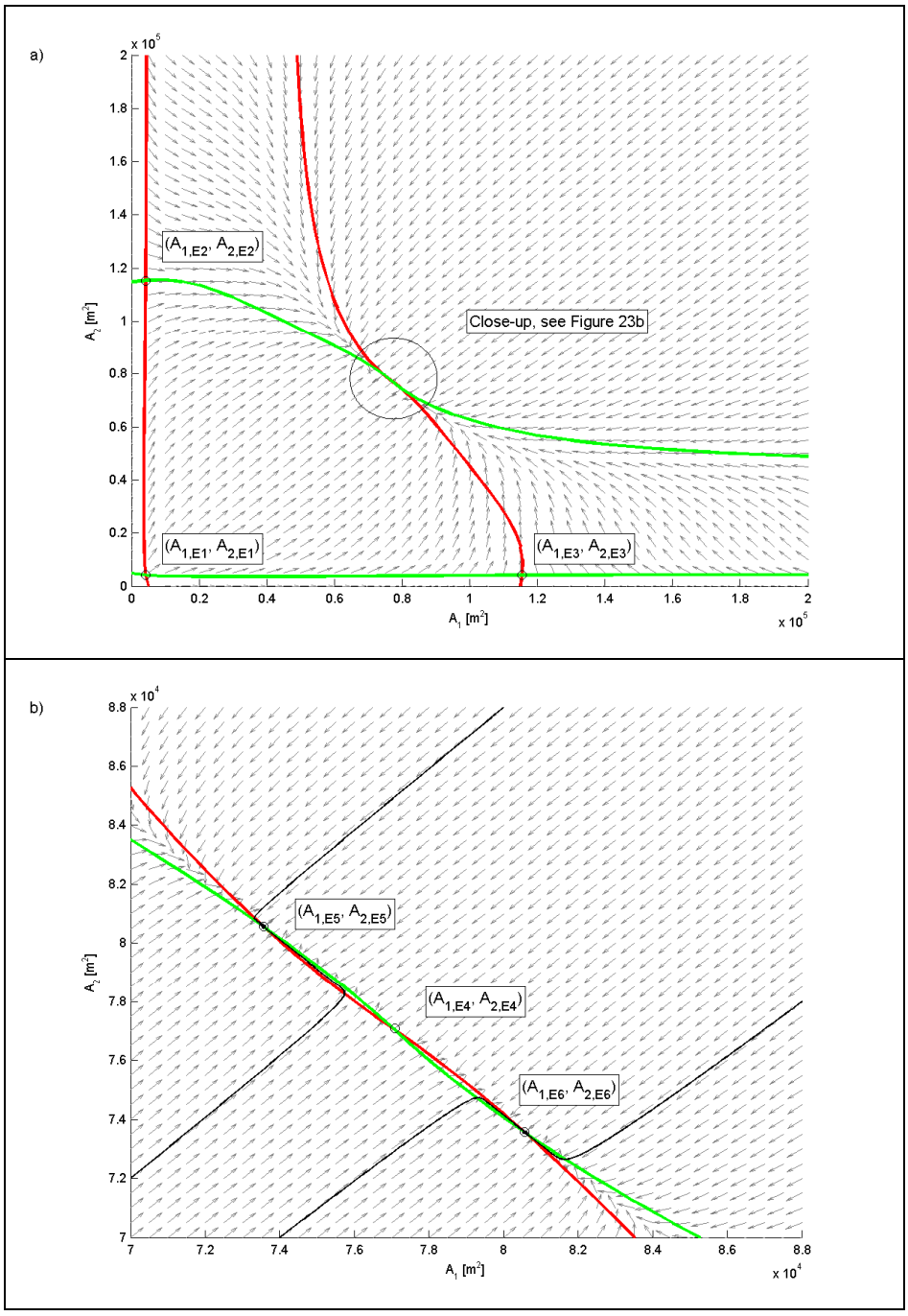

Figure 23: a) Flow diagram and equilibrium flow curves (red for inlet 1 and green for inlet 2) for a double inlet system with partition with A_3 = 20,000 m^2 and b) Close-up equilibriums ($A_{1,E4}$, $A_{2,E4}$), ($A_{1,E5}$, $A_{2,E5}$) and ($A_{1,E6}$, $A_{2,E6}$).

Case IV: A_3 = 30,000 m^2

This case shows the same features as case III with respect to the number of equilibriums. In the flow diagram there are six combinations of equilibrium cross-sectional areas with ($A_{1,E5}$, $A_{2,E5}$) and ($A_{1,E6}$, $A_{2,E6}$) being the stable equilibriums (Figure 24a). The interaction between the basins has increased even more and the distance between the fifth equilibrium ($A_{1,E5}$, $A_{2,E5}$) and sixth equilibrium ($A_{1,E6}$, $A_{2,E6}$) has also become larger (see Figure 24b).

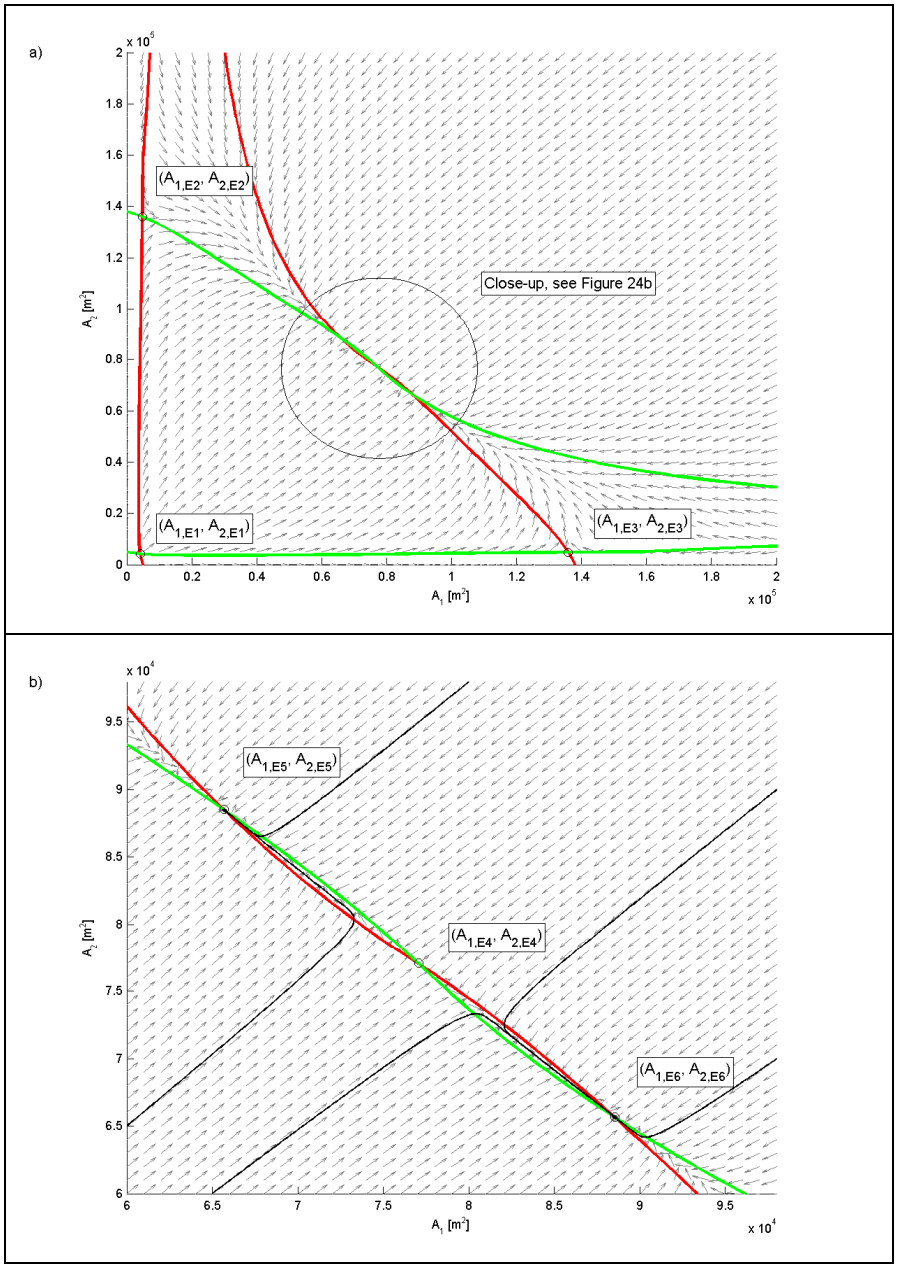

Figure 24: a) Flow diagram and equilibrium flow curves (red for inlet 1 and green for inlet 2) for a double inlet system with partition with A_3 = 30,000 m^2 and b) Close-up equilibriums ($A_{1,E4}$, $A_{2,E4}$), ($A_{1,E5}$, $A_{2,E5}$) and ($A_{1,E6}$, $A_{2,E6}$)

Case V: A_3 = 40,000 m^2

For case V the flow diagram again renders six combinations of equilibrium cross-sectional areas, where equilibrium ($A_{1,E4}$, $A_{2,E4}$) again is an unstable situation flanked by two unconditionally stable equilibriums ($A_{1,E5}$, $A_{2,E5}$) and ($A_{1,E6}$, $A_{2,E6}$) (Figure 25a and b). Equilibriums 5 and 6 are each others mirror image. The interaction between the two basins has increased again and the distance between equilibrium 5 and 6 has become larger.

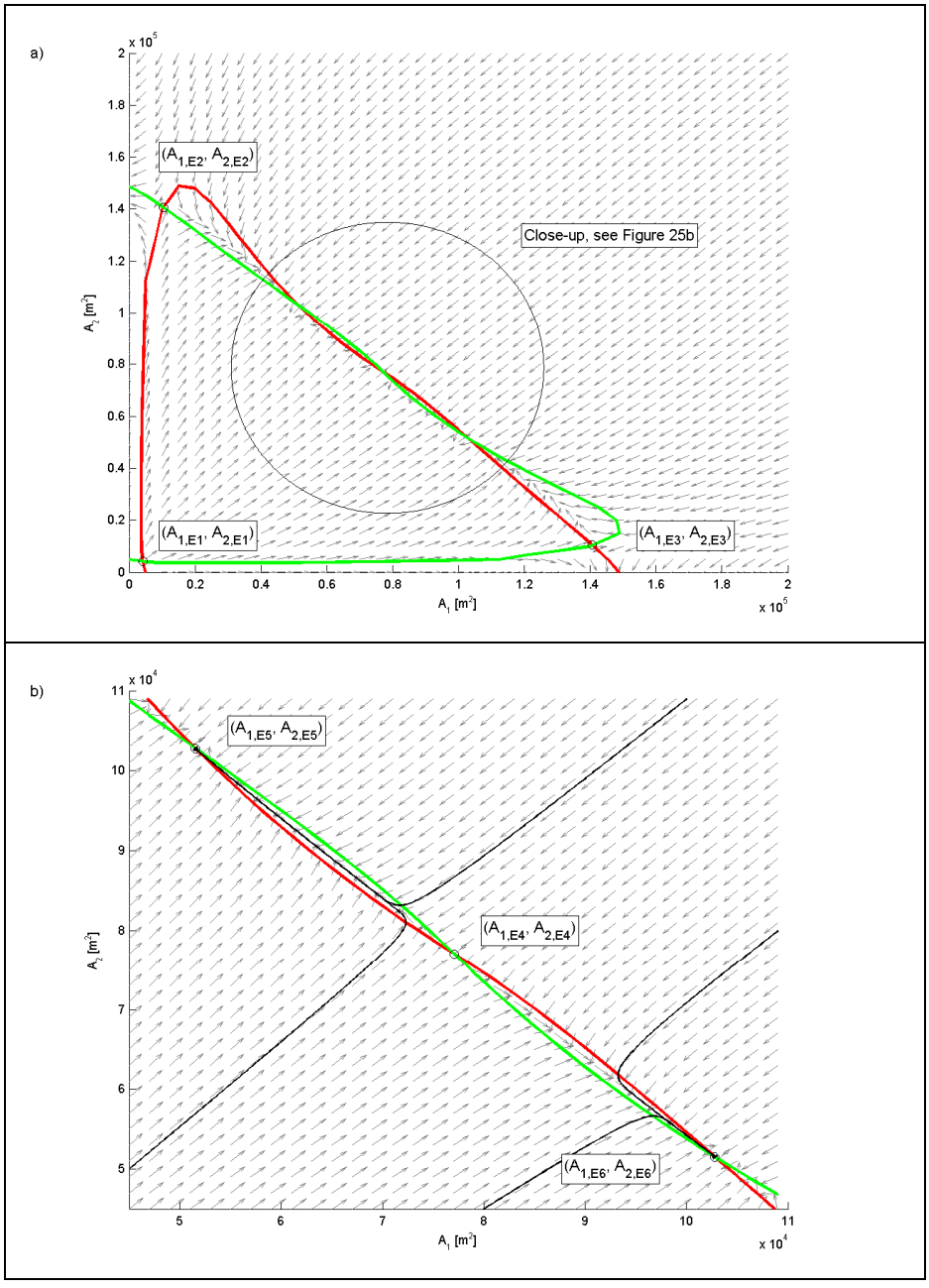

Figure 25: a) Flow diagram and equilibrium flow curves (red for inlet 1 and green for inlet 2) for a double inlet system with partition with A_3 = 40,000 m^2 and b) Close-up equilibriums ($A_{1,E4}$, $A_{2,E4}$), ($A_{1,E5}$, $A_{2,E5}$) and ($A_{1,E6}$, $A_{2,E6}$)

Case VI: A_3 = 50,000 m^2

For A_3 = 50,000 m^2 the flow diagram shows two combinations of equilibrium cross-sectional areas (Figure 26a). From the close-up of equilibrium 2 (Figure 26b) it can be seen that this is an unstable equilibrium. Apparently the cross-sectional area of the opening has become so large that its influence is very small and the water levels in both basins fluctuate almost uniformly. Figure 26a resembles Figure 16a, corresponding to a double inlet system without partition.

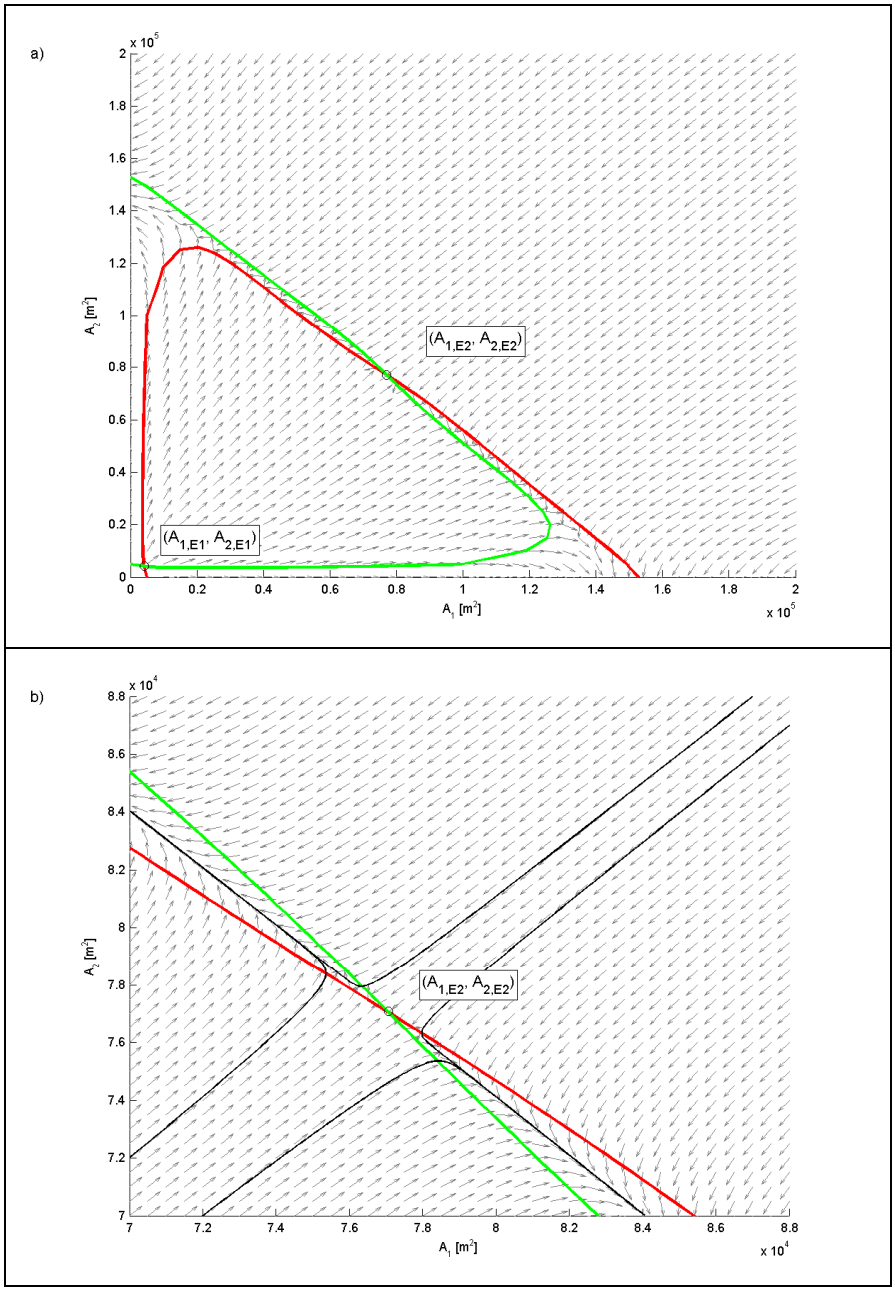

Figure 26: a) Flow diagram and equilibrium flow curves (red for inlet 1 and green for inlet 2) for a double inlet system with partition with A_3 = 50,000 m^2 and b) Close-up equilibrium ($A_{1,E4}$, $A_{2,E4}$)

Case VII: A_3 = 100,000 m^2

For the last case the cross-sectional area of the opening is twice as large as for case VI. The flow diagram in Figure 27a showes two combinations of equilibrium cross-sectional areas. The second equilibrium point is unstable (Figure 27b), just as in the previous case. The cross-sectional area of the opening has become so large that its influence is negligible and the two basins have a uniformly fluctuating water level. The situation is exactly the same as for a double inlet system without opening (Figure 16a).

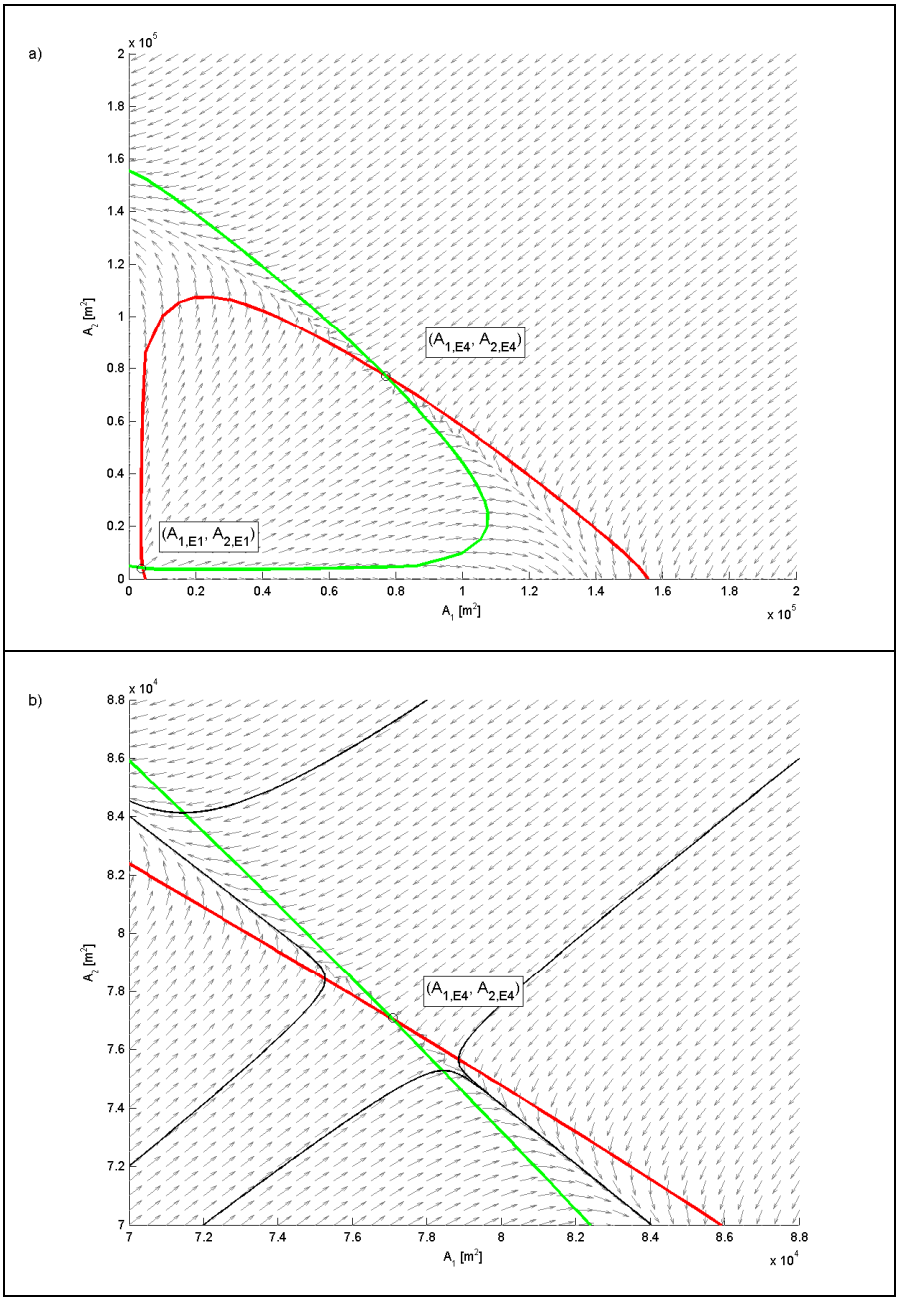

Figure 27: a) Flow diagram and equilibrium flow curves (red for inlet 1 and green for inlet 2) for a double inlet system with partition with A_3 = 100,000 m^2 and b) Close-up equilibrium ($A_{1,E4}$, $A_{2,E4}$)

5.2.2 Effect of the location of the partition on the stability

The combination of the horizontal basin areas of the two sub-basins used in the computations to determine the effect of the location of the partition are:

a) $A_{b,1} = A_{b,2} = 7 \cdot 10^8$ m^2
b) $A_{b,1} = 6 \cdot 10^8$ m^2 and $A_{b,2} = 8 \cdot 10^8$ m^2
c) $A_{b,1} = 4 \cdot 10^8$ m^2 and $A_{b,2} = 10 \cdot 10^8$ m^2
d) $A_{b,1} = 2 \cdot 10^8$ m^2 and $A_{b,2} = 12 \cdot 10^8$ m^2

In all four cases the sum of the sub-basin areas is $14 \cdot 10^8$ m^2. Other relevant parameter values are presented in Table 8.

Table 8: Parameter values for a double inlet system with partition and changing sub-basin areas

Parameter	Value	Parameter	Value
$c_{f,1} = c_{f,2} = c_{f,3}$	0.004 [-]	$\beta_1 = \beta_2 = \beta_3$	π/180 [rad]
m	1 [-]	$\varphi = \psi$	0 [rad]
$L_1 = L_2$	5,000 [m]	g	9.81 [m/s^2]
L_3	1,000 [m]	ω	$1.41 \cdot 10^{-4}$ [s^{-1}]
A_3	30,000 [m^2]	Δt	36 [s]
$\hat{h}_{01} = \hat{h}_{02}$	0.75 [m]	T	44,712 [s]

The influence of the size of the sub-basin areas $A_{b,1}$ and $A_{b,2}$ is shown in Figure 28. Figure 28a shows the symmetrical situation of a double inlet system with equal basin areas and acts as a reference situation. This configuration is the same as Case IV, see Figure 24, and has two stable equilibriums. When the basin surface of inlet 1 is decreased, corresponding to an increase in basin surface for inlet 2, velocities in inlet 1 decrease and velocities in inlet 2 increase. This leads to an equilibrium flow curve for inlet 1 that covers less space in the [A_1, A_2] plane and an equilibrium flow curve for inlet 2 that covers more space; see Figure 28b. There is only one stable equilibrium. Decreasing the values for $A_{b,1}$ and increasing the values for $A_{b,2}$ even further leads to the situations illustrated in Figure 28c and d in which there are no stable equilibriums. It follows from Figure 28 that not only the cross-sectional area of the opening but also the position of the partition plays a role in the number of stable equilibriums. Interesting is that the figures show that apparently asymmetric systems are less stable than symmetric systems. However, in this respect Figure 28 is not conclusive and a more detailed investigation on the stability of asymmetric systems will have to be carried out for a definite answer.

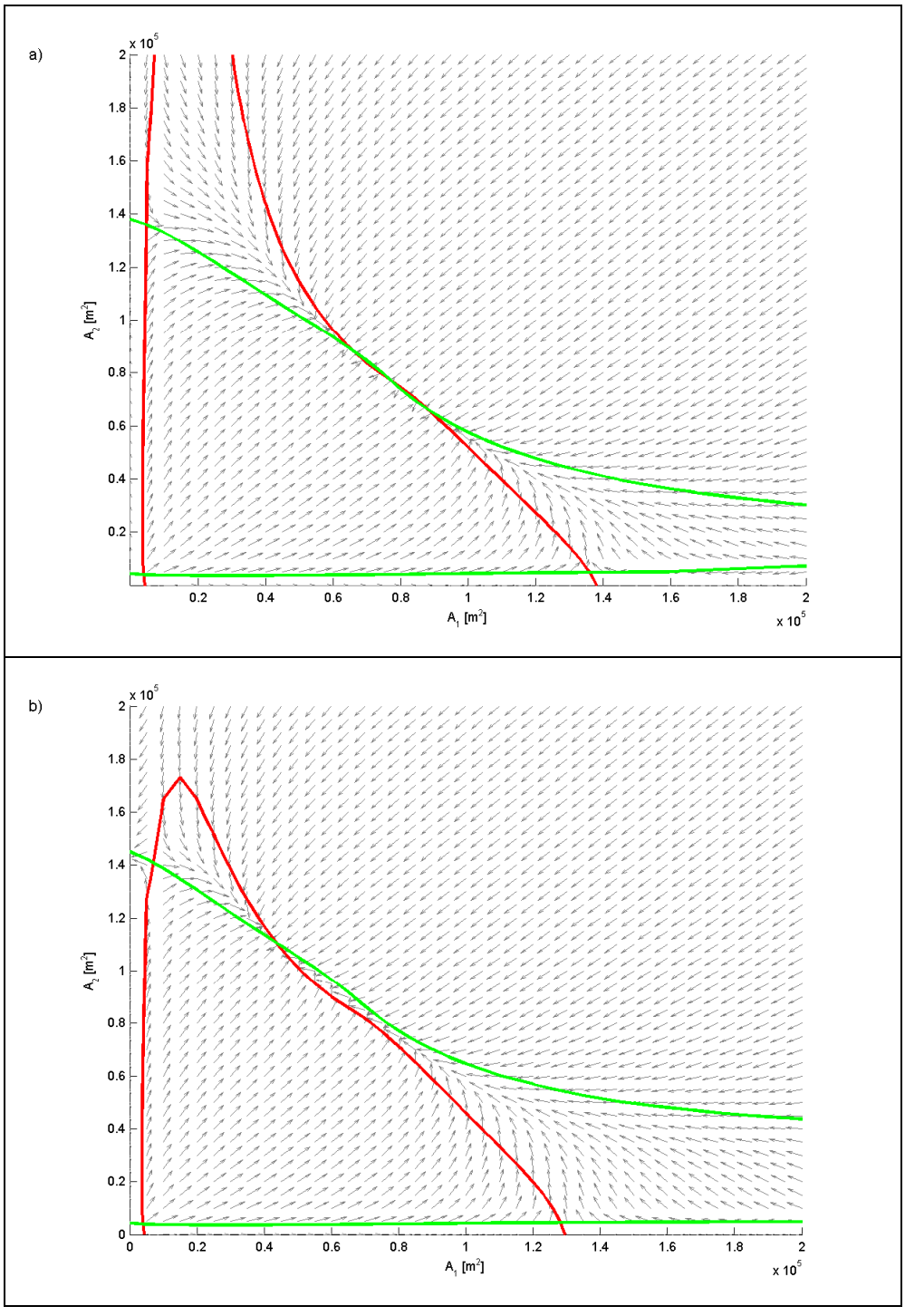
a)
x 10^5
2
1.8
1.6
1.4
1.2
1
0.8
0.6
0.4
0.2
A_2 [m^2]
0.2
0.4
0.6
0.8
1
1.2
1.4
1.6
1.8
2
A_1 [m^2]
x 10^5
b)
x 10^5
2
1.8
1.6
1.4
1.2
1
0.8
0.6
0.4
0.2
0
A_2 [m^2]
0
0.2
0.4
0.6
0.8
1
1.2
1.4
1.6
1.8
2
A_1 [m^2]
x 10^5

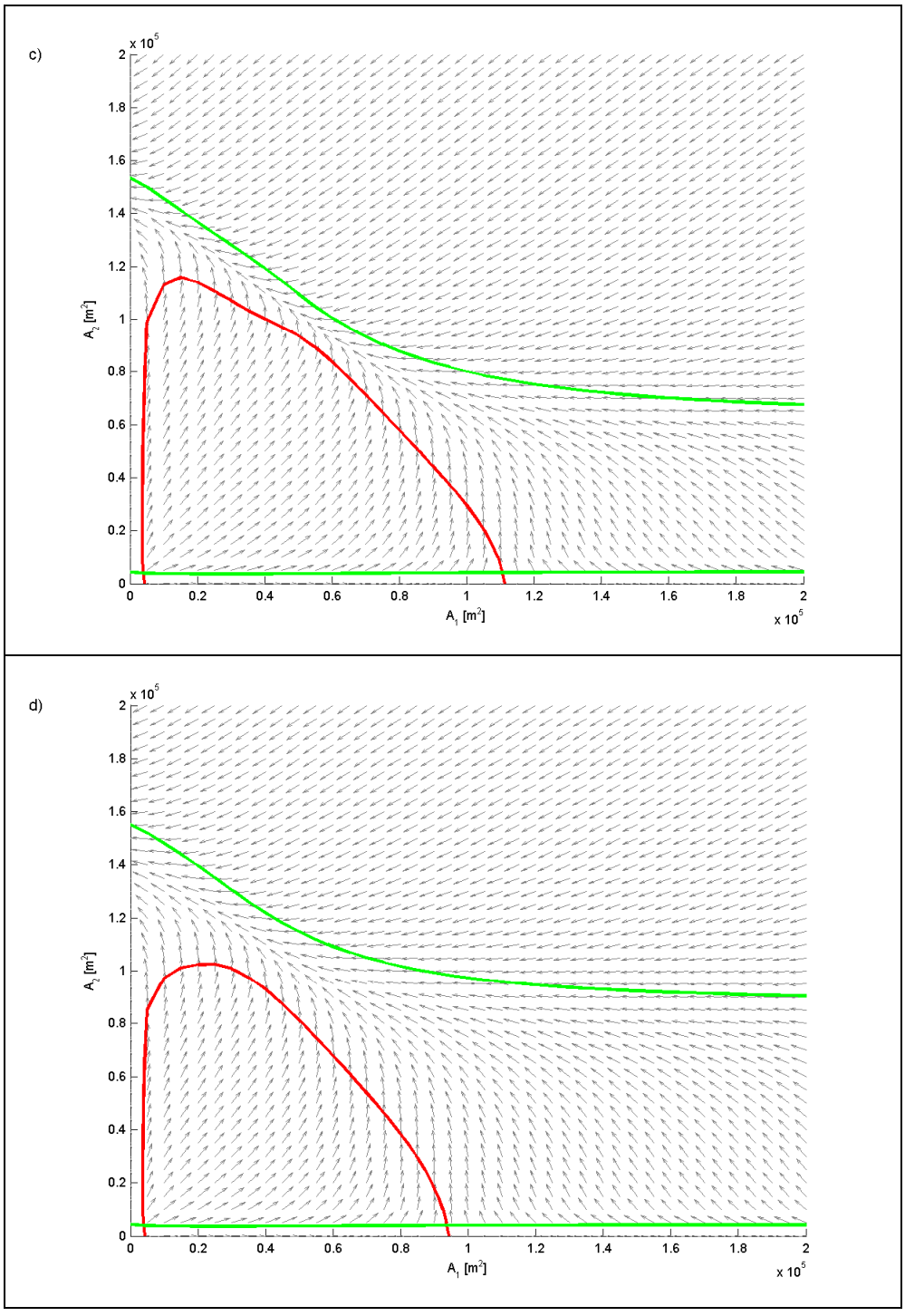

Figure 28: The effect of the location of the partition on the stability for:

a) $A_{b,1} = A_{b,2} = 7 \cdot 10^8$ m^2

b) $A_{b,1} = 6 \cdot 10^8$ m^2 and $A_{b,2} = 8 \cdot 10^8$ m^2

c) $A_{b,1} = 4 \cdot 10^8$ m^2 and $A_{b,2} = 10 \cdot 10^8$ m^2

d) $A_{b,1} = 2 \cdot 10^8$ m^2 and $A_{b,2} = 12 \cdot 10^8$ m^2

5.3 Discussion

The seven cases discussed in Section 5.2.1 to determine the effect of the size of the opening on the stability clearly show that there are three different configurations of the flow diagrams. Each of these configurations is characterized by a different number of intersections of the equilibrium flow curves. As shown in VAN DE KREEKE [1990] the number of intersections has to be at least 4 to have a situation that represents an unconditionally stable equilibrium for both inlets (see also Section 4.1). For the cross-sectional area A_3 smaller than approximately $1.7 \cdot 10^4$ m^2 there are four intersections between the equilibrium flow curves with one unconditionally stable equilibrium. For A_3 larger than approximately $1.7 \cdot 10^4$ m^2 and smaller than approximately $4.6 \cdot 10^4$ m^2 there are six intersections with two unconditionally stable equilibriums, which are each others mirror image. For A_3 larger than approximately $4.6 \cdot 10^4$ m^2 there are two intersections; none of these represent an unconditionally stable equilibrium. Table 9 gives an overview of the number of intersections and unconditionally stable equilibriums. The results agree with the earlier mentioned conclusion in VAN DE KREEKE [1990].

Table 9: Overview of the three configurations found for a double inlet system with partition

A_3	Number of intersections between the equilibrium flow curves of inlet 1 and 2	Number of unconditionally stable equilibriums
$< \pm 1.7 \cdot 10^4$ m^2	4	1
$> \pm 1.7 \cdot 10^4$ m^2 $< \pm 4.6 \cdot 10^4$ m^2	6	2
$> \pm 4.6 \cdot 10^4$ m^2	2	0

For the double inlet system with partition considered in Section 5.2.1 with $L_1 = L_2 = 5{,}000$ m and $A_{b,1} = A_{b,2} = 7 \cdot 10^8$ m^2 the values of the sets of equilibrium cross-sectional areas (E1, E2, E3, E4, E5 and E6 in Figure 21 through Figure 27) as a function of the cross-sectional area of the opening is presented in Figure 29. The figure visualizes the overview given in Table 9. The bold lines represent unconditionally stable equilibriums and the regular lines represent unstable equilibriums. The transition where the number of stable equilibriums goes from one to two and from two to none is indicated by vertical dotted lines. For small values of A_3 the influence of the opening between the two basins is so small that the system behaves almost as two separate single inlet systems. This yields one combination of cross-sections for which both inlets are in stable equilibrium. For the symmetric case considered here the equilibrium cross-sectional areas are the same for both inlets and the velocities in the opening are zero. For large values of A_3 the opening between the two basins is so large that the influence of the opening on the water motion is negligible. The system reduces to a double inlet system with both basin water levels fluctuating uniformly with the same amplitude and phase. As discussed in Chapter 4 this excludes unconditionally stable equilibriums. In the transition region, for each value of A_3 two unconditionally stable equilibriums are found. When the value of A_1 is on the upper branch in the figure, the corresponding value of A_2 is on the lower branch and vice versa. When at a stable equilibrium the cross-sectional areas A_1 and A_2 are different and the velocities in the opening have a finite value. The reason for the existence of the multiple equilibriums will be further discussed in Chapter 6. The ranges used in Figure 29 to delineate the values of A_3 with different numbers of stable equilibriums are approximate and as can be seen from the results of the experiments in section 5.2.2 also depend on the position of the partition.

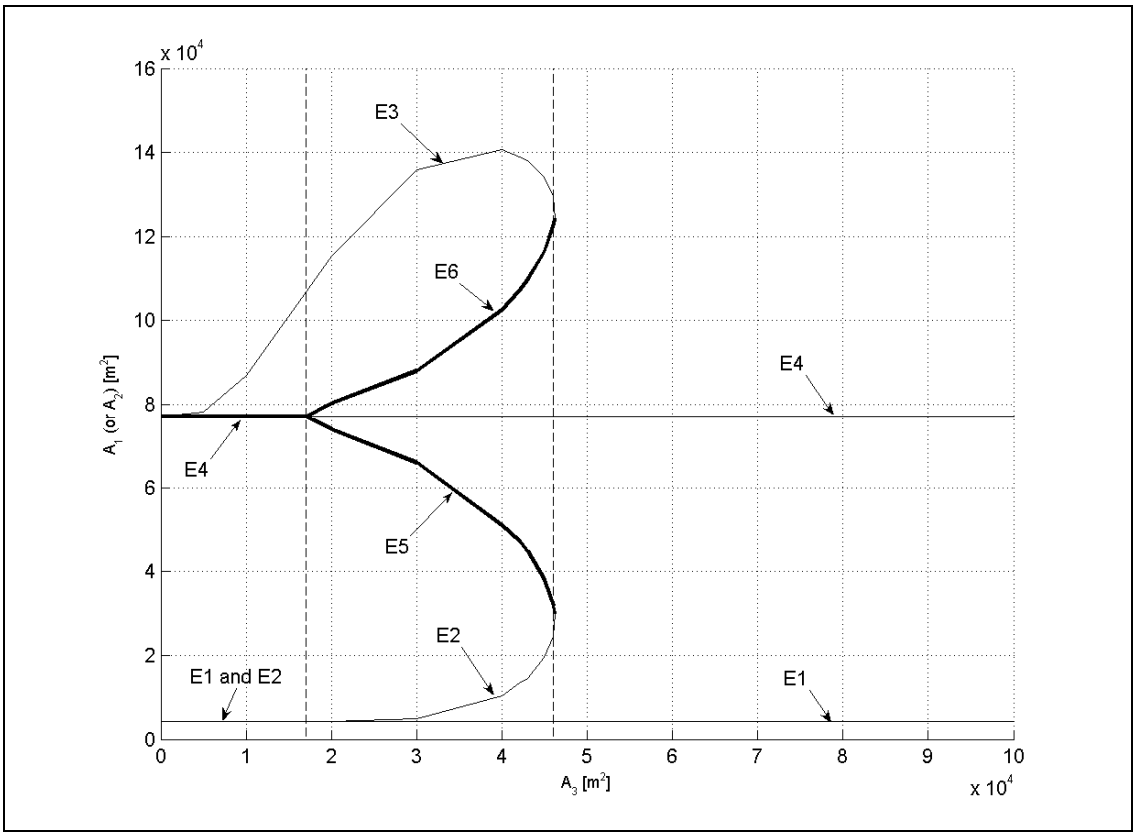

Figure 29: Configurations of the flow diagrams and the number of intersections between the equilibrium flow curves for a double inlet system with partition.

The label of the y-axis states that in the figure either A_1 or A_2 is represented as a function of A_3. The present figure shows A_1 as a function of A_3. When A_2 is plotted as a function of A_3 the labels E_2 and E_3, and E_5 and E_6 need to be interchanged.

Because the figure is based on data gathered from the model runs of the seven cases it has a somewhat discontinuous appearance. Using more data will smooth the curves.

We may use the insight gained in the behaviour of coupled basins to predict the effect of for instance the hypothetical case of dredging in the vicinity of a topographic high. Dredging effectively enlarges the cross-sectional area A_3 of the opening between the two basins. Consider the situation where the cross-sectional area of the opening has a value of 30,000 m^2. For this situation Figure 24 gives two unconditionally stable equilibriums. Assume that the inlets are at the stable equilibrium $(A_{1,E6}, A_{2,E6}) = (8.85 \cdot 10^4, 6.56 \cdot 10^4)$. When the cross-sectional area of the opening is dredged to a value of 40,000 m^2, Figure 25 tells us that the system reacts by increasing the cross-sectional area of inlet 1 and decreasing the cross-sectional area of inlet 2. The new unconditionally stable equilibrium is $(A_{1,E6}, A_{2,E6}) = (10.3 \cdot 10^4, 5.15 \cdot 10^4)$. However, when the cross-sectional area of the opening is dredged to a value of 50,000 m^2, a catastrophic effect occurs. Figure 26 shows that new stability conditions hold for the system and that it reacts by closing inlet 2 and increasing the cross-sectional area of inlet 1 to a value of $15.6 \cdot 10^4$ m^2. The double inlet system thus changes into a single inlet system.

The above implicitly assumes that the system reacts to a change in the cross-sectional area of the opening between the two basins by only adjusting the cross-sectional areas of the inlets connected to the ocean and not that of the opening. As a justification for this, it seems realistic that the morphological time scales of the inlets connected to the ocean are much shorter than for the topographic high between the basins. In that case enlarging the flow area of the topographic high will mainly affect the cross-sectional areas of the inlets connected to the ocean. Ultimately the cross-sectional area of the opening will also react.

6. Multiple stable equilibriums

6.1 Review numerical experiments

In the previous chapter it was shown that for a double inlet system with partition and opening there is a transition area with multiple combinations of inlet cross-sectional areas that represent unconditionally stable equilibriums (Figure 29). To shed some light on the underlying causes of the multiple equilibriums a number of numerical experiments were carried out. Parameter values used in the experiments are listed in Table 7. The cross-sectional area of the opening A_3 is 40,000 m^2.

As a first possible cause of the multiple equilibriums the accuracy of the finite difference solution was looked into. However, increasing the accuracy of the computations by decreasing the time step did not significantly affect the results and multiple equilibriums continued to exist. Next the effect of the inertia terms in the equations of motion (Eqs. (3.52), (3.53) and (3.54)) was investigated. Even though this term is small compared to the other terms in the equations it does contribute to the dynamic balance. Model runs in which the inertia term was deleted in the dynamic equations still showed multiple equilibriums, excluding the inertia as the cause of these equilibriums.

The only remaining cause of the multiple equilibriums appears to be the non-linearity in the friction term. In a separate note (personal communication Van de Kreeke, Appendix C) it is shown that when using linear friction at best one unconditionally stable equilibrium can exist. In the following the results of numerical experiments are presented in which the effect of linear and non-linear friction for the two inlets and opening on the number of equilibriums is further investigated.

6.2 Effect of friction formulation in inlets and opening

Referring to the dynamic equations for the inlets and opening (for example see Equation (3.3)) the non-linear friction term in terms of u is

$$\chi \frac{|u|u}{g} \tag{6.1}$$

The linearized version of the friction term is

$$\frac{8}{3\pi}\chi \frac{\hat{u}u}{g} \tag{6.2}$$

In this equation û is taken as 1 m/s.

With regards to the number of stable equilibriums the results of the computations with different formulations of the friction term in inlets and opening can be summarized as follows:

Definition of friction in:		Number of stable equilibriums
Inlets	Opening	
Non-linear	Non-linear	multiple stable equilibriums
Linear	Linear	one stable equilibrium
Linear	Non-linear	multiple stable equilibriums
Non-linear	Linear	one stable equilibrium

These results show the importance of the formulation of the friction in the opening with regard to multiple equilibriums. A linear friction for the opening results in one stable equilibrium regardless of the formulation of the friction in the inlets. A non-linear formulation of the friction in the opening results in multiple stable equilibriums regardless of the formulation of the friction in the inlets.

To further elucidate the effect of the formulation of the friction in the opening the friction term in de dynamic equation for the opening is split in a linear and a non-linear part

$$\lambda\left(\frac{8}{3\pi}\chi\frac{\hat{u}u}{g}\right)+(1-\lambda)\left(\chi\frac{|u|u}{g}\right) \tag{6.1}$$

In this equation λ has a value between 0 and 1. When the factor λ is 0 the friction term is fully non-linear and when the factor λ is 1 the friction term is fully linear. In this way the transition between a linear and a non-linear friction term in the opening can be ascertained. Figure 30 clearly shows the development of the equilibrium flow curves and the flow diagram when the friction term changes from fully linear to fully non-linear. The transition from one stable equilibrium to two stable equilibriums occurs at a value λ ≈ 0.55. Calculations to determine the sensitivity of the results to other parameter values were not carried out as the main objective of the numerical experiment was to determine whether, depending on the degree of nonlinearity of the friction term in the opening, a clear transition could be found between the occurrence of one and multiple stable equilibriums.

a)

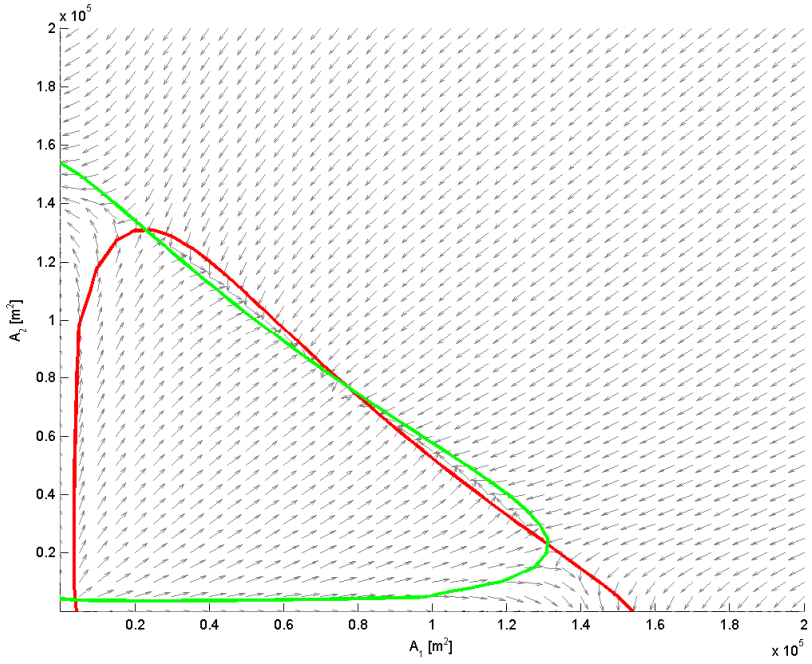
x 10^5
2
1.8
1.6
1.4
1.2
1
0.8
0.6
0.4
0.2
A_2 [m^2]
0.2
0.4
0.6
0.8
1
1.2
1.4
1.6
1.8
2
A_1 [m^2]
x 10^5

b)

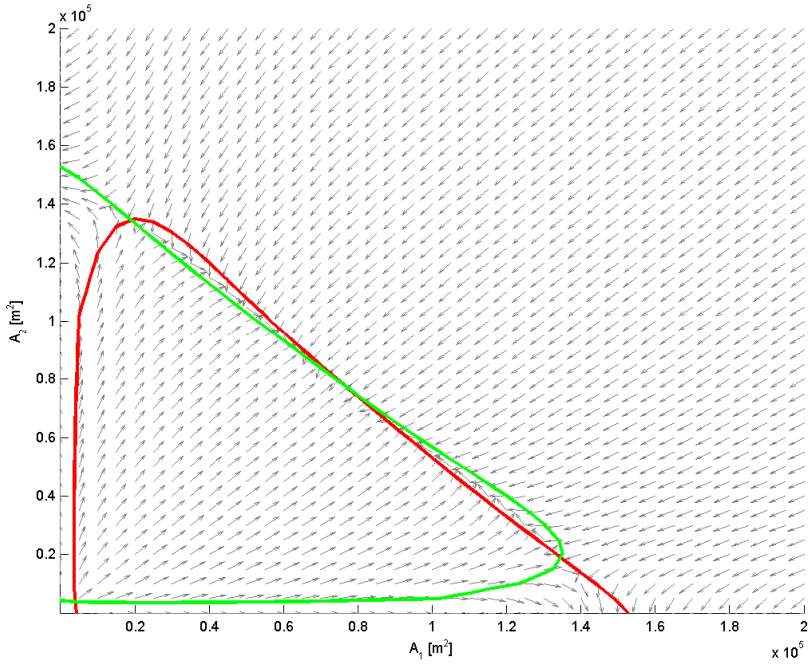
x 10^5
2
1.8
1.6
1.4
1.2
1
0.8
0.6
0.4
0.2
A_2 [m^2]
0.2
0.4
0.6
0.8
1
1.2
1.4
1.6
1.8
2
A_1 [m^2]
x 10^5

c)

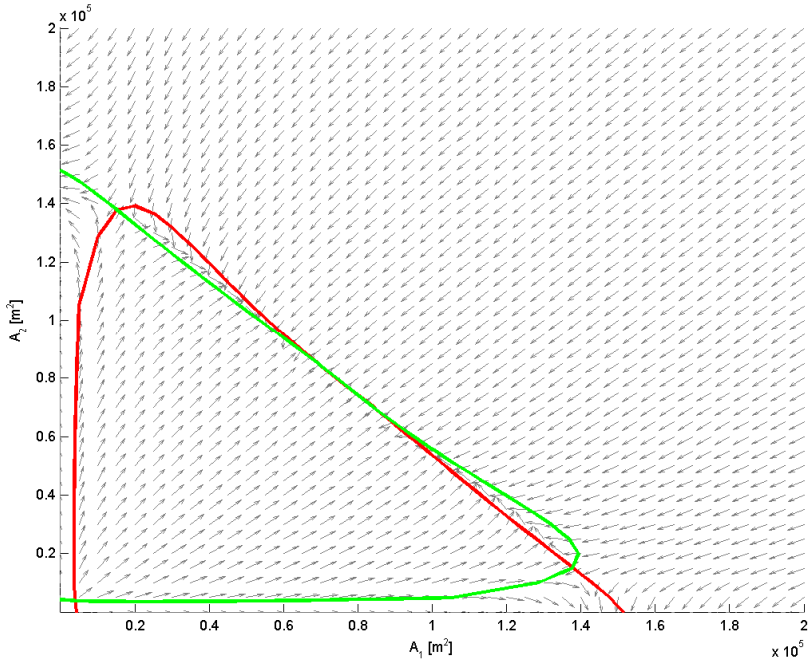
x 10^5
2
1.8
1.6
1.4
1.2
1
0.8
0.6
0.4
0.2
A_2 [m^2]
0.2
0.4
0.6
0.8
1
1.2
1.4
1.6
1.8
2
A_1 [m^2]
x 10^5

d)

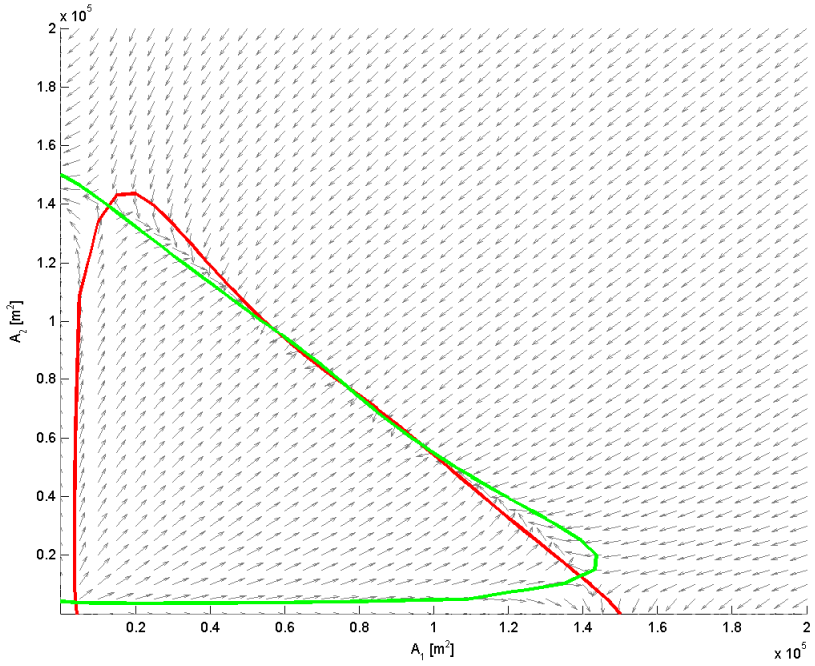
x 10^5
2
1.8
1.6
1.4
1.2
1
0.8
0.6
0.4
0.2
A_2 [m^2]
0.2
0.4
0.6
0.8
1
1.2
1.4
1.6
1.8
2
A_1 [m^2]
x 10^5

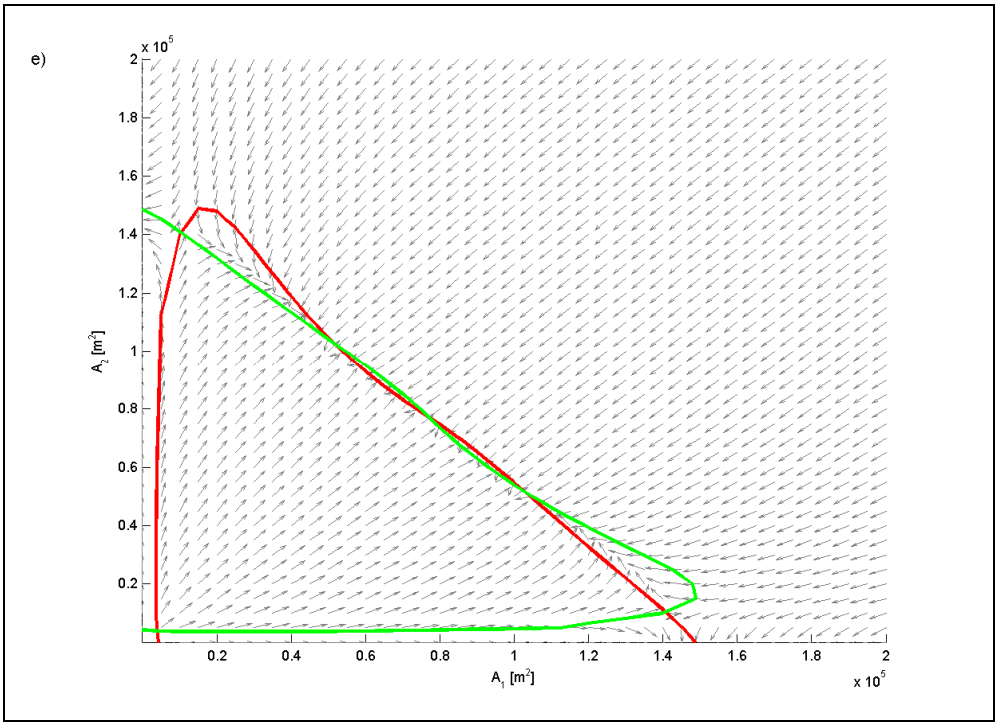

Figure 30: Equilibrium flow curves and flow field for a friction term that is:

a) fully linear (λ=1),

b) 75% linear and 25% non-linear (λ=0.75),

c) 50% linear and 50% non-linear (λ=0.5),

d) 25% linear and 75% non-linear (λ=0.25),

e) fully non-linear (λ=0)

6.3 Water levels and velocities for inlets at equilibrium

The results of the numerical experiments discussed in the previous section gave an indication that it is the formulation of the friction in the opening that is crucial. Still determining the deeper causes of the multiple equilibriums it seems worth while to look at the effect of the friction formulation on the velocities in the inlets. It are the velocities in the inlets, through the equilibrium flow curves, that determine the location and number of equilibriums in the (A_1, A_2) plane. An initial attempt of comparing calculated velocities is presented in Figure 31, Figure 32 and Figure 33. These figures present the velocity curves for the equilibriums discussed in Section 5 i.e. (A_1, A_2) = ($5.2 \cdot 10^4$, $10.3 \cdot 10^4$) and (A_1, A_2) = ($7.7 \cdot 10^4$, $7.7 \cdot 10^4$). It follows that:

> For the equilibrium with different values of A_1 and A_2, in spite of A_1 and A_2 being different, the velocity curves are the same for both inlets; compare Figure 32 and Figure 33.

For both equilibriums the velocity curves in the inlets are the same; compare Figure 31 and Figure 32, and Figure 31 and Figure 33.

It is this type of observations that could lead to a better understanding of the causes for the multiple equilibriums.

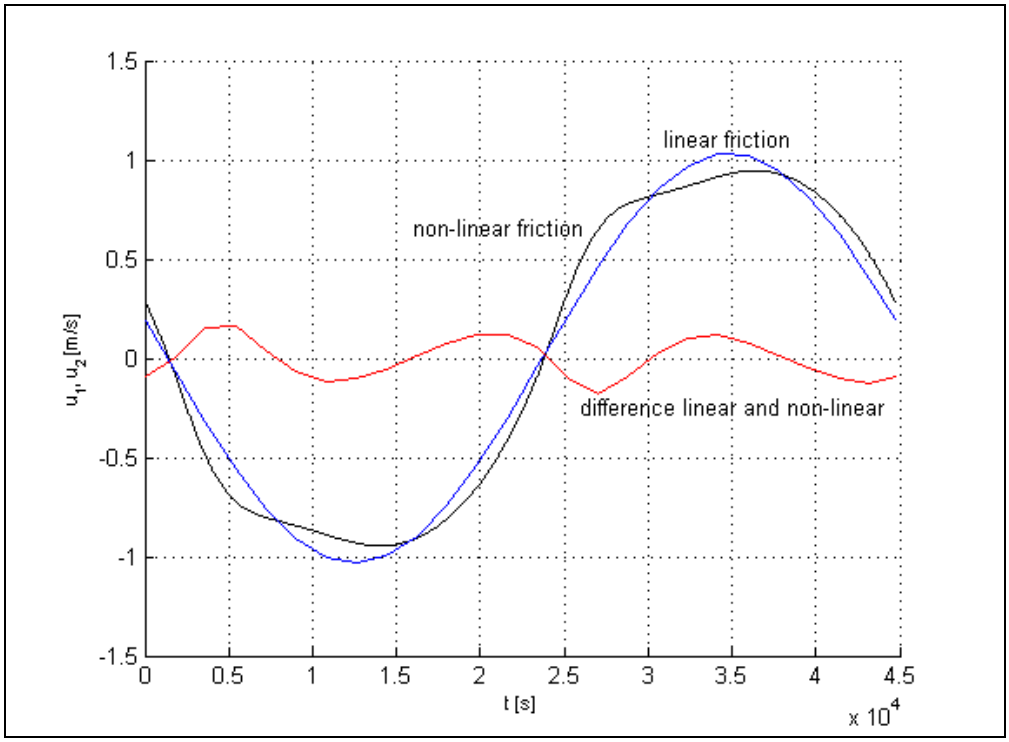

Figure 31: Velocity curves in inlet 1 and inlet 2 at the unstable equilibrium ($7.7 \cdot 10^4$, $7.7 \cdot 10^4$) for linear and non-linear friction

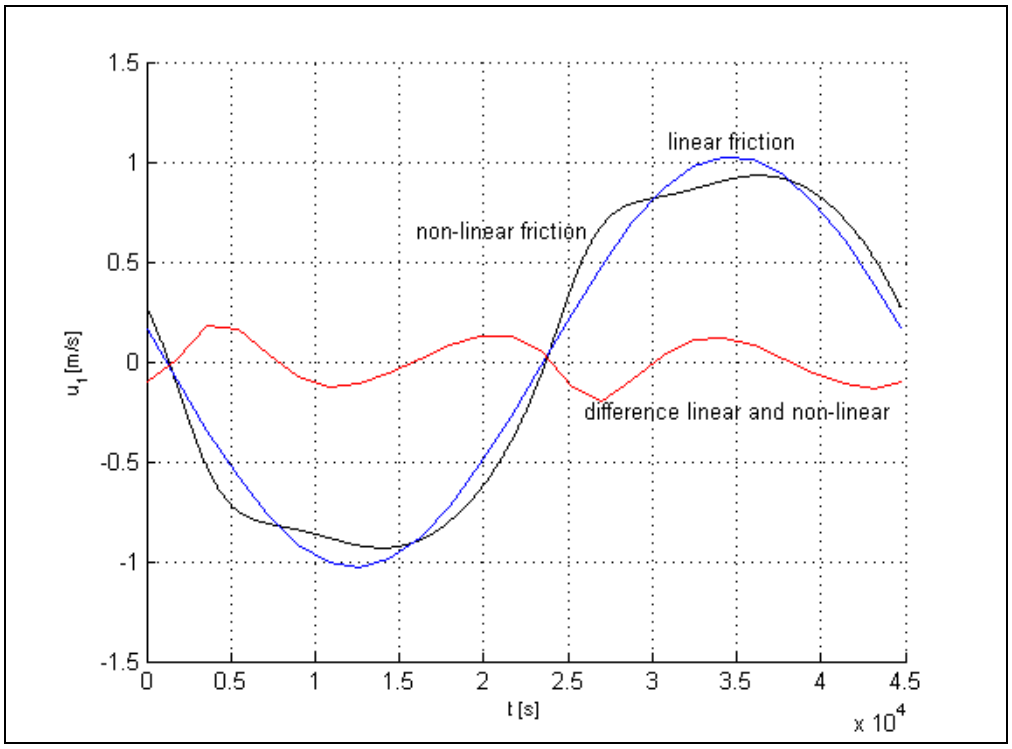

Figure 32: Velocity curves in inlet 1 at the stable equilibrium ($5.2 \cdot 10^4$, $10.3 \cdot 10^4$) for linear and non-linear friction

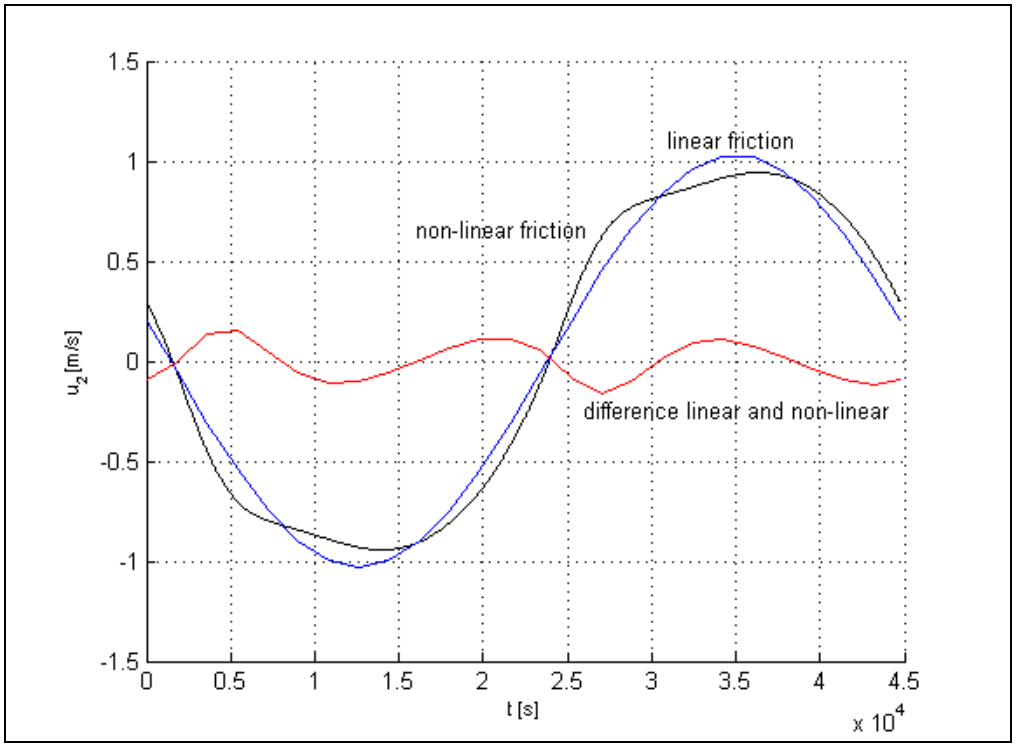

Figure 33: Velocity curves in inlet 2 at the stable equilibrium ($5.2 \cdot 10^4$, $10.3 \cdot 10^4$) for linear and non-linear friction

7. Model application to the Texel and Vlie basins

7.1 Introduction

The motivation to investigate the cross-sectional stability of a double inlet system is, among other, based on observations in the Dutch Wadden Sea. Observations show that the cross-sectional areas of the tidal inlets connecting Wadden Sea and North Sea have changed little over the years. Therefore the assumption that the inlets are in a stable equilibrium seems justified. In Section 1.1 it has already been stated that the Dutch Wadden Sea, and in particular the western part, has been the subject of many studies. As a result a wealth of information exists on bathymetry, tides, morphological changes etc.

The western Wadden Sea consists of two basins; the Texel basin and the Vlie basin (see Figure 1). These basins are connected to the North Sea by respectively the inlets Marsdiep and Vlie. The basins are separated by a topographic high, thus creating a double inlet system with partition. In this chapter an attempt is made to verify whether the hydrodynamic model used in this study (see Chapter 3) is applicable to the western Wadden Sea. For this, emphasis is on water levels.

7.2 Comparison between calculated and predicted water levels in the Texel and Vlie basins

7.2.1 Predicted water levels of the Texel - Vlie system

Predicted water levels (=astronomical tide) are available from www.getij.nl for the stations Texel North Sea, Terschelling North Sea, Vlieland Harbour, Western Terschelling, Harlingen, Den Oever and Kornwerderzand. In Figure 1 the locations of the measurement station are illustrated.

Forcing of the model is by the water levels in the North Sea off Marsdiep and Vlie. For this use is made of the tide stations Texel North Sea and Terschelling North Sea. It is assumed that the predicted water levels at the measurement station Texel North Sea are representative for the forcing at the Marsdiep inlet and the linearly interpolated water levels between the measurement station Texel North Sea and Terschelling North Sea are representative for the forcing at the Vlie inlet. Figure 34 shows the predicted tide at the station Texel North Sea, represented by the blue line, and the tide at Vlie, represented by the red line. In the figure t=0 corresponds to the date 26-5-2006 at 0:00 hrs. Water levels off the Marsdiep inlet lead the water levels at the Vlie inlet by 30-40 minutes. The tidal range off the Vlie inlet is slightly larger than off the Marsdiep inlet.

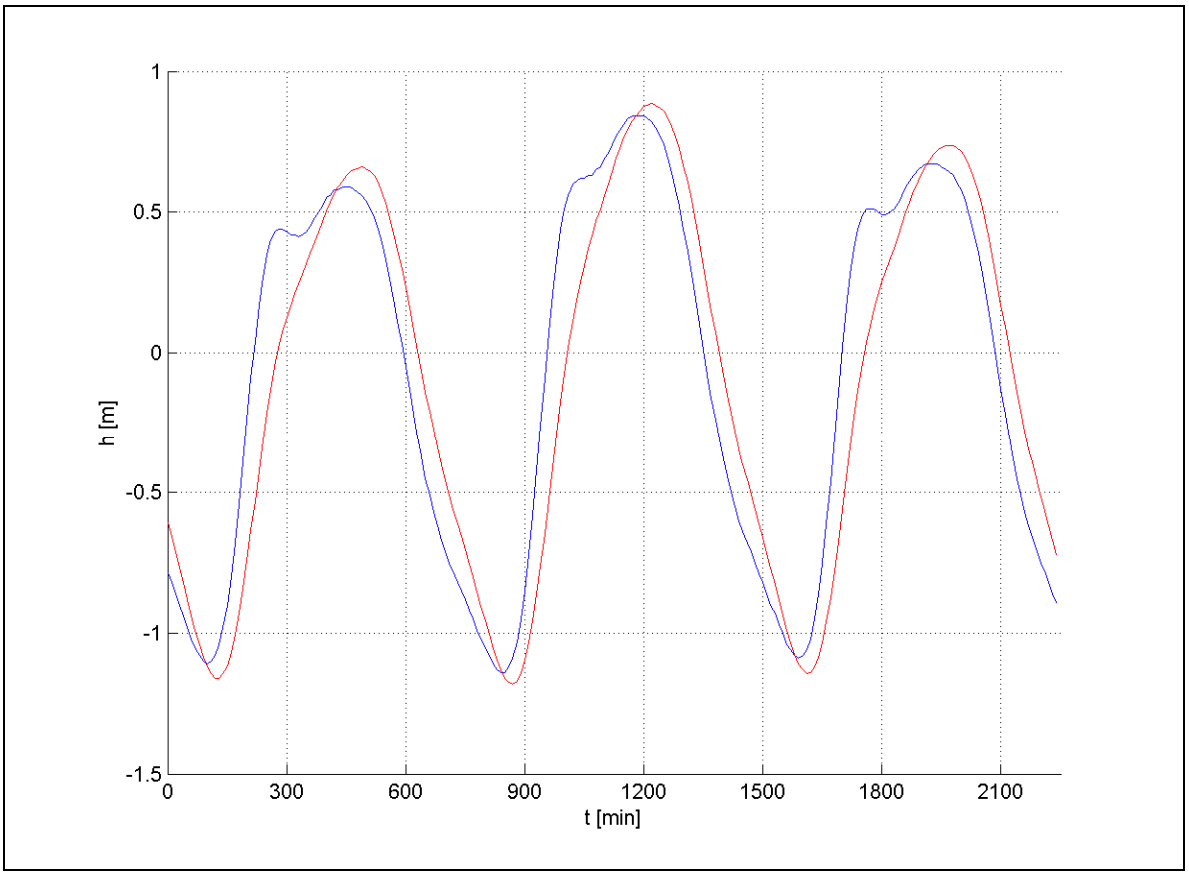

Figure 34: Predicted tide at Texel North Sea (blue line) and Vlie (red line)

Next, the predicted water levels inside the basin are described. In the Texel basin two measurement stations are present, Den Oever and Kornwerderzand. In the Vlie basin three measurement stations are present, Vlieland Harbour, Western Terschelling and Harlingen. Figure 35a illustrates the predicted water levels at the stations in the Vlie basin; the blue line represents the water levels at Vlieland Harbour, the red line represents the water levels at Western Terschelling and the green line represents the water levels at Harlingen. Figure 35b illustrates the predicted water levels in the Texel basin; the blue line represents the water levels at Den Oever and the red line represents the water levels at Kornwerderzand.

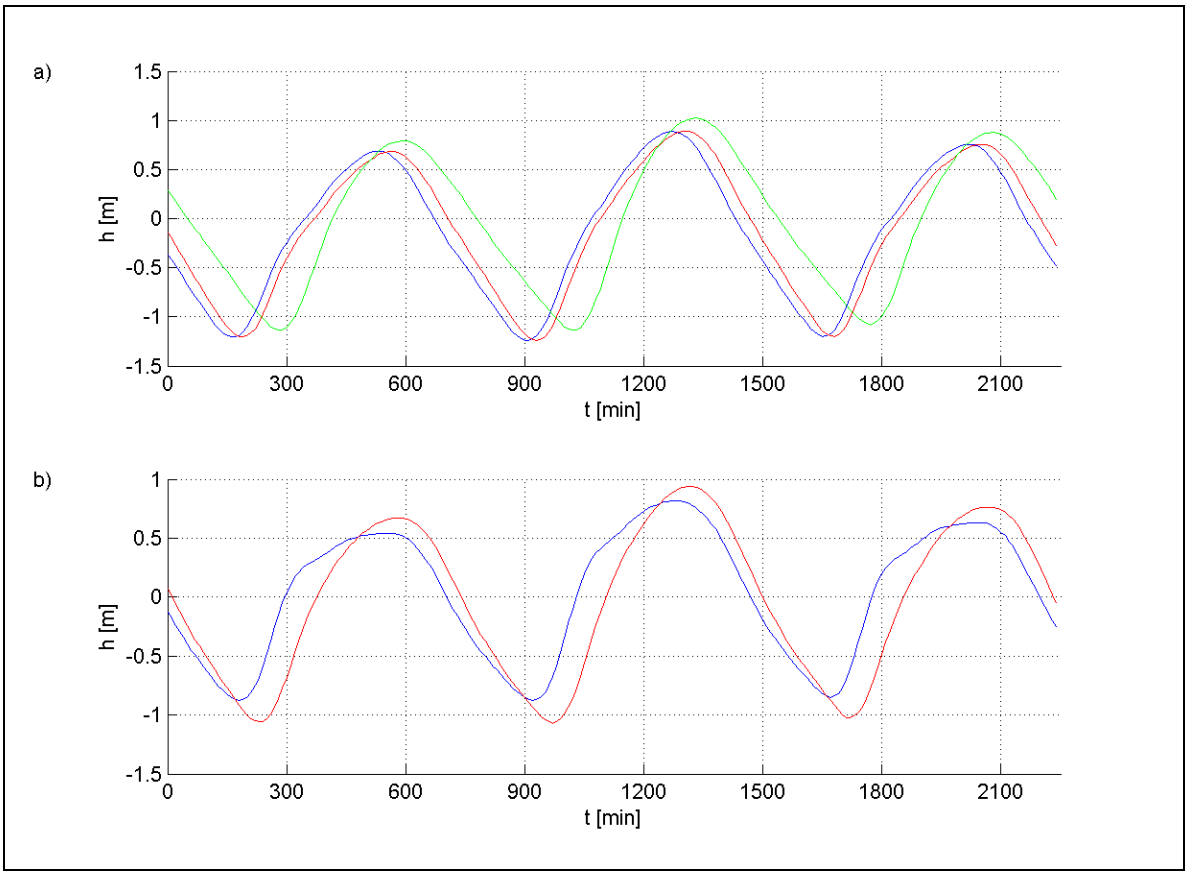

Figure 35: a) Predicted water levels at Vlieland Harbour (blue), Western Terschelling (red) and Harlingen (green) for the Vlie basin and b) Predicted water levels at Den Oever (blue) and Kornwerderzand (red) for the Texel basin.

From Figure 35a and b it can be seen that for the individual basins the amplitudes and the phases at the different stations differ considerably. For example the phase difference between the stations closest to the inlet and farthest removed from the inlet is more than one hour. This means that the assumption made in the model that the water surface of each basin fluctuates uniformly does not hold. In the next section a comparison between calculated and predicted water levels of the Texel - Vlie system is made.

7.2.2 Calculated water levels of the Texel - Vlie system

The parameter values of the Texel - Vlie system used to calculate the water levels are presented in Table 10. The lengths of the Marsdiep and Vlie inlet channels, L_1 and L_2, are measured from available charts of the western Wadden Sea. The value for the length of the opening between the two basins L_3 is difficult to estimate. The opening represents the topographic high between the two basins. As a first estimate a value of L_3 = 3,000 m is chosen. This value originates from a bottom slope of the topographic high of the Texel basin estimated at $i = 1 \cdot 10^{-3}$ m/m and a tidal range for the Wadden Sea of H = 1.5 m. Dividing the tidal range by the bottom slope of the topographic high results in the length of the topographic high of the Texel basin of 1,500 m. Using the same principle on the Vlie basin results in a length of the topographic high of 1,500 m. The value for the cross-sectional area of the opening between the two basins A_3 is also

difficult to estimate. As a first estimate a value of A_3 = 10,000 m^2 is chosen. This value originates from a width of the topographic high between the Texel and Vlie basins of approximately $2 \cdot 10^4$ m and a mean water level of 0.5 m. The values of the horizontal basin areas of the Texel and Vlie basins, $A_{b,1}$ and $A_{b,2}$, and the cross-sectional areas of the Marsdiep and Vlie inlets, A_1 and A_2, are based on personal communication with E. Elias. Both surface areas and cross-sectional areas pertain to mean water level.

Table 10: Parameter values for the Texel and Vlie basins

Parameter	Value	Parameter	Value
$A_{1,E}$	$7.19 \cdot 10^4$ [m^2] w.r.t. NAP	$c_{f,1} = c_{f,2} = c_{f,3}$	0.004 [-]
$A_{2,E}$	$6.19 \cdot 10^4$ [m^2] w.r.t. NAP	m	1 [-]
A_3	10,000 [m^2] w.r.t. NAP	$\beta_1 = \beta_2 = \beta_3$	$\pi/180$ [rad]
L_1	4,000 [m]	$\varphi = \psi$	0 [rad]
L_2	5,500 [m]	g	9.81 [m/s^2]
L_3	3,000 [m]	ω	$1.41 \cdot 10^{-4}$ [s^{-1}]
$A_{b,1}$	$6.76 \cdot 10^8$ [m^2] w.r.t. NAP	T	44,712 [s]
$A_{b,2}$	$6.18 \cdot 10^8$ [m^2] w.r.t. NAP	Δt	36 [s]

The calculated water levels for the Texel basin and Vlie basin together with the predicted water levels at the different tide stations are presented in respectively Figure 36a and b. It follows that for the Vlie basin calculated and predicted water levels for the stations closest to the inlet show reasonable agreement. However, the station farthest removed (Harlingen) shows a considerable difference, especially in the phase. For the Texel basin calculated and predicted water levels show a sizable difference in both amplitude and phase.

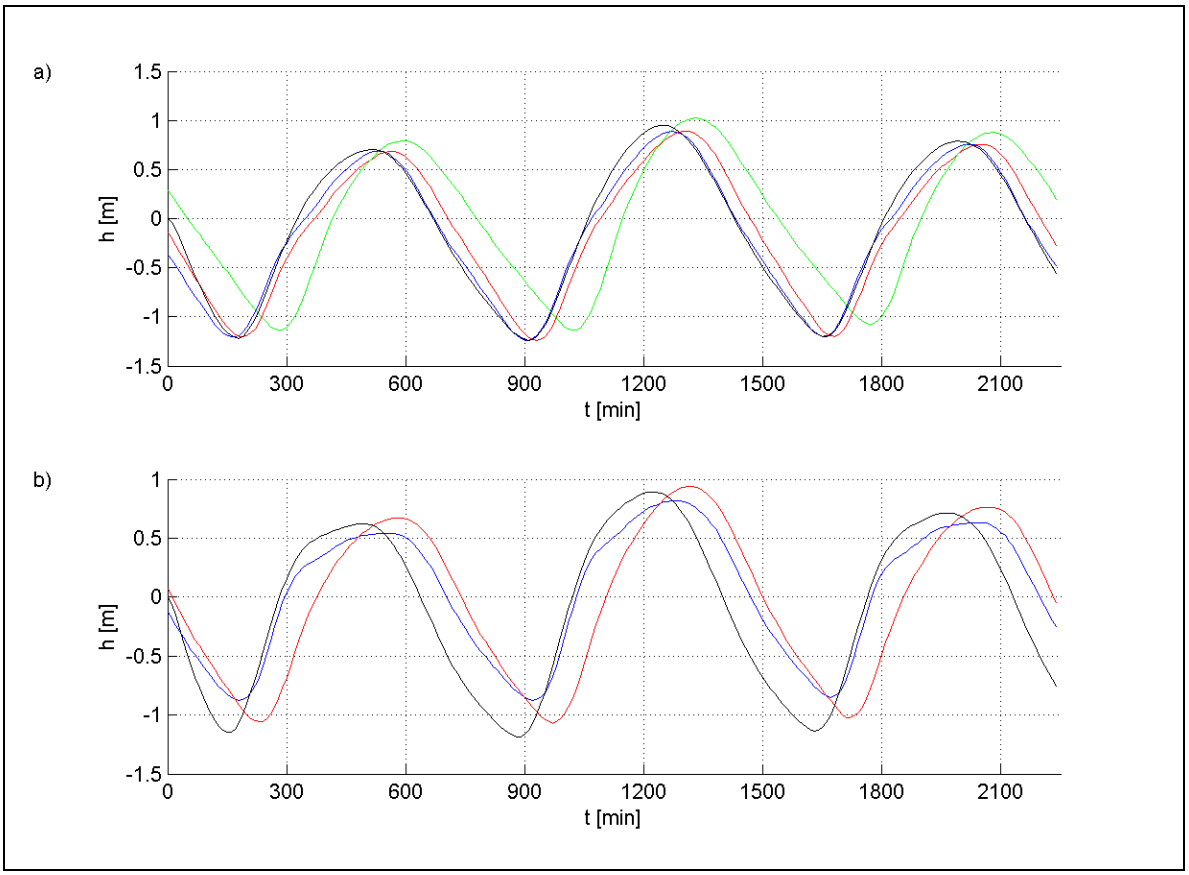

Figure 36: a) Predicted (blue, red and green lines; see Figure 35a) and calculated (black line) water levels in the Vlie basin and b) Predicted (blue and red lines; see Figure 35b) and calculated (black line) water levels in the Texel basin

7.3 Discussion

It follows from the predicted water levels in Figure 36 that in the case of the Texel - Vlie system the assumption of a uniformly fluctuating water level in each basin is not valid. Especially the large difference in phase between the stations closest and farthest removed from the inlet suggests that for a proper representation of the water levels friction in the basin needs to be taken into account. Obviously the basin is not deep/short enough to justify the assumption of a uniformly fluctuating basin level.

A requirement for the evaluation of the stability of the inlets, including the construction of a flow diagram, is that the water motion is represented correctly. In the case of the Texel - Vlie system this implies calculating a spatially variable water level. This can be done with a 2D horizontal hydrodynamic model. Even though the hydrodynamic model described in Chapter 3 is not applicable to the Texel - Vlie system, the conclusion arrived at in Chapter 5, that where there are phase and or amplitude differences in the interior water level stable equilibriums are possible, remains. This finding is an important step in a further understanding of double inlet systems.

In spite of the fact that the assumption of a uniformly fluctuating water level is not valid for the Texel - Vlie system it is interesting to determine which equilibriums the model generates. Figure 37 shows the combination of cross-sectional areas (A_1, A_2) of the Texel - Vlie system when at a stable equilibrium calculated with the model for different combinations of L_3 and A_3. The values of L_3 are in the range between 500 m and 5,000 m and the values of A_3 are in the range between 2,500 m^2 and 20,000 m^2 (see appendix D for a detailed list of combinations of L_3 and A_3 and the corresponding equilibrium cross-sectional areas). It follows from the figure that the calculated equilibriums are located approximately along the same line. Furthermore, it shows that the calculated stable equilibriums are located in the vicinity of the present cross-sectional areas of the Marsdiep and Vlie inlets.

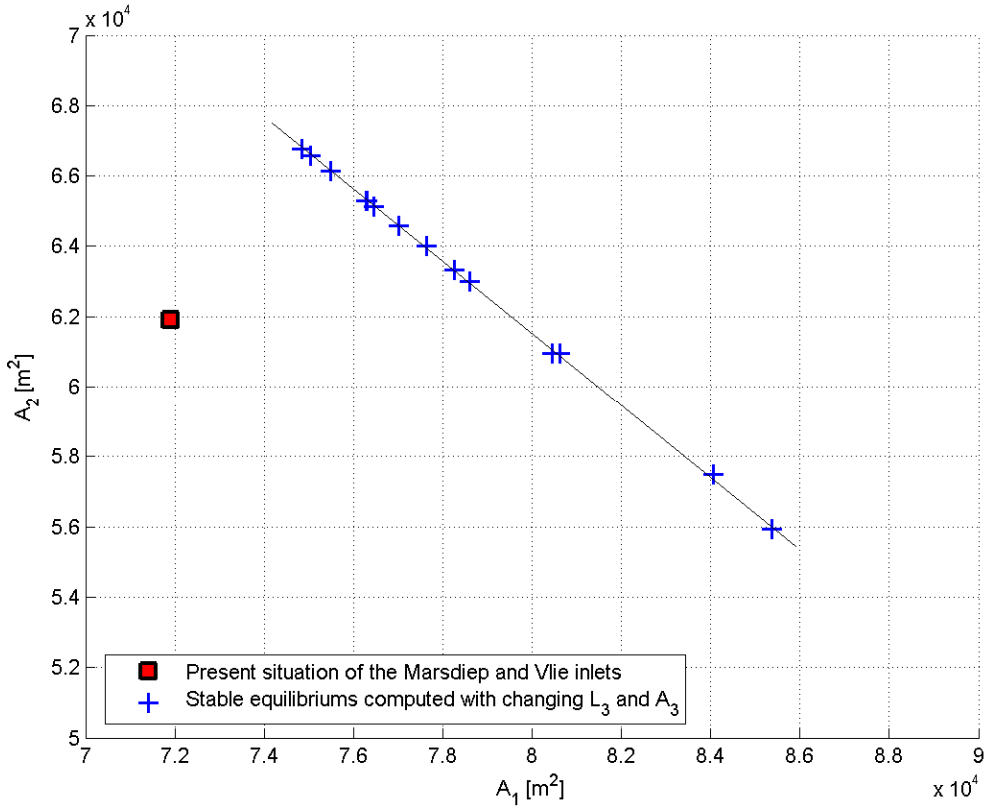

Figure 37: Calculated stable equilibriums for the application to the Texel - Vlie system for different combinations of L_3 and A_3. L_3 is in the range between 500 m and 5,000 m and A_3 is in the range between 2,500 m^2 and 20,000 m^2.

8. Conclusions and recommendations

8.1 Conclusions

This study explores the cross-sectional stability of a double inlet system by means of a simplified mathematical model. Double inlet systems consist of two inlets connecting a lagoon or bay to the ocean. Previous studies of VAN DE KREEKE [1990] and BORSJE [2003] proved to be a useful starting point for the present study. Assuming a uniform fluctuating basin level the equations governing the flow in the inlets are derived. The equations are solved using a finite difference method. The equilibrium cross-sectional areas of the inlets are determined with a method first proposed by Escoffier (1940). The stability of the equilibriums is investigated with the help of a flow diagram. To introduce the effect of topographic highs as found in the Wadden Sea a partition with opening was added to the model, essentially dividing the bay in two separate basins. The following conclusions can be drawn from the mathematical modelling presented in Chapters 2 and 3, the mathematical stability analysis in Chapter 4, 5 and 6 and the application of the suggested model to the Texel and Vlie basins in Chapter 7.

Initial computations with the harmonic method used in previous studies (Borsje, 2003) to solve the governing equations showed that when including a partition the system not always converged to the proper solution. The finite difference method developed in Section 3.2.3 proves to be an adequate answer to the shortcomings of the harmonic method.

The application of flow diagrams in Chapter 2 proves to be a useful tool for analyzing the stability of a double inlet system. By visual interpretation of the flow diagram and equilibrium flow curves a reliable prediction can be made for the stability of a double inlet system.

Stability analysis of a double inlet system without a partition (Chapter 4), making use of the flow diagrams, suggests that such a system can never be unconditionally stable. To be more precise, it always leads to a situation where one of the two inlets closes while the other remains open, thus changing into a single inlet system. This confirms the conclusions drawn by VAN DE KREEKE [1990] and BORSJE [2003].

Stability analysis of a double inlet system with partition (Chapter 5), making use of the flow diagrams, showed that such a system can be unconditionally stable. In the analysis particular attention was given to the effect of the size of the opening in the partition and the position of the partition on the stability of the inlets. Investigations with different cross-sectional areas of the opening in the partition showed that, depending on the number of unconditionally stable equilibriums, three ranges of cross-sectional areas can be distinguished. For a small opening the system almost behaves like two single inlets, resulting in one unconditionally stable equilibrium. For a large opening the influence of the opening is negligible and the system acts as a double inlet system with a uniformly fluctuating water level yielding a situation where one of the two inlets closes while the other remains open. In the transition region the opening has a large influence on the

interaction between the two basins. This leads to a situation where two unconditionally stable equilibriums exist. Investigations with different positions of the partition showed that the exact boundaries between the ranges of cross-sectional areas of the opening depend on the location of the partition, i.e. the size of the sub-basins.

Investigations into the cause of multiple stable equilibriums showed that the formulation of the friction term is paramount. A linear friction for the opening results in one stable equilibrium regardless of the formulation of the friction in the inlets. A non-linear formulation of the friction in the opening results in multiple stable equilibriums regardless of the formulation of the friction in the inlets.

Application of the model to the western Wadden Sea showed that the model is not able to accurately reproduce the water motion in the Texel - Vlie system. The assumption that the water surface area fluctuates uniformly in the individual basins is too restrictive. Measurements showed that in the Texel and Vlie basin considerable differences in water level amplitude and phase exist depending on location.

The model as used in this study still provides useful information. The model does prove that incorporating a partition with opening between the two basins leads to a situation where stable equilibriums exist for which both inlets remain open. This finding is an important step in the further understanding in the stability of double inlet systems.

8.2 Recommendations

- The application of the model to the western Wadden Sea showed that the model suggested in this study is not able to reproduce the water motion in the Texel - Vlie system. The reason is that the assumption of a uniformly fluctuating water level is too restrictive. In reality water levels at different locations in each basin show phase and amplitude differences. Furthermore, throughout the course of this study a constant basin surface area was assumed, while in reality the basin surface area is dependent on the water level in the basin, also known as hypsometry. To alleviate these shortcomings it is proposed to add the hypsometry to the presented model and to investigate the possibility of using a 2D horizontal model to calculate the water motion.

- In this study the adaptation of the inlet cross-sections when out of equilibrium is described with the morphodynamic, semi-empirical model ASMITA. This model is based on limited physics. It is proposed to develop a model for the adaptation of the inlets that includes more physics.

- In determining the morphodynamic equilibrium for an inlet system, in this study use is made of the assumption that when an inlet system is in equilibrium the amplitude of the velocity û equals 1 m/s. An alternate and probably more accurate way of describing the equilibrium conditions for inlets is to make use of the cross-sectional area tidal prism relationship $A_E = C \cdot P_E^q$.

- Numerical experiments carried out as part of this study showed the existence of multiple stable equilibriums. The cause of these multiple equilibriums is not clear and should be further investigated.

- In addition to the western Wadden Sea there exist multiple double inlet systems in other parts of the world that possibly have different features. To strengthen the model, it is recommended to apply the stability analysis to these multiple inlet systems.

References

[1] BORSJE, C.S. (2003). Cross-sectional stability of a two inlet bay system. *M.Sc. Thesis, Delft University of Technology.*

[2] DRAPER, N.R., SMITH, H. (1981). Applied regression analysis, second edition. *John Wiley & Sons*, New York. pp 709.

[3] ESCOFFIER, F.F. (1940). The stability of tidal inlets. *Shore and Beach*, 8 (4), pp 114-115.

[4] O'BRIEN, M.P. (1931). Estuary and tidal prisms related to entrance areas. *Civil Engineering*, 1 (8), pp 738-739.

[5] STIVE, M.F.J., CAPOBIANCO, M., WANG, Z.B., RUOL, P. AND BUIJSMAN, M.C. (1998). Morphodynamics of a tidal lagoon and the adjacent coast. *8th International Biennial Conference on Physics of Estuaries and Coastal Seas*, The Hague, September 1996, pp 397-407.

[6] VAN DE KREEKE, J. (1990). Can multiple tidal inlets be stable?. *Estuarine, Coastal and Shelf Science*, 30, pp 261-273.

[7] VAN DE KREEKE, J. (1998). Adaptation of the Frisian Inlet to a reduction in basin area with special reference to the cross-sectional area of the inlet channel. *Physics of Estuaries and Coastal Seas*, pp 335-362.

[8] WANG, Z.B., FOKKINK, R.J., DE VRIES, M. AND LANGERAK, A. (1995). Stability of river bifurcations in 1D morphodynamic models. *Journal of Hydraulic Research*, 33 (6), pp 739-750.

Appendix A: Stability of a single inlet system using ASMITA

In this study ASMITA is used to determine the cross-sectional equilibrium and stability of tidal inlets. Therefore, the inlet is schematized to a basin connected to the ocean by a channel (Figure 38). The channel length is restricted to the length of the inlet gorge and is assumed to be prismatic. The channel and ocean exchange sediment through a diffusion-type transport, where the diffusion is assumed to take into account all the possible transport processes. There is no sediment exchange between the channel and the basin, in contrast to the original ASMITA concept. In this study we are interested in the development of the cross-sectional area of the inlet. A major difference with the previous applications of ASMITA is that during the adaptation of the cross-sectional area the tidal prism varies with the cross-sectional area. For simplification it is assumed that the important sediment processes take place in the gorge of the inlet and that sediment exchange with the basin does not contribute to the stability of the inlet.

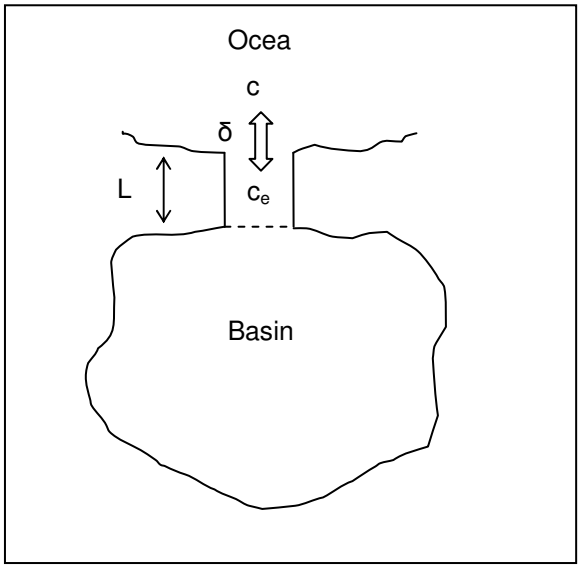

Figure 38: Model schematization ASMITA

A key element in the modelling concept of ASMITA is the equilibrium concentration. The definition of this parameter is based on the following arguments. When the inlet channel is in equilibrium the sediment concentration is the same as in the ocean. This concentration is referred to as the overall equilibrium concentration c_E. For the channel a local equilibrium sediment concentration c_e is defined such that it is equal to c_E when the channel is in morphological equilibrium, larger than c_E if tendency of erosion exist, and smaller than c_E if tendency of sedimentation exists. The local equilibrium concentration and the overall equilibrium concentration are assumed proportional to the velocity amplitude to the power n:

$$c_e \therefore \hat{u}^n \quad and \quad c_E \therefore \hat{u}_E^n \tag{A.1}$$

The power n is larger than one. Most commonly it is taken as 2 in compliance with a third power for the sediment transport as a non-linear function of the mean flow velocity. It follows from Equation (A.1):

$$c_e = c_E \left(\frac{\hat{u}}{\hat{u}_E} \right)^n \tag{A.2}$$

Here $\hat{u}$ is the actual velocity amplitude and $\hat{u}_E$ is the velocity amplitude when the inlet is at equilibrium.

The extent to which the local sediment demand in the channel is satisfied depends on the difference c_e - c, just like exchange between the channel and the ocean is controlled by the difference c - c_E. This results in the following representation of the sediment balance for the channel:

$$\delta \left(c - c_E \right) = wBL \left(c_e - c \right) \tag{A.3}$$

in which:	δ	= horizontal exchange rate	[m^3/s]
	w	= vertical exchange coefficient	[m/s]
	B	= width of the channel	[m]
	L	= length of the channel	[m]

The left-hand side of Equation (A.3) represents the diffusive sediment exchange between channel and ocean. The right-hand side reflects local erosion or sedimentation. According to the modelling concept morphological changes occur when the local sediment concentration deviates from the local equilibrium sediment concentration. Provided that the mean water level in the channel remains unchanged the rate of change of the cross-sectional area of the channel can be written as:

$$\frac{dA}{dt} = wB \left(c_e - c \right) \tag{A.4}$$

Making use of Equations (A.2), (A.3) and (A.4) and eliminating c and c_e the expression for the rate of change of the cross-sectional area of the channel in terms of the velocity amplitudes is:

$$\frac{dA}{dt} = \frac{wBc_E\delta}{\delta + wBL} \left(\left(\frac{\hat{u}}{\hat{u}_E} \right)^n - 1 \right) \tag{A.5}$$

Appendix B: Calculating the amplitude and phase of the first harmonic using the least square method

To calculate the amplitude and the phase of the first harmonic of Q and h, the least square method can be used [DRAPER AND SMITH, 1981]. Here this method is demonstrated for Q.
We assume that the first harmonic is equal to a cosine function:

$$Q^*(t) = \hat{Q}\cos(\omega t + \alpha) \tag{B.1}$$

which can be rewritten as:

$$Q^*(t) = \hat{Q}(\cos\omega t\cos\alpha - \sin\omega t\sin\alpha) = \hat{Q}_c\cos\omega t + \hat{Q}_s\sin\omega t \tag{B.2}$$

so $\hat{Q}_c = \hat{Q}\cos\alpha$ and $\hat{Q}_s = -\hat{Q}\sin\alpha$ (B.3)

The least square method states:

$$\sum_i \left(Q^*(t_i) - v(1,i)\right)^2 = \text{minimal}$$, where v(1,i) is the calculated time series (B.4)

this leads to:

$$\frac{\partial}{\partial\hat{Q}_c}\sum_i \left(Q^*(t_i) - v(1,i)\right)^2 = \sum_i 2\left(Q^*(t_i) - v(1,i)\right)\cdot\frac{\partial}{\partial\hat{Q}_c}Q^*(t_i) = 0$$

$$\sum_i \left(\hat{Q}_c\cos\omega t_i + \hat{Q}_s\sin\omega t_i - v(1,i)\right)\cos\omega t_i \tag{B.5}$$

$$\Rightarrow \hat{Q}_c\sum_i\cos^2\omega t_i + \hat{Q}_s\sum_i\cos\omega t_i\sin\omega t_i = \sum_i v(1,i)\cos\omega t_i$$

the same holds when differentiating with respect to $\hat{Q}_s$. Thus, we now have a set of two equations:

$$\hat{Q}_c\sum_i\cos^2\omega t_i + \hat{Q}_s\sum_i\cos\omega t_i\sin\omega t_i = \sum_i v(1,i)\cos\omega t_i \tag{B.6}$$

$$\hat{Q}_c\sum_i\cos\omega t_i\sin\omega t_i + \hat{Q}_s\sum_i\sin^2\omega t_i = \sum_i v(1,i)\sin\omega t_i \tag{B.7}$$

in matrix form:

$$\begin{pmatrix} \sum_i \cos^2 \omega t_i & \sum_i \cos \omega t_i \sin \omega t_i \\ \sum_i \cos \omega t_i \sin \omega t_i & \sum_i \sin^2 \omega t_i \end{pmatrix} \cdot \begin{pmatrix} \hat{Q}_c \\ \hat{Q}_s \end{pmatrix} = \begin{pmatrix} \sum_i v(1,i) \cos \omega t_i \\ \sum_i v(1,i) \sin \omega t_i \end{pmatrix} \tag{B.8}$$

from this the amplitude and the phase can be calculated with:

$$\hat{Q} = \sqrt{\hat{Q}_c^2 + \hat{Q}_s^2} \tag{B.9}$$

and

$$\tan \alpha = \frac{\hat{Q}_s}{\hat{Q}_c} \tag{B.10}$$

Appendix C: Equilibrium cross-sectional areas of a double inlet system with partition assuming linear friction

February 1, 2006

In a personal note to the writer VAN DE KREEKE showed that for a double inlet system with opening and linear friction there is only one combination of inlet cross-sectional areas for which both inlets are in equilibrium. The following is the model that proofs the statement made above.

Length, friction, etc. of inlets 1 and 2 is the same.

$A_{b1} = A_{b2} = A_b$

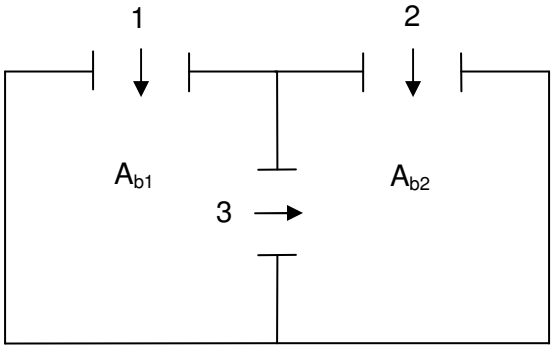

Equations of continuity:

$$A_b \frac{d\eta_{b1}}{dt} = u_1 A_1 - u_3 A_3 \tag{C.1}$$

$$A_b \frac{d\eta_{b2}}{dt} = u_2 A_2 + u_3 A_3 \tag{C.2}$$

Equations of motion:

$$u_1 = c(\eta_0 - \eta_{b1}) \tag{C.3}$$

$$u_2 = c(\eta_0 - \eta_{b2}) \tag{C.4}$$

$$u_3 = c_3(\eta_{b1} - \eta_{b2}) \tag{C.5}$$

The five Equations with 5 unknowns are reduce to two equations with unknowns u_1 and u_2 in the following manner.

Differentiating Equation (C.3) w.r.t. t and multiplying by A_b leads to:

$$A_b \frac{du_1}{dt} = A_b c \frac{d\eta_0}{dt} - A_b c \frac{d\eta_{b1}}{dt} \tag{C.6}$$

From Eqs. (C.1) and (C.6)

$$A_b \frac{du_1}{dt} = A_b c \frac{d\eta_0}{dt} - c u_1 A_1 + c u_3 A_3 \tag{C.7}$$

From Eqs. (C.3) and (C.4)

$$u_1 - u_2 = c\left(\eta_{b2} - \eta_{b1}\right) = -\frac{u_3}{c_3} c \tag{C.8}$$

From Eqs. (C.5) and (C.8)

$$u_3 = \frac{c_3}{c}\left(u_2 - u_1\right) \tag{C.9}$$

Substitution of u_3 from (C.9) in (C.7) leads to:

$$\frac{A_b}{c}\frac{du_1}{dt} + \left(A_1 + \frac{c_3 A_3}{c}\right) u_1 - \frac{c_3 A_3}{c} u_2 = A_b \frac{d\eta_0}{dt} \tag{C.10}$$

similar for u_2:

$$\frac{A_b}{c}\frac{du_2}{dt} + \left(A_2 + \frac{c_3 A_3}{c}\right) u_2 - \frac{c_3 A_3}{c} u_1 = A_b \frac{d\eta_0}{dt} \tag{C.11}$$

with $\eta_0 = \hat{\eta}_0 e^{i\sigma t}$, assume a trial solution:

$$u_1 = \hat{u}_1 e^{i\varphi_1} e^{i\sigma t} \tag{C.12}$$

$$u_2 = \hat{u}_2 e^{i\varphi_2} e^{i\sigma t} \tag{C.13}$$

Substituting in (C.10) and (C.11):

$$\hat{u}_1 \frac{A_b}{c} i\sigma e^{i\varphi_1} + \left(A_1 + \frac{c_3 A_3}{c}\right)\hat{u}_1 e^{i\varphi_1} - \frac{c_3 A_3}{c}\hat{u}_2 e^{i\varphi_2} = A_b \sigma \hat{\eta}_0 i \tag{C.14}$$

$$\hat{u}_2 \frac{A_b}{c} i\sigma e^{i\varphi_2} + \left(A_2 + \frac{c_3 A_3}{c}\right)\hat{u}_2 e^{i\varphi_2} - \frac{c_3 A_3}{c}\hat{u}_1 e^{i\varphi_1} = A_b \sigma \hat{\eta}_0 i \tag{C.15}$$

Introducing the equilibrium conditions $\hat{u}_1 = \hat{u}_2 = 1$ m/s, and solving for $e^{i\varphi_1}$ and $e^{i\varphi_2}$.

$$e^{i\varphi_1} = \frac{\begin{vmatrix} A_b\sigma\hat{\eta}_0 i & -\frac{c_3 A_3}{c} \\ A_b\sigma\hat{\eta}_0 i & \frac{A_b i\sigma}{c} + \left(A_2 + \frac{c_3 A_3}{c}\right) \end{vmatrix}}{\begin{vmatrix} \frac{A_b i\sigma}{c} + \left(A_1 + \frac{c_3 A_3}{c}\right) & -\frac{c_3 A_3}{c} \\ -\frac{c_3 A_3}{c} & \frac{A_b i\sigma}{c} + \left(A_2 + \frac{c_3 A_3}{c}\right) \end{vmatrix}} \tag{C.16}$$

The determinant in the denominator is:

$$-\left(\frac{A_b\sigma}{c}\right)^2 + A_1 A_2 + \left(A_1 + A_2\right)\left(\frac{c_3 A_3}{c}\right) + i\frac{A_b\sigma}{c}\left(A_1 + A_2 + \frac{2c_3 A_3}{c}\right) = a + ib \tag{C.17}$$

The determinant in the nominator is:

$$-\frac{A_b^2\sigma^2}{c}\hat{\eta}_0 + i\left(2A_b\sigma\hat{\eta}_0\frac{c_3 A_3}{c} + A_b\sigma\hat{\eta}_0 A_2\right) = x + iy \tag{C.18}$$

and thus:

$$e^{i\varphi_1} = \frac{x + iy}{a + ib} \tag{C.19}$$

Similar for $e^{i\varphi 2}$ the determinant in the denominator is a+ib. The determinant in the nominator is:

$$-\frac{A_b^2\sigma^2}{c}\hat{\eta}_0 + i\left(2A_b\sigma\hat{\eta}_0\frac{c_3 A_3}{c} + A_b\sigma\hat{\eta}_0 A_1\right) = x + iz \tag{C.20}$$

and thus:

$$e^{i\varphi_2} = \frac{x + iz}{a + ib} \tag{C.21}$$

It follows that:

$$\left|e^{i\varphi_1}\right| = \sqrt{\frac{x^2 + y^2}{a^2 + b^2}} = 1 \tag{C.22}$$

$$\left|e^{i\varphi_2}\right| = \sqrt{\frac{x^2 + z^2}{a^2 + b^2}} = 1 \tag{C.23}$$

and therefore y = z.
It then follows from the definitions of y and z that $A_1 = A_2$.

Conclusion: There is only one combination of cross-sectional areas for which $\hat{u}_1 = \hat{u}_2 = 1$ m/s, For that combination $A_1 = A_2$.The actual value of the cross-sectional areas would have to be calculated from Eqs. (C.1) to (C.5).

Note: The foregoing conclusion holds as long as $\hat{u}_1 = \hat{u}_2$. The value of the equilibrium velocity does not necessarily have to be 1 m/s

Appendix D: List of combinations of A_3 and L_3 and the corresponding stable equilibrium cross-sectional areas

A_3 [m^2]	L_3 [m]	Stable equilibrium cross-sectional areas	
		A_1 [m^2]	A_2 [m^2]
2,500	500	$7.484 \cdot 10^4$	$6.677 \cdot 10^4$
5,000	1,000	$7.629 \cdot 10^4$	$6.529 \cdot 10^4$
5,000	2,000	$7.548 \cdot 10^4$	$6.613 \cdot 10^4$
5,000	3,000	$7.504 \cdot 10^4$	$6.658 \cdot 10^4$
7,500	1,000	$7.826 \cdot 10^4$	$6.333 \cdot 10^4$
7,500	2,000	$7.702 \cdot 10^4$	$6.459 \cdot 10^4$
7,500	3,000	$7.631 \cdot 10^4$	$6.53 \cdot 10^4$
7,500	5,000	$7.548 \cdot 10^4$	$6.613 \cdot 10^4$
10,000	1,000	$8.046 \cdot 10^4$	$6.095 \cdot 10^4$
10,000	2,000	$7.861 \cdot 10^4$	$6.301 \cdot 10^4$
10,000	3,000	$7.764 \cdot 10^4$	$6.4 \cdot 10^4$
10,000	5,000	$7.647 \cdot 10^4$	$6.514 \cdot 10^4$
15,000	1,000	$8.538 \cdot 10^4$	$6.594 \cdot 10^4$
15,000	3,000	$8.062 \cdot 10^4$	$6.095 \cdot 10^4$
20,000	3,000	$8.405 \cdot 10^4$	$5.75 \cdot 10^4$